Regulatory T Cell Function in Established Systemic Autoimmune Inflammation: Reversal and Containment of a Fatal Disease

Alexander Rudensky (rudenska@mskcc.org)
Sloan Kettering Institute, and Ludwig Center at Memorial Sloan Kettering Cancer Center
https://orcid.org/0000-0003-1280-2898

Wei Hu
Sloan Kettering Institute, and Ludwig Center at Memorial Sloan Kettering Cancer Center
https://orcid.org/0000-0002-0392-6939

Zhong-Min Wang
Sloan Kettering Institute, and Ludwig Center at Memorial Sloan Kettering Cancer Center
https://orcid.org/0000-0002-5538-1969

Yongqiang Feng
St. Jude Children's Research Hospital https://orcid.org/0000-0002-2320-5063

Michail Schizas
Sloan Kettering Institute, and Ludwig Center at Memorial Sloan Kettering Cancer Center

Beatrice Hoyos
Sloan Kettering Institute, and Ludwig Center at Memorial Sloan Kettering Cancer Center

Joris van der Veeken
Memorial Sloan Kettering Cancer Center

Jacob Verter
Sloan Kettering Institute, and Ludwig Center at Memorial Sloan Kettering Cancer Center

Regina Bou Puerto
Sloan Kettering Institute, and Ludwig Center at Memorial Sloan Kettering Cancer Center
https://orcid.org/0000-0002-7546-3312

Article

Keywords: autoimmunity, inflamation

Posted Date: February 5th, 2021

DOI: https://doi.org/10.21203/rs.3.rs-153417/v1

Version of Record: A version of this preprint was published at Nature Immunology on August 23rd, 2021.
See the published version at https://doi.org/10.1038/s41590-021-01001-4.

Regulatory T Cell Function in Established Systemic Autoimmune Inflammation: Reversal and Containment of a Fatal Disease

Wei Hu[1]*, Zhong-Min Wang[1,2]*, Yongqiang Feng[1,3], Michail Schizas[1], Beatrice E. Hoyos[1], Joris van der Veeken[1], Jacob Verter[1], Regina Bou Puerto[1,4], Alexander Y. Rudensky[1]

[1] Howard Hughes Medical Institute, Immunology Program, and Ludwig Center, Memorial Sloan Kettering Cancer Center, New York, NY 10065, USA; [2] Gerstner Sloan Kettering Graduate School of Biomedical Sciences, Memorial Sloan Kettering Cancer Center, New York, NY 10065, USA; [3] Present address: Department of Immunology, St. Jude Children's Research Hospital, Memphis, TN 38105, USA. [4] Immunology and Microbial Pathogenesis Program, Weill Cornell Graduate School of Medical Sciences, New York, NY 10021, USA.

** These authors contributed equally to this work*

The immunosuppressive function of regulatory T (Treg) cells is dependent on continuous expression of the transcription factor Foxp3. *Foxp3* loss-of-function or induced ablation of Treg cells results in a fatal autoimmune disease featuring all known types of inflammatory responses with every manifestation stemming from Treg cell paucity, highlighting a vital function of Treg cells in preventing fatal autoimmune inflammation. However, a major question remains whether Treg cells can persist and effectively exert their function in a disease state, where broad spectrum of inflammatory mediators can either inactivate Treg cells or render innate and adaptive pro-inflammatory effector cells insensitive to suppression. By reinstating Foxp3 protein expression and suppressor function in cells expressing a reversible *Foxp3* null allele in severely diseased mice, we found that the resulting single pool of "redeemed" Treg cells normalized immune activation, quelled severe tissue inflammation, reversed fatal autoimmune disease and provided long-term protection against them. Thus, Treg cells are functional in settings of established broad spectrum systemic inflammation and are capable of affording sustained reset of the immune homeostasis.

35 Regulatory T (Treg) cells expressing the X chromosome-encoded transcription factor Foxp3
36 have been implicated in the control of inflammation in diverse physiological and pathological
37 settings[1-9]. Mice and humans lacking functional *Foxp3* gene develop fatal autoimmune and
38 inflammatory disease affecting skin, lung, endo- and exocrine glands, and gastro-intestinal tract,
39 autoimmune anemia, lymphadenopathy and splenomegaly, eosinophilia, hyper IgE syndrome,
40 and markedly increased systemic levels of a wide range of pro-inflammatory cytokines,
41 including IL-6, TNFα, IL-4, IL-5, IL-13, IFNγ, IL-17, IL-23, and GM-CSF[1-3]. Foxp3 protein
42 expression is required for Treg cell differentiation[4-7]. Previous analyses of mice harboring a
43 functional *Foxp3*^{GFP} reporter and a *Foxp3*^{GFPKO} reporter null allele revealed a critical requirement
44 for Foxp3 protein for Treg cell suppressor function. Foxp3-deficient GFP^{+} Treg "wannabes",
45 while exhibiting considerable similarity to their Foxp3-sufficient GFP^{+} counterparts, are devoid of
46 suppressor capacity[8,9]. Accordingly, retroviral expression of a *Foxp3* transgene in Treg
47 "wannabes" confers characteristic Treg cell gene expression and suppressor function[10]. Foxp3-
48 deficient mice present with marked immune activation, increased pro-inflammatory cytokines,
49 IgE and IgG1 levels, blepharitis, dermatitis, and lymphadenopathy by day 10 of life with the
50 majority of mice succumbing to the disease by 3-4 wks of age[5,11,12]. Likewise, Treg cell ablation
51 induced upon diphtheria toxin (DT) treatment of healthy adult *Foxp3*$^{DTR\text{-}GFP}$ mice, which express
52 a simian diphtheria toxin receptor (DTR)-GFP fusion protein encoded by the endogenous *Foxp3*
53 locus, leads to similar widespread autoimmune inflammation to which they succumb within 2
54 wks[13]. Adoptive transfer of wild-type Treg cells into *Foxp3*$^{DTR\text{-}GFP}$ mice at the time of DT
55 administration or into 1-day-old *Foxp3* mutant mice prevents the disease[5,13]. These studies have
56 unequivocally demonstrated a critical role of Treg cells in preventing autoimmunity and
57 inflammation and associated pathologies.
58
59 However, a major outstanding issue is whether Treg cells can effectively function in settings of
60 established systemic inflammation and are capable of reversing and containing severe
61 autoimmune diseases. In fact, a large body of work in experimental animal models of infection,
62 inflammation, and cancer suggests that major immune effector cytokines, including IL-6, IL-1,
63 type I and II IFNs, IL-23, and IL-4, can cause 1) loss of Foxp3 expression in, functional
64 inactivation of, and acquisition of pro-inflammatory features by Treg cells, or 2) make immune
65 effector cells refractory to Treg-mediated suppression[14-20]. Accordingly, numerous analyses of
66 Treg cells present at the inflammatory sites of autoimmune patients suggested that their
67 function is impaired[21-25]. Additional uncertainty stems from a possibility that the three archetypal
68 inflammatory immune responses (types 1, 2, and 3), recognized based on their distinct spectra

of secreted and cellular effectors, may differ in their ability to compromise Treg functionality or in their sensitivity to, and requirements for, Treg mediated suppression. In this regard, variation in Treg cell frequencies was reported to result in a disproportionate dysregulation of type 2 vs. type 1 autoimmunity[26]. Thus, to address the major outstanding question above, we sought to employ an experimental animal model which would: 1) exhibit systemic mixed type 1, 2, and 3 autoimmunity and tissue inflammation; 2) enable temporal control and efficient switching of Treg suppressor function in an established disease; 3) eschew adoptive transfer of Treg cells, which does not guarantee their migration to and accumulation at the inflammatory sites; and 4) allow for an extended longitudinal observation.

We reason that the cardinal features of the aforementioned archetypal inflammatory responses are shared by a broad spectrum of autoimmune and inflammatory diseases. The breadth and severity of the autoimmune inflammatory disease resulting from Foxp3 deficiency, characterized by the activation and expansion of all major immune cell types (Th1, Th2, Th17, CD8, B cells, monocytes, neutrophils, eosinophils, etc.) and rampant cytokine storm (IFNγ, IL-4, IL-5, IL-17, IL-6, TNFα, GM-CSF, IL-1β), make it an ideal experimental setting for testing the ability of Treg cells to operate in established inflammation. By engineering mice where an inducible Cre recombinase allowed for the installation of Treg cells in severely diseased animals, we found that Treg cells were functional in settings of established systemic mixed type 1, 2, and 3 inflammation and capable of resetting immune homeostasis and restoring health. Upon sensing the inflammatory environment, Treg cells became activated, rapidly expanded, and exhibited heightened suppressive capacity. These Treg cells stably persisted for an extended period of time with no signs of dysfunction or sexhaustion and were enriched for a sub-polulation featuring enhanced self-renewing properties.

Results

Restoration of Foxp3 expression in Treg “wannabe” cells

To investigate the ability of Treg cells to function in settings of established severe autoimmune inflammation, we generated mice harboring a reversible *Foxp3*$^{loxP\text{-}Thy1.1\text{-}STOP\text{-}loxP\text{-}GFP}$ reporter null allele (*Foxp3*^{LSL}). In these mice, a loxP site-flanked Thy1.1 reporter coding sequence followed by a STOP cassette was inserted into the *Foxp3* locus in front of the *Foxp3* coding sequence preceded by a GFP reporter (Extended Data Fig. 1a, b). Since *Foxp3* transcription was halted by the STOP cassette, effectively creating a null allele, expression of Thy1.1 marked a population of Treg “wannabe” cells in these mice (Extended Data Fig. 1c, d). These cells were

similar to the aforementioned cells expressing the *Foxp3*^{GFPKO} allele[8], with phenotypic features distinct from either naïve or activated conventional CD4 T cells, or Foxp3-sufficient Treg cells (Extended Data Fig. 1e). Combining the *Foxp3*^{LSL} allele with a *Cd4* allele expressing a tamoxifen-inducible Cre-ERT2 fusion protein (*Cd4*^{creERT2}) enabled Cre-mediated excision of the STOP cassette upon 4-hydroxytamoxifen (4-OHT) treatment and conversion of Foxp3-deficient Thy1.1^{+} cells into Foxp3-sufficient GFP^{+} Treg cells (Fig. 1a and 1b). The latter, when co-transferred with effector Foxp3^{-} CD4 T cells into lymphopenic recipients, were able to suppress the wasting disease similar to Treg cells isolated from control *Foxp3*^{GFP} mice (Extended Data Fig. 1f). Thus, re-expression of Foxp3 in Treg "wannabes" confers suppressor function and fitness in accordance with previous findings.

Reversal of established autoimmune inflammation in young mice by Treg cells

Hemizygous male *Foxp3*^{LSL} mice developed early onset, multi-organ autoimmune inflammation indistinguishable from that of Foxp3-deficient mice and succumbed to the disease within 3-4 wks with few mice surviving for up to 6 wks after birth. To test whether Treg cells can suppress ongoing inflammation, male *Foxp3*^{LSL}*Cd4*^{creERT2} or *Foxp3*^{LSL}*Cd4*^{wt} mice were administered with a single dose of 4-OHT at 2 wks of age, when they exhibited pronounced autoimmune syndrome with frank clinical manifestations including blepharitis and macroscopic skin lesions. By measuring 4-OHT induced Cre recombinase activity in Treg cells in mice simultaneously treated with the S1P receptor antagonist FTY720, we assessed the recombination efficiency in the absence of the confounding effects of ongoing thymic output and T cell recirculation, which were abolished upon S1P receptor blockage. We found that the recombination efficiency was comparable in the secondary lymphoid organs, lung, and liver on day 3 following 4-OHT administration (Extended Data Fig. 2a). Within 4 wks after 4-OHT administration, the disease in *Foxp3*^{LSL}*Cd4*^{creERT2} mice was greatly reduced with the extent of activation of innate and adaptive immune cells approaching the level of healthy *Foxp3*$^{DTR\text{-}GFP}$*Cd4*^{creERT2} controls. In contrast, the disease in 4-OHT treated control *Foxp3*^{LSL}*Cd4*^{wt} mice rapidly progressed unabatedly with prominent splenomegaly, lymphadenopathy and thymic atrophy; none of the mice survived beyond 6 wks of age (Fig. 1c-e; Extended Data Fig. 2b-f).

4-OHT treatment led to the recombination of the *Foxp3*^{LSL} allele in CD4 expressing cells in the thymus and the periphery. Therefore, the observed reversal of inflammation could be due to either transient restoration of thymic Treg cell output following Foxp3 restoration in double positive and CD4 single positive thymocytes or due to conversion of peripheral Treg "wannabe"

137 cells into Treg cells. To assess whether rescue of the peripheral pool of Treg cells in disease
138 settings is sufficient to restrain immune activation and inflammation, we induced Foxp3
139 expression in Treg "wannabe" cells upon 4-OHT treatment in the presence of continuous
140 administration of FTY720 (Extended Data Fig. 3a). We observed diminished immune activation
141 and inflammation in *Foxp3*^{LSL}*Cd4*^{creERT2} mice, compared to *Foxp3*^{LSL}*Cd4*^{wt} controls, on day 14
142 following combined 4-OHT and FTY720 treatment, suggesting that peripheral "redeemed" Treg
143 cells were effective at controlling inflammation and could rescue disease in the absence of
144 thymic output (Extended Data Fig. 3b-c).
145
146 Detailed kinetic analysis revealed that aggressive lymphoproliferation and activation of
147 conventional CD4 (Foxp3^{-}Thy1.1^{-}) and CD8 T cells were suppressed within a wk after 4-OHT-
148 induced restoration of Treg cell function, as evidenced by reduced expression of Ki67, CD44,
149 CD25, IFNγ, and IL-4 (Fig. 1d; Extended Data Fig. 2d-e). Likewise, myelo-proliferation marked
150 by expansion of neutrophils, monocytes and eosinophils also retreated (Fig. 1e; Extended Data
151 Fig. 2f). During the course of the disease, control *Foxp3*^{LSL}*Cd4*^{wt} mice displayed increasingly
152 severe acute phase response reflected in high levels of serum amyloid P (SAP) and
153 haptoglobin, both of which were brought to basal levels in treated *Foxp3*^{LSL}*Cd4*^{creERT2} mice (Fig.
154 1f and data not shown). In addition, levels of IgE, IgG1 and IgM, sharply increased in control
155 *Foxp3*^{LSL}*Cd4*^{wt} mice, were brought down by newly minted Treg cells in *Foxp3*^{LSL}*Cd4*^{creERT2} mice
156 (Fig. 1g, Extended Data Fig. 2g). Histopathological analysis of the skin, lung and liver showed
157 manifest immune infiltration and lymphocytic and myeloid inflammation in both control
158 *Foxp3*^{LSL}*Cd4*^{wt} and untreated *Foxp3*^{LSL}*Cd4*^{creERT2} mice; however, the tissue pathology
159 disappeared in *Foxp3*^{LSL}*CD4*^{creERT2} mice within 4 wks after 4-OHT administration (Fig. 1h and
160 1i). A closer examination of the skin pathology in both *Foxp3*^{LSL}*Cd4*^{creERT2} and *Foxp3*^{LSL}*Cd4*^{wt}
161 mice before 4-OHT treatment revealed lichenoid interface dermatitis with edema in the dermis
162 and focal pyknotic keratinocytes, epidermal hyperplasia and hyperkeratosis, with sizeable areas
163 of serocellular crust. These autoimmune manifestations were ameliorated in *Foxp3*^{LSL}*Cd4*^{creERT2}
164 mice, but continued to worsen in *Foxp3*^{LSL}*Cd4*^{wt} mice 4 wks following 4-OHT treatment
165 (Extended Data Fig. 4a-b). Additionally, TUNEL staining showed a pronounced increase in
166 apoptotic cells in the liver of *Foxp3*^{LSL}*Cd4*^{creERT2} mice before the treatment, which was
167 completely reverted to control levels 4 wks post restoration of Treg function following 4-OHT
168 treatment (Extended Data Fig. 4c-d). Consistent with the observed liver damage, serum
169 albumin concentration in *Foxp3*^{LSL}*Cd4*^{creERT2} mice at 2 wks of age was significantly diminished
170 but restored to normal within 4 wks after 4-OHT treatment. (Extended Data Fig. 4e).

171

172 The reversed immune activation and tissue inflammation was unlikely to be a mere
173 consequence of subtracting the Treg "wannabe" cells from the CD4 T cell pool, as our previous
174 studies demonstrated that the disease severity in Foxp3-deficient mice harboring Treg
175 "wannabe" cells was identical to that of neonates subjected to chronic Treg cell ablation[13],
176 suggesting that Treg "wannabe" cells do not provide a notable non-redundant contribution to the
177 severity and time course of the disease in Foxp3-deficient mice. These results show that Treg
178 cells are capable of effectively exerting their function in settings of established inflammatory
179 disease and suppressing multiple arms of the inflammatory immune response, causing their
180 reversal. It can be argued, however, that the observed Treg cell-mediated restoration of the
181 "normalcy" might be limited to an early age when the immune system is not fully developed.
182

183 **Reversal of established autoimmune inflammation by Treg cells in adulthood**

184 To assess whether Treg cells are capable of suppressing ongoing inflammatory responses in
185 adulthood, we took advantage of the fact that *Foxp3*, as an X chromosome-encoded gene, is
186 subject to random X-inactivation. Thus, we generated healthy mosaic heterozygous female
187 *Foxp3*$^{DTR\text{-}GFP/LSL}$*Cd4*^{creERT2} mice, which harbor both a functional Treg population and a non-
188 functional Treg "wannabe" population expressing the *Foxp3*$^{DTR\text{-}GFP}$ and *Foxp3*^{LSL} allele,
189 respectively. Acute depletion of Treg cells in homozygous *Foxp3*$^{DTR\text{-}GFP}$ females or hemizygous
190 *Foxp3*$^{DTR\text{-}GFP}$ males upon recurrent diphtheria toxin (DT) administration causes an even more
191 aggressive widespread autoimmune inflammatory disease to which mice succumb within 10-14
192 days[13]. Indeed, DT-mediated Treg cell depletion in adult (8-10-wks-old) *Foxp3*$^{DTR\text{-}GFP/LSL}$
193 heterozygous females caused similarly massive immune activation by day 7, at which point the
194 diseased *Foxp3*$^{DTR\text{-}GFP/LSL}$*Cd4*^{creERT2} and control *Foxp3*$^{DTR\text{-}GFP/LSL}$*Cd4*^{wt} mice were administered
195 with tamoxifen to induce conversion of Treg "wannabes" to functional Treg cells (Fig. 2a). Within
196 2 wks post tamoxifen treatment, the rehabilitated Treg cells suppressed T cell activation,
197 whereas in tamoxifen-treated control *Foxp3*$^{DTR\text{-}GFP/LSL}$*Cd4*^{wt} mice the disease progressed (Fig.
198 2b, Extended Data Fig. 5). Although the numbers of CD4 and CD8 T cells no longer decreased
199 beyond wk 2 post Treg cell restoration (data not shown), the percentages of activated CD4 and
200 CD8 T cells continued to decline during the 5 wk observation period post tamoxifen treatment
201 (Fig. 2b). Furthermore, the rehabilitated Treg cells ameliorated the inflammatory lesions in the
202 skin, lung, and liver induced upon Treg cell depletion in *Foxp3*$^{DTR\text{-}GFP/LSL}$*Cd4*^{creERT2} mice by wk 5
203 post tamoxifen administration (Fig. 2c-e). Therefore, the revived Treg cells were able to protect
204 the adult mice from autoimmune inflammation until at least 5 wks post tamoxifen administration,

205 the longest period of time we could confidently ensure that the mice would not develop DT-
206 specific antibodies, which would interfere with DT-mediated ablation of *Foxp3*$^{DTR\text{-}GFP}$ Treg cells.
207 Thus, Treg cells can function under inflammatory settings and suppress established lethal
208 inflammation in both neonates and adults.
209
210 **Foxp3 expression imparts Treg cell functionality in inflammatory environment**
211 The remarkable effect of restored Foxp3 expression in a cohort of Treg "wannabe" cells led us
212 to explore the intrinsic and extrinsic phenotypic shifts it afforded to these cells in inflammatory
213 vs. non-inflammatory settings. Compared to *Foxp3*$^{DTR\text{-}GFP}$*Cd4*^{creERT2} healthy littermate control
214 mice, we observed a transient increase in Treg cell proportion in male *Foxp3*^{LSL}*Cd4*^{creERT2} mice,
215 which peaked on day 7 post 4-OHT treatment and decreased to the level of control healthy mice
216 after 4 wks, when the autoimmune disease was largely eradicated (Fig. 3a). On day 7, the
217 Thy1.1^{-}GFP^{+} Treg cell population in rescued *Foxp3*^{LSL}*Cd4*^{creERT2} mice was more proliferative
218 than Treg cells in healthy *Foxp3*$^{DTR\text{-}GFP}$*Cd4*^{creERT2} controls, as indicated by increased proportion
219 of Ki67^{+} cells. Furthermore, the former cells expressed higher amounts of GITR and CTLA4,
220 both of which contribute to their functionality (Fig. 3b, c). To gain a transcriptome-wide view of
221 the effects of Foxp3 expression in diseased *Foxp3*^{LSL}*Cd4*^{creERT2} mice, we performed RNA-seq
222 analysis of Thy1.1^{-}GFP^{+} Treg cells and Thy1.1^{+} GFP^{-} Treg "wannabes" isolated from *Foxp3*^{LSL}
223 males on day 7 following 4-OHT treatment, and of control GFP^{+} Treg cells isolated from
224 similarly treated *Foxp3*$^{DTR\text{-}GFP}$*Cd4*^{creERT2} mice. Principal component analysis (PCA) of the RNA-
225 seq data showed that Thy1.1^{-}GFP^{+} Treg cells from diseased mice were considerably different
226 from control Treg cells from *Foxp3*$^{DTR\text{-}GFP}$*Cd4*^{creERT2} mice (PC2; 30% variance) with the
227 differentially regulated genes in the former enriched for previously reported Treg cell[27] and
228 STAT5[28] activation gene signatures (Fig. 3d). Notably, the transcriptomes of both Treg cell
229 groups were markedly different – equidistant in PCA – from Thy1.1^{+}GFP^{-} Treg "wannabe" cells
230 (Fig. 3d). These results suggested that Treg cells in *Foxp3*^{LSL}*Cd4*^{creERT2} mice were more
231 activated, potentially due to heightened STAT5 signaling. These cells expressed lower levels of
232 *Tcf7*, *Sell*, and *Ccr7* transcripts consistent with their pronounced activation. Moreover, they
233 expressed higher levels of cell cycle and anabolism-related genes as well as genes whose
234 products have been implicated in Treg cell mediated suppressor function (*Gzma*, *Gzmb*, *Lgals1*,
235 *Lgals3*, *Il10*, *Fgl2*, *Ctla4*, *Entpd1*, *Icos*, and *Tigit*)[29,30], suggesting that these cells were more
236 metabolically active and potentially more suppressive than Treg cells present in healthy control
237 mice (Fig. 3e). Indeed, we found that Thy1.1^{-}GFP^{+} Treg cells from diseased *Foxp3*^{LSL}*Cd4*^{creERT2}
238 mice isolated on day 7 post 4-OHT administration were significantly more potent on a per cell

basis at suppressing T cell proliferation *in vitro* than their counterparts from control healthy *Foxp3*$^{DTR\text{-}GFP}$*Cd4*^{creERT2} mice (Fig. 3g).

Notably, activated Treg "wannabe" cells from DT treated *Foxp3*$^{LS/\,DTR\text{-}GFP}$ sick female mice, compared to their resting counterparts from similarly treated healthy *Foxp3*$^{LSL/WT}$ mice, shared some gene expression changes observed in activated Foxp3-sufficient Treg cells in rescued *Foxp3*$^{LSL/y}$ mice vs. resting Treg cells in control *Foxp3*$^{DTR\text{-}GFP/y}$ male mice described above (Fig. 3d, Extended Data Fig. 6). However, this acquisition of activated phenotype by the Treg "wannabe" cells did not endow them with any appreciable suppressive capacity, as *Foxp3*$^{LSL/DTR}$*Cd4*^{wt} mice, in which tamoxifen treatment did not restore Foxp3-expressing Treg cells, died of systemic multi-organ inflammation similar to that seen in the male *Foxp3*$^{LSL/y}$ mice (data not shown). These results suggested that restoration of Foxp3 expression allows rehabilitated Treg cells to mobilize their functionality upon exposure to an inflammatory environment, resulting in their heightened suppressor capacity as compared to their basal state in non-inflammatory settings. Alternatively, the observed functional superiority of the rehabilitated Treg cells in *Foxp3*^{LSL}*Cd4*^{creERT2} mice could have been a cell-intrinsic effect of a delayed Foxp3 expression regardless of the inflammatory environment. To distinguish between these two possibilities, we analyzed the corresponding Thy1.1^{-}GFP^{+} Treg and Thy1.1^{+}GFP^{-} Treg "wannabe" cell subsets under basal non-inflammatory conditions in healthy heterozygous female *Foxp3*$^{LSL/WT}$*Cd4*^{creERT2} mice and control GFP^{+} Treg cells in heterozygous female *Foxp3*$^{DTR\text{-}GFP/WT}$*Cd4*^{creERT2} mice on day 7 post 4-OHT treatment. In contrast to Treg cells exposed to the pro-inflammatory environment in male mice, Thy1.1^{-}GFP^{+} Treg cells in 4-OHT treated mosaic *Foxp3*$^{LSL/WT}$*Cd4*^{creERT2} females failed to exhibit increased proliferative activity, or enhanced CTLA4 and GITR expression, compared to GFP^{-}Foxp3^{+} Treg cells expressing the *Foxp3*^{WT} allele in the same mice (Fig. 3f). Expression of these markers was also similar to that of control GFP^{+} Treg cells in heterozygous female *Foxp3*$^{DTR\text{-}GFP/WT}$*Cd4*^{creERT2} mice (Fig. 3f). Likewise, comparable suppressor activity was observed for Thy1.1^{-}GFP^{+} Treg cells and control GFP^{+} counterparts on day 7 from 4-OHT treated healthy *Foxp3*$^{LSL/WT}$*Cd4*^{creERT2} and *Foxp3*$^{DTR\text{-}GFP/WT}$*Cd4*^{creERT2} female mice, respectively (Fig. 3g). To the contrary, sick *Foxp3*$^{DTR\text{-}GFP/LSL}$*Cd4*^{creERT2} mosaic female mice, subjected to DT-induced ablation of *Foxp3*$^{DTR\text{-}GFP}$ Treg cells and tamoxifen-induced Foxp3 restoration in *Foxp3*^{LSL} cells, showed a transient increase in Treg cell percentages at 1 and 2 wks post tamoxifen-mediated rescue, which disappeared by wk 5 (Fig. 3h). This trend was similar to that observed in sick *Foxp3*$^{LSL/y}$*Cd4*^{creERT2} male mice. Likewise, Treg cells rehabilitated under inflammatory conditions exhibited enhanced proliferation

273 as well as heightened activation evidenced by elevated expression of Ki67, CTLA4, GITR and
274 ICOS on day 7 post tamoxifen treatment (Fig. 3i, j). Thus, the enhanced proliferative potential
275 and superior suppressive capacity of Treg cells in diseased *Foxp3*^{LSL}*Cd4*^{creERT2} male and DT-
276 treated *Foxp3*$^{DTR\text{-}GFP/LSL}$*Cd4*^{creERT2} female mice was likely due to sensing inflammation by these
277 cells assisted by restored Foxp3 expression.
278
279 **A single cohort of Treg cells provides long-term protection against autoimmunity**
280 Our observation that Treg cells introduced into diseased *Foxp3*^{LSL}*Cd4*^{creERT2} males were highly
281 functional in disease settings raised the question whether the containment of autoimmunity
282 afforded by a sole cohort of Treg cells was durable. To address this question, we monitored 4-
283 OHT treated male *Foxp3*^{LSL}*Cd4*$^{\mathrm{creERT2}}$ mice for an extended period of time (Fig. 4a). To "time
284 stamp" the Treg cell populations in these studies, we introduced into *Foxp3*^{LSL}*Cd4*^{creERT2} and
285 control *Foxp3*$^{DTR\text{-}GFP}$*Cd4*^{creERT2} mice a *Rosa26*$^{loxP\text{-}STOP\text{-}loxP\text{-}tdTomato}$ (*R26*^{Tom}) recombination reporter
286 allele, which allows for irreversible labeling of all CD4 T cells undergoing Cre-mediated
287 recombination induced by 4-OHT with the red fluorescent tdTomato protein. Within a month
288 after 4-OHT treatment, the *Foxp3*^{LSL}*Cd4*^{creERT2}*R26*^{Tom} mice recovered completely from otherwise
289 lethal disease and continued to gain weight (Extended Data Fig. 7a). When analyzed at the 4-
290 month time point, Foxp3^{+} Treg cells detected in the thymus of these mice were exclusively
291 CD73 positive and were devoid of the CD73-negative subset representing newly generated
292 thymic Treg cells (Fig. 4b)[31]. This observation implied a lack of new thymic output of Treg cells
293 with all thymic Foxp3^{+} cells being recirculating cells, in agreement with our observation that
294 CD4-creERT2-mediated recombination, reported by the *R26*^{Tom} allele, ceased within 48 to 72
295 hours after 4-OHT administration (Extended Data Fig. 7b). The peripheral "4-month-old" Treg
296 cell pool in these mice was well maintained both in the lymphoid and non-lymphoid tissues (Fig.
297 4c), and remained functionally competent as documented using *in vitro* suppression assay
298 (Extended Data Fig. 7c). Nearly all Thy1.1^{-}GFP^{+} Foxp3^{+} Treg cells at all sites examined in
299 *Foxp3*^{LSL}*Cd4*^{creERT2}*R26*^{Tom} mice expressed the tdTomato reporter whereas the Tshy1.1^{+}GFP^{-}
300 Treg "wannabe" cells and conventional Thy1.1^{-}GFP^{-} Foxp3^{-}CD4 T cells in the same mice, as
301 well as Treg and conventional CD4 T cell subsets in control *Foxp3*$^{DTR\text{-}GFP}$*Cd4*^{creERT2}*R26*^{Tom} mice
302 contained only a small fraction of tdTomato "fate-mapped" cells (Fig. 4d). Thus, Treg cells
303 generated as a single cohort in diseased *Foxp3*^{LSL}*Cd4*^{creERT2} mice continued to persist while the
304 other analyzed T cell subsets turned over most likely due to continuous thymic output.
305 Impressively, even after 4 months, the reversal of autoimmune disease seemed complete with
306 no pathology observed in the skin, lung, liver and small intestine (Fig. 4e). Likewise, T cell

activation and effector cytokine production, as well as myelo-proliferation, at best minimally increased (Fig. 4f-h, Extended Data Fig. 7d-f). Thus, a single cohort of Treg cells is capable of reversing established inflammation and affording long-term protection against autoimmunity. Remarkably, the rescued mice continued to survive for at least 7 months post 4-OHT treatment (Fig. 5a). Even at this time point, the rescued mice remained largely healthy with only moderately increased T cell activation and effector cytokine production with Treg cell population well maintained in both the lymphoid and non-lymphoid tissues (Extended Data Fig. 8a-c). Despite moderately increased serum IgG1and IgE levels in comparison to the 4-wk time point, the other Ig isotype levels remained comparable to those in control *Foxp3*$^{DTR\text{-}GFP/y}$*Cd4*^{creERT2} mice (Extended Data Fig. 8d and data not shown). Neither did we observe prominent immune infiltrates in the skin, liver, and small intestine (Extended Data Fig. 8e).

Transcriptional features of long-lived protective Treg cells

The extraordinarily long-term protection against autoimmunity by a single cohort of Treg cells, as well as their impressive self-renewing potential, suggested that these cells, despite their prolonged persistence and continuous self-antigen stimulation, do not exhibit dysfunction typical of chronically stimulated CD4 and CD8 T cells. However, population level analyses of these Treg cells may obscure their potential heterogeneity in relation to their self-renewing potential or exhaustion. Thus, we sought to analyze this long-lived Treg cell population at a single-cell resolution using single cell RNA sequencing (scRNA-seq). We compared GFP^{+} Treg cells from *Foxp3*$^{LSL/y}$*CD4*^{creERT2}*R26*^{Tom} mice and *Foxp3*$^{DTR\text{-}GFP/y}$*CD4*^{creERT2}*R26*^{Tom} control mice 7 months after 4-OHT treatment (Fig. 5b). Treg cells in experimental and control mice were efficiently and comparably labeled by tdTomato protein shortly after 4-OHT induction (Fig. 5c). The percentage of tdTomato^{+} cells among Thy1.1^{-}GFP^{+} Treg cells in *Foxp3*$^{LSL/y}$*CD4*^{creERT2}*R26*^{Tom} mice remained high (>80%) over time, demonstrating that this long-lived cell population persisted in an impressively stable manner. The percentage of tdTomato^{+} cells among control *Foxp3*$^{DTR\text{-}GFP}$ Treg cells, however, gradually declined with only about 15% tdTomato^{+} cells found within GFP^{+} Treg cells at the time of analysis, most likely as a result of continuous thymic output replenishing the peripheral Treg cell pool with non-tdTomato-labeled Treg cells (Fig. 5c).

We pooled the scRNA-seq data from *Foxp3*$^{LSL/y}$*Cd4*^{creERT2}*R26*^{Tom} and *Foxp3*$^{DTR\text{-}GFP/y}$*Cd4*^{creERT2}*R26*^{Tom} mice and performed uniform manifold approximation and projection (UMAP) for visualization. To distinguish “old” and “young” cells among the control Treg cells from *Foxp3*$^{DTR\text{-}GFP/y}$*Cd4*^{creERT2}*R26*^{Tom} mice, we computationally separated them into tdTomato

341 positive (“old”) and negative (“young”) cells based on the expression of the tdTomato transcript
342 by individual cells. Thy1.1^{-}GFP^{+} Treg cells in *Foxp3*$^{LSL/y}$*Cd4*^{creERT2}*R26*^{Tom} mice, as well as the
343 tdTomato^{+} and tdTomato^{-} control GFP^{+} Treg cells in *Foxp3*$^{DTR\text{-}GFP/y}$*Cd4*^{creERT2}*R26*^{Tom} mice,
344 exhibited distinct distribution patterns in the UMAP plot (Fig. 5d). To better understand the most
345 significant sources of variation among the three Treg cell populations, we performed diffusion
346 map analysis. The first diffusion component (DC1) had a distribution of gene expression highly
347 similar to that of activated Treg cell gene signature[27] (Fig. 5e). The long-lived Thy1.1^{-}GFP^{+} Treg
348 cells had a DC1 density similar to that of the tdTomato^{+} cells in control mice, which was higher
349 than that of the tdTomato^{-} cells (Fig. 5f). This result indicates that long-lived Treg cells in
350 *Foxp3*$^{LSL/y}$*Cd4*^{creERT2}*R26*^{Tom} mice and control mice tagged with tdTomato 7 month earlier and
351 their offsprings exhibited a similarly activated phenotype. Upon examining the genes whose
352 expression patterns highly correlated with this diffusion component, we found transcripts
353 associated with Treg cell activation (*Cd44*, *Sell*, *Tnfrsf18*, *Icos*, *Ctla4*). Additionally, we also
354 found genes whose products promote cell migration to non-lymphoid tissues (*Ccr4*, *Cxcr3*, *Ccr6,*
355 *Itgae*), as well as tissue adaptation and suppressor function[32,33] (*Maf*, *Ahr*) (Fig. 5g, Extended
356 Data Fig.9a). Flow cytometric analysis of expression of some of these genes confirmed the
357 scRNA-seq results across multiple tissues. The CD62L^{hi} (encoded by *Sell*) cells were greatly
358 reduced while cells expressing CD103, encoded by *Itgae,* were markedly increased within the
359 Thy1.1^{-}GFP^{+} Treg population in *Foxp3*$^{LSL/y}$*Cd4*^{creERT2}*R26*^{Tom} mice (Extended Data Fig. 9b).
360 Furthermore, flow cytometric analysis of the tdTomato^{+} fraction of control Treg cells showed
361 enrichment for Ly6C^{-}CD103^{+} and CD44^{high}CD62L^{lo} cells, consistent with their heightened
362 activation state (Extended Data Fig. 9c). Despite the burden of being the sole Treg cells
363 responsible for immunosuppression, the Thy1.1^{-}GFP^{+} Treg cells did not appear less fit than
364 their “age-matched” counterparts in control mice with continuous Treg cell turnover. Compared
365 to tdTomato^{+} GFP^{+} Treg cells in *Foxp3*$^{DTR\text{-}GFP/y}$*Cd4*^{creERT2}*R26*^{Tom} mice, Thy1.1^{-}GFP^{+} Treg cells in
366 *Foxp3*$^{LSL/y}$*Cd4*^{creERT2}*R26*^{Tom} mice exhibited comparable expression of genes associated with T
367 cell exhaustion[34] and apoptosis, and similar levels of *Mcl1*, an anti-apoptotic gene critical for the
368 Treg cell survival[35] (Fig. 5f). Genes involved in cell cycle progression and various metabolic
369 pathways were also comparably expressed by tdTomato^{+} GFP^{+} Treg cells in *Foxp3*$^{DTR\text{-}}$
370 $^{GFP/y}$*Cd4*^{creERT2}*R26*^{Tom} mice and Thy1.1^{-}GFP^{+} Treg cells in *Foxp3*$^{LSL/y}$*Cd4*^{creERT2}*R26*^{Tom} mice
371 (Extended Data Fig. 9d). These shared transcriptional features highlight the similarities in
372 metabolic status and proliferative potential between the long-lived Treg cells in
373 *Foxp3*$^{LSL/y}$*Cd4*^{creERT2}*R26*^{Tom} mice and age matched tdTomato^{+} control *Foxp3*$^{DTR\text{-}GFP/y}$ Treg cells.
374

375 The observed heightened activation and self-renewal of functional Thy1.1^{-}GFP^{+} Treg cells in
376 *Foxp3$^{LSL/y}$Cd4^{creERT2}R26^{Tom}* mice might represent a cell state unique to these mice or
377 characteristic features of long-lived cells present within the peripheral Treg cell pool under
378 physiologic conditions. To address this question, we performed trajectory analysis on combined
379 experimental and control Treg cell scRNA-seq datasets using the Palantir algorithm, which
380 generates a high-resolution pseudotime ordering of cells at different developmental stages[36].
381 The pseudotime gradient started from resting ("naïve") Treg cells, proceeded towards activated
382 Treg cells, and ended with activated cells with transcriptional features of "tissue" Treg cells
383 found in non-lymphoid organs in agreement with a previous report[37] (Fig. 5h). The analysis
384 successfully recapitulated known gene expression dynamics during Treg cell activation
385 including downregulation of *Tcf7*, *Sell*, and *Klf2,* and upregulation of *Foxp3*, *Ctla4*, and *Ikzf2*
386 transcripts (Fig. 5i). Next, we compared the pseudotemporal ordering of Thy1.1^{-}GFP^{+} Treg cells
387 from *Foxp3$^{LSL/y}$Cd4^{creERT2}R26^{Tom}* mice, originating from cells whose Foxp3 expression was
388 restored 7 months ago, with that of similarly "old" tdTomato^{+} and of "young" tdTomato^{-} GFP^{+}
389 Treg cells from control *Foxp3$^{DTR\text{-}GFP/y}$Cd4^{creERT2}R26^{Tom}* mice. Both "old" Treg cell populations
390 were positioned late in the inferred differentiation trajectory in comparison to tdTomato^{-} Treg
391 cells –s consistent with their activated phenotype – and were characterized by similarly high
392 pseudotime values (Fig. 5j). Thus, Thy1.1^{-}GFP^{+} Treg cells in *Foxp3$^{LSL/y}$Cd4^{creERT2}R26^{Tom}* mice
393 closely resemble a set of long-lived cells present in the normal Treg cell pool under physiologic
394 conditions.
395
396 To gain further insights into the long-term persistence of Thy1.1^{-}GFP^{+} Treg cells in
397 *Foxp3^{LSL}Cd4^{creERT2}R26^{Tom}* mice, we performed a refined clustering analysis of the Thy1.1^{-}GFP^{+}
398 and *Foxp3$^{DTR\text{-}GFP}$* Treg cell scRNA-seq datasets. Among the 13 clusters identified, clusters 0
399 and 3 were primarily composed of tdTomato^{-} *Foxp3$^{DTR\text{-}GFP}$* control Treg cells, whereas clusters
400 1, 6, 7 and 8 were enriched for Thy1.1^{-}GFP^{+} Treg cells (Fig. 6a). Importantly, cells from cluster 1
401 were enriched for IL-2-Stat5 and Wnt-β-catenin pathway gene signatures (Fig. 6b), which have
402 been implicated in Treg cell maintenance and self-renewal[38-40]. Moreover, these cells were
403 lower in pseudotime values compared to the majority of the Thy1.1^{-}GFP^{+} Treg cells, suggesting
404 that they were less differentiated and had the potential to differentiate into the rest of the cells to
405 sustain the Treg cell pool (Fig. 6c). Gene expression analysis revealed transcripts enriched
406 (*Ifngr1*, *Epcam*, *Lrrc32*, *Il4ra, etc.*) and depleted (*Sell*, etc.) in cluster 1 cells (Fig. 6d, Extended
407 Data Table 1). Using flow cytometry, we corroborated these results by demonstrating a marked
408 enrichment of IL4Rα^{hi}IFNγR1^{hi}Epcam^{+}GARP^{hi}CD25^{hi} (γREG^{+}) cell subset within rescued

409 activated CD62L^{lo} Treg population in *Foxp3*^{LSL}*Cd4*^{creERT2}*R26*^{Tom} mice (Fig. 6e, Extended Data
410 Fig. 10a-c). In unperturbed mice, these cells were also present, albeit at a lower frequency,
411 within Treg cell population in the secondary lymphoid organs and at even lower frequency in
412 non-lymphoid tissues such as liver and lung, but were virtually undetectable among newly
413 differentiated CD73^{-} thymic Treg cells (Fig. 6f). γREG^{+} Treg cells were enriched in the
414 parenchyma of highly vascularized organs such as the spleen and the lung, as evidenced by
415 their higher frequency among cells not labeled by intravenously administered CD45 antibody,
416 suggesting that these cells were largely non-circulatory and likely contributed to local
417 maintenance of the Treg cell pools (Extended Data Fig. 10d). To compare the capacity of
418 perinatal and adult Treg cell populations to give rise to γREG^{+} Treg cells, we labeled Treg cells
419 in healthy 2-wk-old and 8-wk-old *Foxp3*$^{DTR-GFP}$*Cd4*^{creERT2}*R26*^{Tom} mice upon 4-OHT treatment and
420 assessed the frequencies of γREG^{+} Treg cells within tdTomato^{+} and tdTomato^{-} Treg cell subsets
421 4 months later. In the former experimental group, tdTomato^{+} Treg subset harbored higher
422 frequencies of γREG^{+} Treg cells than their tdTomato^{-} counterparts (Fig. 6g). In contrast,
423 tdTomato^{+} Treg cell population "time-stamped" in adult *Foxp3*$^{DTR-GFP}$*Cd4*^{creERT2}*R26*^{Tom} mice failed
424 to show an enrichment of γREG^{+} Treg cells over their tdTomato^{-} counterpart; rather, both
425 populations contained similar percentages of γREG^{+} Treg cells as the tdTomato^{-} Treg cells in
426 perinatally labeled mice, which is reduced in comparison to the tdTomato^{+} Treg cells in these
427 mice (Fig. 6g). These observations were independently confirmed by similar "time-stamping" of
428 Treg cells in young vs. adult *Foxp3*^{creERT2}*R26*^{Tom} mice (Fig. 6g). These results were consistent
429 with the enrichment in γREG^{+} Treg cells observed within the peripheral Treg populations in the
430 secondary lymphoid organs and non-lymphoid tissues in unmanipulated 2-wk-old vs. 8-wk-old
431 mice (Extended Data Fig. 10e). Our results suggest γREG^{+} Treg cells, capable of persisting in
432 peripheral lymphoid and non-lymphoid organs, are selectively prominent within Treg cell
433 population generated early in life.
434

435 **Discussion**

436 The cardinal features of the adaptive immune system, including its essentially unlimited antigen
437 recognition specificity, amplification of innate immune responses, novel effector functions and
438 memory, afford vertebrates with a versatile anticipatory defense against rapidly evolving
439 infectious agents. This superior protection is confounded by a major fitness constraint due to a
440 threat of autoimmunity and inflammation posed by the inherent self-reactivity of T cells. A
441 singular vital role and broad purview of Treg cells in countering this threat - forestalling

442 autoimmunity – has been most vividly demonstrated by wide-ranging clinical manifestations of
443 human monogenic disorders resulting from Treg cell deficiency or dysfunction due to *FOXP3*,
444 *STAT5B, IL2RA,* and *LRBA* mutations or *CTLA4* haplo-insufficiency[41,42]. In IPEX patients, these
445 manifestations include endocrinopathies (diabetes, thyroiditis, pancreatitis, adrenal dysfunction),
446 hepatitis, enteropathies (autoimmune gastritis, IBD, celiac disease), skin disorders (exudative
447 dermatitis, alopecia), food allergy, hyper-IgE syndrome, autoimmune hematologic disorders
448 (autoimmune thrombocytopenia, hemolytic anemia), myelo- and lymphoproliferation
449 (splenomegaly, lymphadenopathy), polyneuropathy, as well as pulmonary and nephrotic
450 syndromes[43]. In mice, Treg deficiency or depletion cause equally widespread and fatal
451 autoimmune inflammatory disease[13].
452
453 However, the potent immunosuppressive function of Treg cells indispensable for preventing
454 autoimmune inflammation can in turn compromise protective immunity against infection. This
455 consideration provided rationale for the concept that in the inflammatory settings of an infection
456 Treg cells are ineffectual. Indeed, numerous studies showed that infection associated
457 inflammatory milieu can cause downregulation of Foxp3 expression by Treg cells, impede their
458 suppressor and proliferative capacity, or even confer pro-inflammatory properties, i.e. effector
459 cytokine production; furthermore, pro-inflammatory cytokines, IL-6 and IL-1 in particular, can
460 make effector cells refractory to Treg cell mediated suppression[14,16,18,19,44,45]. On the other hand,
461 some studies suggested that Treg cells are capable of modulating virus-specific immune
462 responses and limiting associated pathologies[46-51]. However, in all of these studies, Treg cells
463 were present from the onset of infection, making it impossible to discriminate their activity prior
464 to, or after the onset of infection-induced inflammation. Thus, the ability of Treg cells to function
465 in infection induced inflammation remains an open question.
466
467 Since inflammation elicited by various infectious, metabolic and genetic causes, including Treg
468 cell deficiency, shares principal cellular and soluble mediators, a corollary to the above concept
469 is the notion that in established autoimmune inflammation, Treg cell activity is also expected to
470 be severely attenuated or even lacking. In this regard, autoimmune and inflammatory
471 pathologies were reported to exert varying effects on Treg cell numbers. In contrast to the
472 aforementioned monogenic Treg deficiency-linked disorders, many studies of polygenic
473 autoimmune diseases have found unchanged or even increased frequencies of Treg cells at
474 inflammatory sites and in circulation[52]. Meanwhile, functional and gene expression analyses of
475 Treg cells isolated from autoimmune patients suggested that their function is impaired in the

476 inflammatory environment[21-23,52-54]. However, numerous genetic polymorphisms have been
477 linked to the pathophysiological manifestations of polygenic autoimmune diseases. Thus, the
478 reported inferior Treg functionality in autoimmune patients can be one of these phenotypic
479 manifestations. Indeed, an enrichment for such autoimmunity associated single nucleotide
480 polymorphisms has been observed within Treg cell-specific regulatory elements identified by
481 histone modifications and DNA demethylation analyses[10,55,56]. As a potential counterargument to
482 the above findings, adoptive transfer of Treg cells after the initiation of T cell-induced colitis was
483 shown to cause its amelioration, highlighting their potential to control local inflammation. In this
484 model, however, colonic inflammation was elicited upon homeostatic expansion of a relatively
485 small number of naïve CD4 T cells upon their transfer into lymphopenic mice. Although the
486 disease receded, it did so very slowly after transfer of a large number of $CD25^{+}CD4^{+}$ Treg cells
487 in a strictly IL-10 dependent manner[57,58]. Thus, it remained possible that the observed reparative
488 activity of Treg cells in this setting may be specific to the colon aided by its continuous epithelial
489 cell turnover, or due to the numerical imbalance between the transferred Treg and effector T
490 cells and the limited repertoire of the latter.
491
492 By genetically installing a limited Treg cell pool in *Foxp3*^{LSL} mice, we demonstrated that Treg
493 cells are able to function in settings of systemic autoimmune inflammation, reverse fatal disease
494 and tissue pathology, and offer its long-term containment. The reversal of inflammation was not
495 a simple diversion of a large number of pro-inflammatory effector T cells into Treg cells as only
496 approximately 5-6% of CD4 T cell population is represented by Treg "wannabe" cells at the time
497 of 4-OHT treatment (data not shown). While induced Foxp3 expression could have "subtracted"
498 no more than 6% cells from the total CD4 T cell pool, within a week of 4-OHT administration we
499 observed ~40% and ~60% decrease in the absolute numbers of $Foxp3^{-}CD44^{hi}$ activated CD4 T
500 cells in the spleen and the lymph nodes, respectively (data not shown). This finding was fully
501 consistent with the indistinguishable fatal autoimmune diseases reported in Foxp3-deficient
502 mice harboring Treg "wannabe" cells and *Foxp3*^{DTR} neonates subjected to chronic ablation of
503 Treg cells, which demonstrated that Treg "wannabes" do not provide notable non-redundant
504 contribution to the pathogenic self-reactive T cell pool in Foxp3 deficient mice that would affect
505 severity and time course of the disease[5,8,13]. The ability of Treg cells to suppress established
506 inflammation was not limited to young (2-3 wk-old) mice but was also observed in adult animals.
507 Notably, Treg cells introduced into the inflammatory environment suppressed Th2 autoimmunity
508 including increased serum IgG1 and IgE levels, as efficiently as Th1 and Th17 responses, even

509 though Th2 responses are known to be most sensitive to diminished Treg cell numbers or
510 functionality[26,59] .
511
512 The observed normalization of lympho- and myeloproliferation, acute phase response, and
513 reversal of tissue inflammation highlighted the ability of Treg cells to function in settings of
514 autoimmunity accompanied by a cytokine storm. Rather than impeding functionality, we found
515 that exposure to this highly inflammatory milieu endowed the newly minted Treg cells with
516 heightened suppressor activity in comparison to Treg cells isolated from control healthy mice
517 while the latter and Treg cells generated upon a similar conversion of Treg "wannabe" cells in
518 healthy heterozygote female mice had indistinguishable suppressor activity. It is widely
519 accepted that Treg cells employ multiple and partially redundant modes of suppression,
520 including secreted immunomodulatory factors, IL-2 consumption, and ATP to adenosine
521 conversion, and may directly partake in tissue regeneration and repair via production of
522 amphiregulin (Areg)[60,61]. Consistent with these findings and the observed efficient reversal of
523 inflammatory disease by Treg cells in *Foxp3*^{LSL} mice, these cells exhibited increased expression
524 of numerous molecules implicated in Treg mediated immunomodulation and tissue repair
525 including IL-2R, IL-10, Galectin-1 and -3 (*Lgals1* and *Lgals3*), Fgl2, CTLA4, CD39 (*Entpd1*),
526 ST2 (*Il1rl1*), and Areg. While we cannot unambiguously pinpoint inflammation sensing pathways
527 responsible for potentiation of Treg cell function, prominent STAT5 activation gene expression
528 signature discerned in redeemed Treg cells in 4-OHT-treated male *Foxp3*^{LSL} mice implicates
529 cytokines signaling through common γ-chain receptors including IL-2. Accordingly,
530 administration of therapeutic IL-2 formulations and expression of an active form of STAT5b in
531 Treg cells have been reported to promote their expansion and superior suppressor
532 function[28,62,63]. It is important to note that the observed suppressor activity of Treg cells in
533 inflammatory settings was not limited to recent thymic emigrants as Foxp3 expression induced
534 in peripheral Treg "wannabe" cells present in the secondary lymphoid organs led to efficient
535 suppression of autoimmunity in systemically inflamed mice in the absence of thymus export
536 upon S1P1 receptor blockage. The reversal of inflammatory disease and restoration and long-
537 term health maintenance by a single pool of redeemed Treg cells was enabled by its stability. At
538 a population level, these cells remained functional and did not exhibit signs of dysfunction and
539 were similar to time-stamped long-lived "old" Treg cells in a healthy mouse. Single cell
540 transcriptomic analyses of these redeemed Treg cells revealed a subset of preferentially tissue-
541 residing cells, marked by increased expression of IFNγR, IL-4Rα, EpCAM, and GARP. Based
542 on gene set enrichment and pseudo-time analyses, it is possible that these cells may contribute

543 to the long-term maintenance of the Treg pool, by giving rise to terminally differentiated
544 progenies locally.
545
546 By demonstrating that Treg cells are functional in severe established inflammation and can
547 suppress and reverse all known types of and key common features of inflammation and that a
548 single cohort of Treg cells can afford a long-lasting protection against autoimmunity and
549 inflammation, our findings provide general rationale and support for the emerging efforts to
550 develop adoptive Treg cell therapy not only for intrauterine and neonatal IPEX syndrome and
551 other monogenic Treg deficiencies, but for a broad spectrum of autoimmune and inflammatory
552 disorders.
553
554 **Acknowledgements:**
555 We thank Elham Azizi for advice on scRNA-seq data analysis and members of the Rudensky
556 lab for technical support and discussion. We acknowledge the use of the Integrated Genomics
557 Operation Core facility at MSKCC led by C. Cobbs for RNA-extraction, library preparation and
558 high-throughput sequencing. We thank L. Mazutis and the staff at the MSKCC Single Cell
559 Research Initiative for sample processing and library generation. This work was supported
560 by NIAID grant RO1 AI034206 (A.Y.R), Irvington-Cancer Research Institute Postdoctoral
561 Fellowship (W.H.), the Ludwig Center at Memorial Sloan Kettering, Parker Institute for Cancer
562 Immunotherapy (PICI) (A.Y.R.), NCI Cancer Center grant P30 CA08748. A.Y.R is an
563 investigator with the Howard Hughes Medical Institute. Z.-M.W. is supported by a Bruce Charles
564 Forbes Fellowship.
565
566 **Author contributions:**
567 W.H. and A.Y.R. conceived the study and designed experiments. W.H., Z.-M.W. and A.Y.R.
568 interpreted the data and wrote the manuscript; W.H. and Z.-M.W. performed the experiments.
569 Y.F. designed the targeting construct and generated the *Foxp3*^{LSL} mouse. B.E.H. performed the
570 antibody ELISA assays. J.V., J.v.d.V. and R.B.P. provided assistance with some experiments.
571 J.V. assisted with mouse generation and animal colony maintenance. Z.-M.W. and M.S.
572 performed analysis of the bulk RNA-seq experiment. M.S. performed analysis of scRNA-seq
573 datasets. W.H. and A.Y.R. supervised the study.
574
575 **Author information:**

576 A.Y.R. is a co-founder and SAB member of and holds stock options in Vedanta Bioscience and
577 Sonoma Biotherapeitics. Correspondence and requests for materials should be addressed to
578 A.Y.R. (rudenska@mskcc.org)
579

580 **Methods**

581

582 **Mice**

583 Experiments in this study were approved by the Sloan Kettering Institute (SKI) Institutional
584 Animal Care and Use Committee under protocol 08-10-023. Mice were housed at the SKI
585 animal facility under SPF conditions on a 12-hour light/dark cycle with free access to water and
586 regular chow diet. All control and experimental animals were age-matched, and littermates were
587 used as controls unless otherwise indicated.
588 *Foxp3*$^{DTR\text{-}GFP}$ [13], *Foxp3*^{GFP} [6], *Foxp3*^{creERT2} [28],*Foxp3*$^{GFP\text{-}BirA\text{-}AVI\text{-}TEV/y}$ (in preparation), *Cd4*^{creERT2} [64],
589 *Tcrb*$^{-/-}$*Tcrd*$^{-/-}$ [65] and *Rosa26*$^{LSL\text{-}tdTomato}$ [66] mice were maintained in the the Sloan Kettering Institute
590 animal facility. The *Rosa26*$^{LSL\text{-}tdTomato}$ allele was bred to homozygosity for fate mapping studies.

591

592 **Generation of *Foxp3*^{LSL} mice**

593 The targeting construct was made by first subcloning an 8.5 kb *SphI* fragment harboring the
594 *Foxp3* genomic sequence from exon -1a to exon 7 obtained from the RP23-143D8 cosmid into
595 a cloning vector carrying a Pgk-DTA-polyA cassette allowing for negative selection of random
596 genomic integration. The FRT-PGK-neo-polyA-FRT positive selection cassette was then cloned
597 into the *DraIII* site within the intron between exons -1b and 1, and the loxP-Thy1.1 coding
598 sequence-triple-tandem SV40 polyA-eGFP coding sequence cassette was cloned into the *AvrII*
599 site within exon 1. The Thy1.1 and eGFP sequences are preceded by a start codon (ATG). The
600 targeting construct was then electroporated into albino C57BL/6 ES cells. After neomycin
601 selection, Southern blotting and karyotyping, correctly targeted clones were injected into WT
602 C57BL/6 blastocysts. The resulting chimeric mice were bred to albino C57BL/6 mice. Founders
603 identified based on the coat color and genotyping were mated to a Flp deleter strain of mice to
604 remove the neo cassette.

605

606 **4-hydroxytamoxifen, diphtheria toxin, and tamoxifen treatment**

607 4-hydroxytamoxifen (4-OHT, Sigma-Aldrich, H7904) stock solution was made by reconstituting
608 in ethyl alcohol 200 proof (Sigma-Aldrich, E-7023) at a concentration of 20 mg/mL, then diluting
609 1:1 (v/v) with Cremophor EL (Sigma-Aldrich, 238470). 20 μg/g body weight of 4-OHT diluted in
610 PBS was administered intraperitoneally.

611

612 Diphtheria toxin (DT, List Biological Laboratories, 150) was dissolved in PBS. 1μg (first dose) or
613 250 ng (subsequent doses) was injected intraperitoneally for each mouse. For tamoxifen

614 administration, 20 mg of tamoxifen (Sigma-Aldrich, T5648) was resuspended in 1 mL corn oil
615 (Sigma-Aldrich, C8267) by rotating and tilting at 37°C until fully dissolved. Each mouse was
616 orally gavaged with 4 mg of tamoxifen per treatment.
617
618 4-OHT was used whenever possible because it bypasses the conversion of tamoxifen to 4-
619 hydroxytamoxifen in the liver. Compared to tamoxifen, 4-OHT offers a much sharper
620 pharmacokinetics and enables a highly synchronized labeling of cells. In addition, 4-OHT has a
621 much shorter half-life than tamoxifen, particularly in adults. Therefore, tamoxifen instead of 4-
622 OHT was used for *in vivo* suppression assays (Extended Data Fig. 1f) and in studies of adult
623 female mice (Fig. 2, Fig. 3h-j, and Extended Data Fig. 7) to achieve sufficient recombination of
624 the *Foxp3*^{LSL} allele.
625
626 FTY720 stock solution was made by reconstituting in dimethyl sulfoxide at a concentration of 20
627 mg/ml. 0.8 μg/g body weight of FTY720 diluted to 0.1 mg/ml in 2% β-
628 hydroxypropanylcyclodextrin was administered intraperitoneally.
629
630 **Reagents and antibodies**
631 The following clones of fluorescently conjugated or biotinylated antibodies were obtained from
632 BD Biosciences, BioLegend, ThermoFisher, or Tonbo and were used in this study for
633 flowcytometry: anti-Siglec-F (E50-2440), anti-I-A/I-E (M5/114.15.2), anti-NK1.1 (PK136), anti-
634 CD45 (30-F11), anti-CD11b (M1/70), anti-CD3ε (17A2), anti-Ly-6C (HK1.4), anti-CD90.2 (30-
635 H12), anti-Foxp3 (FJK-16s), anti-CD19 (6D5), anti-Ly-6G (1A8), anti-TCRβ (H57-597), anti-
636 F4|80 (BM8), anti-CD90.1 (HIS51), anti-CD4 (RM4-5), anti-CD8α (53-6.7), anti-GITR (DTA-1),
637 anti-CD73 (TY/11.8), anti-CD44 (IM7), anti-CD103 (M290), anti-CD62L (MEL-14), anti-CTLA4
638 (UC10-4B9), anti-Helios (22F6), anti-Ki-67 (16A8), anti-CD25 (PC61.5), anti-CD45.1 (A20), anti-
639 CD45.2 (104), anti-IL-2 (JES6-5H4), anti-IL-17A (17B7), anti-IFNγ (XMG1.2), anti-IL-4 (BVD6-
640 24G2), anti-GARP (YGIC86), anti-CD119 (2E2), anti-EpCAM (G8.8), anti-CD124 (mIL4R-M1).
641
642 The following antibodies were used to capture antigens for ELISA in this study: purified anti-
643 mouse IgE (R35-72, BD Pharmingen, 553413), Goat Anti-Mouse IgG1 (RRID: AB_2794408,
644 SouthernBiotech, 1070-01), Goat Anti-Mouse IgG3 (RRID: AB_2794567, SouthernBiotech,
645 1100-01), Goat Anti-Mouse IgG2a (RRID: AB_2794475, SouthernBiotech, 1080-01), Goat Anti-
646 Mouse IgG2b (RRID: AB_2794517, SouthernBiotech, 1090-01), Goat Anti-Mouse IgG2c (RRID:
647 AB_2794464, SouthernBiotech, 1079-01), Goat Anti-Mouse IgA (RRID: AB_2314669,

648 SouthernBiotech, 1040-01), Goat Anti-Mouse IgM (RRID: AB_2794197, SouthernBiotech, 1020-
649 01), Mouse Pentraxin 2/SAP Antibody (R & D Systems, MAB2558).
650
651 The following antibodies were used to detect antigens for ELISA in this study: Goat Anti-Mouse
652 Ig-HRP (RRID: AB_2728714, SouthernBiotech, 1010-05), Biotin Rat Anti-Mouse IgE (R35-118,
653 BD Pharmingen, 553419), Biotinylated Pentraxin 2/SAP Antibody (R & D Systems, BAF2558).
654
655 The following reagents were used to construct standard curves for ELISA in this study: Purified
656 Mouse IgE, kappa, Isotype Control (BD Pharmingen, 557079), Purified Mouse IgA, kappa,
657 Isotype Control (BD Pharmingen, 553476), Purified Mouse IgG3, kappa, Isotype Control (BD
658 Pharmingen, 553486), Purified Mouse IgG1, kappa, Isotype Control (SouthernBiotech, 0100-
659 01), Purified Mouse IgG2a, kappa, Isotype Control (Sigma, M5409), IgM Isotype Control from
660 murine myeloma (Sigma, M5909), IgG2b Isotype Control from murine myeloma (Sigma,
661 M5534), Mouse IgG2c (RRID: AB_2794064, SouthernBiotech, 0122-01), Recombinant Mouse
662 Pentraxin 2 (R & D Systems, 2558-SA-050).
663
664 **Enzyme-linked immunosorbent assay (ELISA)**
665 ELISA experiments were conducted as previously described[67]. Briefly, mouse peripheral blood
666 was collected via cardiac puncture immediately after euthanasia into BD SST microcontainer
667 tubes (02-675-185) and sera were harvested after centrifugation. F-bottom 96-well plates were
668 coated with capturing antibodies in 50 μL 0.1 M $NaHCO_3$ solution at pH 9.5 O/N at 4°C. The
669 plates were then emptied, blocked with 200 μL 1% bovine serum albumin (VWR, 97061-422) in
670 PBS, and washed 3 times with PBS containing 0.05% Tween-20 (Sigma-Aldrich, P1379). 50 μL
671 of sera at appropriate dilutions was added and incubated O/N at 4°C. The plate was then
672 incubated in sequential orders with 50 μL of biotinylated detection antibodies for 2-3 hours, 50
673 μL of avidin-HRP (ThermoFisher, 18-4100-51) for 30 minutes, and 100 μL of TMB solution
674 (ThermoFisher, 00-4201-56) at room temperature, with 3-4 washes with PBS-Tween in between
675 each incubation steps. The colorimetric reaction was stopped with 100 μL of 1M H_3PO_4 (Sigma-
676 Aldrich, P5811) after 5-10 minutes of adding TMB and absorbance at 450 nm was measured
677 with a Synergy HTX plate reader (BioTek). Concentrations of antigens were determined using
678 standard curves constructed with purified recombinant proteins and calculated with Gen5 3.02.2
679 (BioTek).
680
681 **Isolation of cells from lymphoid organs, livers, lungs, and colonic lamina propria**

682 For flow cytometric analyses, animals were perfused with a total of 20 mL PBS into both left and
683 right ventricles immediately after euthanasia. Cells were retrieved from spleens, peripheral
684 (brachial, axillary and inguinal) lymph nodes, mesenteric lymph nodes, thymuses, and livers by
685 meshing the organs through a 100 μm strainer (Corning, 07-201-432) with a syringe plunger.
686 Cells in the colonic lamina propria were isolated as previously described[68]. Briefly, colons were
687 cleaned by flushing the luminal content out with PBS using a syringe, defatted, opened up
688 longitudinally and diced into 1-2 cm pieces. Tissues were then incubated in 25 mL IEL solution
689 [1x PBS w/ 2% FBS (ThermoFisher, 35010CV), 10 mM HEPES buffer (ThermoFisher, MT 25–
690 060-CI), 1% penicillin/streptomycin (ThermoFisher, MT 30–002-CI), 1% L-glutamine
691 (ThermoFisher, MT 25–005-CI), plus 1 mM EDTA (Sigma-Aldrich, E4884) and 1 mM DTT
692 (Sigma-Aldrich, D9779) added immediately before use] for 15 minutes at 37°C with vigorous
693 shaking (250 rpm) to remove the epithelial fraction. Tissues were then retrieved, washed
694 extensively, and digested in 25 mL LPL solution [1x RPMI 1640 w/2% FBS, 10 mM HEPES
695 buffer, 1% penicillin/streptomycin, 1% L-glutamine, 0.2 U/mL collagenase A (Sigma,
696 11088793001) and 1 U/mL DNase I (Sigma-Aldrich, 10104159001)] for 30 minutes at 37°C with
697 vigorous shaking (250 rpm). ¼inch ceramic beads (MP Biomedicals, 116540034) were added
698 during this step (3–4 per sample) to facilitate tissue dissociation. The digested samples were
699 passed through a 100 μm strainer, pelleted at 450 g for 5 minutes and washed extensively.
700 Lungs were digested in the same fashion as the lamina propria fraction of the colons but for 45
701 minutes. Cells from non-lymphoid organs were centrifugated in 40% PBS-adjusted Percoll (v/v,
702 ThermoFisher, 45–001-747) in PBS to enrich for lymphocytes. Erythrocytes in the spleen, lung,
703 and liver samples were lysed with ACK lysis buffer [150 mM NH_4Cl (Sigma-Aldrich, A9434), 10
704 mM $KHCO_3$ (Sigma-Aldrich, P7682), 0.1 mM Na_2EDTA, pH 7.4].
705
706 For fluorescence-activated cell sorting, cell suspension was made from pooled secondary
707 lymphoid organs (spleen; peripheral and mesenteric lymph nodes) as above and CD4 T cells
708 were enriched with the Dynabeads Flowcomp Mouse CD4 Kit (ThermoFisher, 11461D)
709 according to manufacturer's instructions, stained with antibodies, washed extensively,
710 resuspended in isolation buffer (PBS w/ 2% FBS, 10 mM HEPES buffer, 1% L-glutamine, and 2
711 mM EDTA) containing 0.01% SYTOX Blue dead cell stain (ThermoFisher, S34857) to facilitate
712 dead cell exclusion, and sorted on a FACSAria (BD) instrument. Treg cells ($TCR\beta^+CD4^+CD8^-$
713 $NK1.1^-Foxp3^+Thy1.1^-$), Treg "wannabes" ($TCR\beta^+CD4^+CD8^-NK1.1^-Thy1.1^+Foxp3^-$) and naïve
714 conventional CD4 T cells ($TCR\beta^+CD4^+CD8^-NK1.1^-Foxp3^-Thy1.1^-CD44^{lo}CD62L^{hi}$) were sorted by
715 gating on the respective populations.

716

717 **Histology and TUNEL assay**

718 Sample embedding, sectioning, haematoxylin and eosin staining, pathology grading, and
719 TUNEL (terminal deoxynucleotidyl transferase dUTP nick end labeling) assay were conducted
720 at HistoWiz (Brooklyn, NY). Tissues were fixed in 10% neutral buffered formalin and embedded
721 in paraffin before sectioned into 5-micron slices. Lymphocytic and acute (neutrophils) or chronic
722 (monocytes) myeloid inflammation was blindly scored with the following criteria: 0-normal, 1-
723 mild increase, 2-moderate increase, 3-medium increase, 4-sever increase.

724

725 For TUNEL assay, liver sample sections were processed under standardized conditions using
726 the DeadEnd Fluorometric Detection System (Promega, G3250), and subsequent
727 immunohistochemistry was carried out using BOND Polymer Refine Detection Kit (Leica,
728 DS9800) according to manufacturers' instructions. $TUNEL^+$ cells were quantified with ImageJ
729 v2.0.0-rc-69/1.52p.

730

731 **Measurement of serum albumin**

732 Serum albumin level was measured by Laboratory of Comparative Pathology, SKI, using the
733 Albumin kit (Beckman Coulter, OSR6102), according to manufacturer's instruction.

734

735 **Flow cytometric analysis of cytokine production**

736 To measure cytokine production after *ex vivo* restimulation, single cell suspensions were
737 incubated at 37°C for 3-4 hours with 5% CO_2 in 96-well flat-bottom plates in the presence of 50
738 ng/mL phorbol-12-myristate-13-acetate (PMA, Sigma-Aldrich, P8139) and 500 ng/mL ionomycin
739 (Sigma-Aldrich, I0634) with 1 μg/mL brefeldin A (Sigma-Aldrich, B6542) and 2 μM monensin
740 (Sigma-Aldrich, M5273) to inhibit ER and Golgi transport. Cells were then stained with Ghost
741 Dye Violet 510 (Tonbo, 13-0870), Ghost Dye Red 780 (Tonbo, 13-0865), or Zombie NIR
742 Flexible Viability Kit (Biolegend, 423106) in PBS for 10 minutes at 4°C to help identify dead cells
743 and then with purified anti-Mouse CD16/CD32 (2.4G2, Tonbo, 70-0161) in staining buffer [0.5%
744 (w/v) BSA, 2 mM EDTA, 10 mM HEPES, 0.02% NaN_3 (Sigma-Aldrich, S2002) in 1x PBS] for 10
745 minutes at 4°C to block the Fc receptors. Samples were then incubated with fluorescently-
746 conjugated antibodies against cell surface antigens in staining buffer for 25 minutes at 4°C and
747 then washed extensively. For accessing intracellular antigens, cells were fixed and
748 permeabilized with the BD Cytofix/Cytoperm Kit for measuring cytokine production, or with the
749 ThermoFisher Transcription Factor Fix/Perm Kit for staining cytosolic and nuclear antigens,

750 according to manufacturers' instructions. Samples were recorded on an LSR II cytometer (BD)
751 or an Aurora cytometer (Cytek) and analyzed with FlowJo v10.6.1 (BD).
752
753 ***In vitro* suppression assay**
754 A 2-fold titration series of FACS-sorted Treg cells starting from 40,000 cells/well was set up in
755 U-bottom 96-well plates. 40,000 FACS-sorted, CellTrace Violet (ThermoFisher, C34571)-
756 labeled naïve CD4 T cells and 100,000 erythrocyte-lysed splenocytes from *Tcrb*$^{-/-}$*Tcrd*$^{-/-}$ mice as
757 antigen-presenting cells were then added to each well. α-mouse CD3 (145-2C11, BioXCell,
758 BE0001-1) was then added to a final concentration of 1 μg/mL. Cells were incubated in a final
759 volume of 200 μL complete RPMI w/ 10% FBS and with 5% CO_2 at 37°C for 72 hours before
760 analysis. Cells that have had more than 4 rounds of CTV dilution were considered divided for
761 calculating Treg-mediated suppression using the following formula:

762 $$\%Suppression\ (Sample\ X) = \frac{\%divided\ (no\ Treg) - \%divided\ (Sample\ X)}{\%divided\ (no\ Treg)}$$

763
764 **Statistics**
765 Statistical significance was determined using tests indicated in the respective figure legends. P-
766 values for *t*-test were calculated with GraphPad Prism 7 and had been corrected for multiple
767 hypothesis testing using the Holm-Sidak method. P-values for ANOVA were computed with R
768 for Fig. 2b and GraphPad Prism 7 elsewhere and had been corrected for multiple hypothesis
769 testing using the Tukey method (when using R and Prism), the Dunnett's method or the Sidak
770 method (when using Prism, according to its recommendations). P-values for Kolmogorov-
771 Smirnov test were calculated with R. Throughout the entire study, error bars represent mean ±
772 s.e.m., and the following notation was used to report statistical significance: ns, non-significant;
773 *, $p < 0.05$; **, $p < 0.01$; ***, $p < 0.001$; ****, $p < 0.0001$.
774
775 **Bulk RNA sequencing and data analysis**
776 Doubly sorted cells were directly placed into TRIzol reagent (ThermoFisher, 15596-018) for
777 subsequent RNA extraction. RNA was precipitated with isopropanol and linear acrylamide,
778 washed with 75% ethanol, and resuspended in RNase-free water. After RiboGreen
779 quantification and quality control by Agilent BioAnalyzer, 2ng of total RNA underwent
780 amplification using the SMART-Seq v4 Ultra Low Input RNA Kit (Clonetech, 63488), with 12
781 cycles of amplification. 3.8 – 4 ng of amplified cDNA was then used to prepare libraries with the
782 KAPA Hyper Prep Kit (Kapa Biosystems, KK8504) using 8 cycles of PCR. Barcoded samples

783 were run on a HiSeq 4000 instrument in a 50bp/50bp paired-end run, using the HiSeq
784 3000/4000 SBS Kit (Illumina). An average of 41 million paired reads were generated per sample
785 with % mRNA bases per sample ranging from 67% to 77%. In experiments shown in Fig. 3,
786 Treg cells (TCRβ^+CD4$^+$Foxp3$^+$) from *Foxp3*$^{DTR\text{-}GFP/y}$ and *Foxp3*$^{LSL/y}$*Cd4*$^{creERT2/+}$ mice and Treg
787 "wannabe" (TCRβ^+CD4$^+$Foxp3$^-$Thy1.1$^+$) cells from *Foxp3*$^{LSL/y}$*Cd4*$^{+/+}$ mice were analyzed (2-3
788 biological replicates). In experiments shown in Extended Data Fig. 6, Treg "wannabe" cells from
789 3 *Foxp3*$^{LSL/+}$ mice and 2 *Foxp3*$^{LSL/DTR\text{-}GFP}$ mice were analyzed. RNA-seq reads from fastq files
790 were aligned to the reference mouse genome GRCm38 using the STAR aligner[69], and local
791 realignment was performed using the Genome Analysis Toolkit[70]. For each sample, raw count of
792 reads per gene was measured using R, and the DESeq2 R package[71] was used to perform
793 differential gene expression analysis across different conditions. A cutoff of 0.05 was set on the
794 obtained FDR-adjusted p-values to get the significant genes of each comparison. All detectable
795 genes were rlog-normalized and then used for the principal component analysis.
796
797 **Single cell RNA sequencing and data analysis**
798 *Library Preparation and sequencing*
799 Library preparation and sequencing for the scRNA-Seq of doubly-FACS-sorted Treg cells isolated
800 from the secondary lymphoid organs of 7 months post-4-OHT treatment *Foxp3*$^{DTR\text{-}GFP}$ (cells
801 pooled from 5 mice) and *Foxp3*^{LSL}*Cd4*$^{creERT2/+}$ mice (cells pooled from 4 mice) were performed by
802 the Single Cell Research Initiative, SKI, using 10X genomics Chromium Single Cell 3' Library &
803 Gel bead Kit V3 according to manufacturer's protocol. Cells, with a mean viability of 75%, were
804 encapsulated in microfluidic droplets at a dilution of ~60 cells/μL with the multiplet fraction being
805 3.5%. After the RT step, the barcoded-cDNA was purified with DynaBeads, followed by 12-cycles
806 of PCR-amplification (98°C for 180 s; [98°C for 15 s, 67°C for 20 s, 72°C for 60 s] x 12-cycles;
807 72°C for 60 s). Next, 50 ng of PCR-amplified barcoded cDNA was fragmented with the reagents
808 provided in the kit and purified with SPRI beads to obtain an average fragment size of 600 bp.
809 The fragmented DNA was ligated to sequencing adapters which was then indexed with PCR
810 (98°C for 45 s; [98°C for 20 s, 54°C for 30 s, 72°C for 20 s] x 10 cycles; 72°C for 60 s). The
811 resulting DNA library was double-size purified (0.6-0.8X) with SPRI beads and sequenced on an
812 Illumina NovaSeq 6000 System (R1 – 26 cycles, i7 – 8 cycles, R2 – 96 cycles) at a depth of 210
813 million reads per sample (average reads per single cell being 31,000 and average reads per
814 transcript 3.96 – 4.10), with a median sequencing saturation of 74%.
815
816 *Data Pre-processing*

817 Fastq files were processed using Cell Ranger (10x Genomics) and reads were aligned to the
818 mouse genome mm10 from ENSEMBL GRCm38 that was modified to include sequences
819 corresponding to the coding region and the 3'UTR of the *R26*^{Tom} allele. Cells containing over 5%
820 mitochondria-derived transcripts were filtered out, resulting in 3,634 *Foxp3*$^{DTR\text{-}GFP}$ cells and
821 3,390 *Foxp3*^{LSL} cells that passed QC metrics, with a median of 3,580 molecules/cell. Cells with
822 total molecule counts below 1000, as determined by the lower mode of the distribution of total
823 molecules per cell, were additionally filtered out to remove putative empty droplets. Genes that
824 were expressed in more than 10 cells were retained for further analysis. The resulting count
825 matrices from both samples were then combined, resulting in a final set of 7,024 cells x 12,432
826 genes, and normalized to median library size, where library size is defined as total molecule
827 counts per cell. The normalized data are then log transformed as log (counts + 1) for
828 downstream analysis.
829
830 *Principal component analysis*
831 For dimensionality reduction and visualization of data, we further excluded genes with very low
832 or very high expression of transcripts (log average expression <0.02 or >3 and dispersion
833 >0.15), and principle component analysis was then performed on the log-transformed
834 normalized data. Using 40 principal components, where the number of principal components
835 was determined by the knee-point in eigenvalues, yielded a good representation of the
836 variability in the data.
837
838 *MAGIC imputation*
839 To account for missing values in scRNA-seq due to a high dropout rate, we employed MAGIC, a
840 method of "de-noising" and imputing missing expression values through data diffusion between
841 cells with similar covariate gene relationships[72]. We constructed the diffusion map matrix using
842 k = 30, ka = 10, and t = 6 as input parameters, where t specifies the number of times the affinity
843 matrix is powered for diffusion.
844
845 *Diffusion components and pseudotime calculation*
846 Instead of constructing a tSNE map using 40 PCs, we followed the strategy outlined by Setty
847 et al.[36] in order to characterize potential pseudotime non-linear trajectories and to visualize
848 single-cell gene expression in a UMAP embedding of diffusion components. Based on the eigen
849 gap, we chose to use 15 diffusion components for downstream analysis in Palantir and for
850 calculating diffusion distances. We scaled each included diffusion component by the factor λ/(1-

851 λ) where λ is the associated eigenvalue, to reflect 'multi-scale' diffusion distances. Then, we
852 calculate each cell position in pseudotime based on modeling cell fate in a continuous
853 probabilistic model.
854
855 *Clustering and gene ranking*
856 Clustering of cells was performed using PhenoGraph[73] setting k = 15 nearest neighbors. A
857 cluster was removed because of its disparity with the rest of the data (t-SNE projected this
858 cluster as a separate component that comprised cells from both populations), and those cells
859 also had a relatively lower number of total molecules compared with other populations.
860 Significant differentially expressed genes in each cluster were identified using *t*-test (where the
861 variance of small groups is overestimated), which was implemented in Single-Cell Analysis in
862 Python[74] with default parameters.
863
864 *tdTomato expression and gene set module score calculation*
865 Because of a high dropout rate of single cell sequencing, we performed MAGIC imputation of
866 tdTomato expression (as described above) only for *Foxp3*$^{DTR\text{-}GFP}$ cells since the overwhelming
867 majority of the *Foxp3*^{LSL} cells were tdTomato^{+} which could potentially cause over-imputation. A
868 cutoff of 1.04 was set for the imputed tdTomato expression where any cells with higher
869 expression were categorized as tdTomato^{+}(~15% of cells) and those with lower expression as
870 tdTomato^{-} (~85% of cells) in agreement with flow cytometric measurements. Gene set module
871 scores for Il2-Stat5 (GSEA HALLMARK_IL2_STAT5_SIGNALING) and Wnt/β-catenin (GSEA
872 HALLMARK_WNT_BETA_CATENIN_SIGNALING) were calculated with the AddModuleScore
873 function in Seurat v 3.1.5[75] using the default parameters.
874
875

876 **References**

877 1 Kanangat, S. *et al.* Disease in the scurfy (sf) mouse is associated with overexpression of
878 cytokine genes. *Eur J Immunol* **26**, 161-165, doi:10.1002/eji.1830260125 (1996).
879 2 Chatila, T. A. Role of regulatory T cells in human diseases. *J Allergy Clin Immunol* **116**, 949-
880 959; quiz 960, doi:10.1016/j.jaci.2005.08.047 (2005).
881 3 Godfrey, V. L., Wilkinson, J. E. & Russell, L. B. X-linked lymphoreticular disease in the scurfy
882 (sf) mutant mouse. *Am J Pathol* **138**, 1379-1387 (1991).
883 4 Khattri, R., Cox, T., Yasayko, S. A. & Ramsdell, F. An essential role for Scurfin in CD4+CD25+ T
884 regulatory cells. *Nat Immunol* **4**, 337-342, doi:10.1038/ni909 (2003).
885 5 Fontenot, J. D., Gavin, M. A. & Rudensky, A. Y. Foxp3 programs the development and function
886 of CD4+CD25+ regulatory T cells. *Nat Immunol* **4**, 330-336, doi:10.1038/ni904 (2003).
887 6 Fontenot, J. D. *et al.* Regulatory T cell lineage specification by the forkhead transcription
888 factor foxp3. *Immunity* **22**, 329-341, doi:10.1016/j.immuni.2005.01.016 (2005).
889 7 Hori, S., Nomura, T. & Sakaguchi, S. Control of regulatory T cell development by the
890 transcription factor Foxp3. *Science* **299**, 1057-1061, doi:10.1126/science.1079490 (2003).
891 8 Gavin, M. A. *et al.* Foxp3-dependent programme of regulatory T-cell differentiation. *Nature*
892 **445**, 771-775, doi:10.1038/nature05543 (2007).
893 9 Lin, W. *et al.* Regulatory T cell development in the absence of functional Foxp3. *Nat Immunol*
894 **8**, 359-368, doi:10.1038/ni1445 (2007).
895 10 Ohkura, N. *et al.* T cell receptor stimulation-induced epigenetic changes and Foxp3
896 expression are independent and complementary events required for Treg cell development.
897 *Immunity* **37**, 785-799, doi:10.1016/j.immuni.2012.09.010 (2012).
898 11 Brunkow, M. E. *et al.* Disruption of a new forkhead/winged-helix protein, scurfin, results in
899 the fatal lymphoproliferative disorder of the scurfy mouse. *Nat Genet* **27**, 68-73,
900 doi:10.1038/83784 (2001).
901 12 Ramsdell, F. & Ziegler, S. F. FOXP3 and scurfy: how it all began. *Nat Rev Immunol* **14**, 343-
902 349, doi:10.1038/nri3650 (2014).
903 13 Kim, J. M., Rasmussen, J. P. & Rudensky, A. Y. Regulatory T cells prevent catastrophic
904 autoimmunity throughout the lifespan of mice. *Nat Immunol* **8**, 191-197,
905 doi:10.1038/ni1428 (2007).
906 14 Gangaplara, A. *et al.* Type I interferon signaling attenuates regulatory T cell function in viral
907 infection and in the tumor microenvironment. *PLoS Pathog* **14**, e1006985,
908 doi:10.1371/journal.ppat.1006985 (2018).
909 15 Izcue, A. *et al.* Interleukin-23 restrains regulatory T cell activity to drive T cell-dependent
910 colitis. *Immunity* **28**, 559-570, doi:10.1016/j.immuni.2008.02.019 (2008).
911 16 Nish, S. A. *et al.* T cell-intrinsic role of IL-6 signaling in primary and memory responses. *Elife*
912 **3**, e01949, doi:10.7554/eLife.01949 (2014).
913 17 Overacre-Delgoffe, A. E. *et al.* Interferon-gamma Drives Treg Fragility to Promote Anti-
914 tumor Immunity. *Cell* **169**, 1130-1141 e1111, doi:10.1016/j.cell.2017.05.005 (2017).
915 18 Pasare, C. & Medzhitov, R. Toll pathway-dependent blockade of CD4+CD25+ T cell-mediated
916 suppression by dendritic cells. *Science* **299**, 1033-1036, doi:10.1126/science.1078231
917 (2003).
918 19 Pelly, V. S. *et al.* Interleukin 4 promotes the development of ex-Foxp3 Th2 cells during
919 immunity to intestinal helminths. *J Exp Med* **214**, 1809-1826, doi:10.1084/jem.20161104
920 (2017).
921 20 Srivastava, S., Koch, M. A., Pepper, M. & Campbell, D. J. Type I interferons directly inhibit
922 regulatory T cells to allow optimal antiviral T cell responses during acute LCMV infection. *J*
923 *Exp Med* **211**, 961-974, doi:10.1084/jem.20131556 (2014).

21 Korn, T. *et al.* Myelin-specific regulatory T cells accumulate in the CNS but fail to control autoimmune inflammation. *Nat Med* **13**, 423-431, doi:10.1038/nm1564 (2007).
22 Clough, L. E. *et al.* Release from regulatory T cell-mediated suppression during the onset of tissue-specific autoimmunity is associated with elevated IL-21. *J Immunol* **180**, 5393-5401, doi:10.4049/jimmunol.180.8.5393 (2008).
23 Gao, Y. *et al.* Inflammation negatively regulates FOXP3 and regulatory T-cell function via DBC1. *Proc Natl Acad Sci U S A* **112**, E3246-3254, doi:10.1073/pnas.1421463112 (2015).
24 Komatsu, N. *et al.* Pathogenic conversion of Foxp3+ T cells into TH17 cells in autoimmune arthritis. *Nat Med* **20**, 62-68, doi:10.1038/nm.3432 (2014).
25 Bailey-Bucktrout, S. L. *et al.* Self-antigen-driven activation induces instability of regulatory T cells during an inflammatory autoimmune response. *Immunity* **39**, 949-962, doi:10.1016/j.immuni.2013.10.016 (2013).
26 Tian, L. *et al.* Foxp3(+) regulatory T cells exert asymmetric control over murine helper responses by inducing Th2 cell apoptosis. *Blood* **118**, 1845-1853, doi:10.1182/blood-2011-04-346056 (2011).
27 Arvey, A. *et al.* Inflammation-induced repression of chromatin bound by the transcription factor Foxp3 in regulatory T cells. *Nat Immunol* **15**, 580-587, doi:10.1038/ni.2868 (2014).
28 Chinen, T. *et al.* An essential role for the IL-2 receptor in Treg cell function. *Nat Immunol* **17**, 1322-1333, doi:10.1038/ni.3540 (2016).
29 Vignali, D. A., Collison, L. W. & Workman, C. J. How regulatory T cells work. *Nat Rev Immunol* **8**, 523-532, doi:10.1038/nri2343 (2008).
30 Shevach, E. M. Mechanisms of foxp3+ T regulatory cell-mediated suppression. *Immunity* **30**, 636-645, doi:10.1016/j.immuni.2009.04.010 (2009).
31 Owen, D. L. *et al.* Thymic regulatory T cells arise via two distinct developmental programs. *Nat Immunol* **20**, 195-205, doi:10.1038/s41590-018-0289-6 (2019).
32 Xu, M. *et al.* c-MAF-dependent regulatory T cells mediate immunological tolerance to a gut pathobiont. *Nature* **554**, 373-377, doi:10.1038/nature25500 (2018).
33 Ye, J. *et al.* The Aryl Hydrocarbon Receptor Preferentially Marks and Promotes Gut Regulatory T Cells. *Cell Rep* **21**, 2277-2290, doi:10.1016/j.celrep.2017.10.114 (2017).
34 Pritykin, Y. *et al.* A unified atlas of CD8 T cell dysfunctional states in cancer and infection. *bioRxiv* (2020).
35 Pierson, W. *et al.* Antiapoptotic Mcl-1 is critical for the survival and niche-filling capacity of Foxp3(+) regulatory T cells. *Nat Immunol* **14**, 959-965, doi:10.1038/ni.2649 (2013).
36 Setty, M. *et al.* Characterization of cell fate probabilities in single-cell data with Palantir. *Nat Biotechnol* **37**, 451-460, doi:10.1038/s41587-019-0068-4 (2019).
37 Miragaia, R. J. *et al.* Single-Cell Transcriptomics of Regulatory T Cells Reveals Trajectories of Tissue Adaptation. *Immunity* **50**, 493-504 e497, doi:10.1016/j.immuni.2019.01.001 (2019).
38 Fontenot, J. D., Rasmussen, J. P., Gavin, M. A. & Rudensky, A. Y. A function for interleukin 2 in Foxp3-expressing regulatory T cells. *Nat Immunol* **6**, 1142-1151, doi:10.1038/ni1263 (2005).
39 Xing, S. *et al.* Tcf1 and Lef1 are required for the immunosuppressive function of regulatory T cells. *J Exp Med* **216**, 847-866, doi:10.1084/jem.20182010 (2019).
40 Yang, B. H. *et al.* TCF1 and LEF1 Control Treg Competitive Survival and Tfr Development to Prevent Autoimmune Diseases. *Cell Rep* **27**, 3629-3645 e3626, doi:10.1016/j.celrep.2019.05.061 (2019).
41 Allenspach, E. & Torgerson, T. R. Autoimmunity and Primary Immunodeficiency Disorders. *J Clin Immunol* **36 Suppl 1**, 57-67, doi:10.1007/s10875-016-0294-1 (2016).
42 Georgiev, P., Charbonnier, L. M. & Chatila, T. A. Regulatory T Cells: the Many Faces of Foxp3. *J Clin Immunol* **39**, 623-640, doi:10.1007/s10875-019-00684-7 (2019).

973 43 Park, J. H. *et al.* Immune dysregulation, polyendocrinopathy, enteropathy, X-linked (IPEX)
974 syndrome: A systematic review. *Autoimmun Rev* **19**, 102526,
975 doi:10.1016/j.autrev.2020.102526 (2020).
976 44 Oldenhove, G. *et al.* Decrease of Foxp3+ Treg cell number and acquisition of effector cell
977 phenotype during lethal infection. *Immunity* **31**, 772-786,
978 doi:10.1016/j.immuni.2009.10.001 (2009).
979 45 Schenten, D. *et al.* Signaling through the adaptor molecule MyD88 in CD4+ T cells is required
980 to overcome suppression by regulatory T cells. *Immunity* **40**, 78-90,
981 doi:10.1016/j.immuni.2013.10.023 (2014).
982 46 Lund, J. M., Hsing, L., Pham, T. T. & Rudensky, A. Y. Coordination of early protective
983 immunity to viral infection by regulatory T cells. *Science* **320**, 1220-1224,
984 doi:10.1126/science.1155209 (2008).
985 47 Ruckwardt, T. J., Bonaparte, K. L., Nason, M. C. & Graham, B. S. Regulatory T cells promote
986 early influx of CD8+ T cells in the lungs of respiratory syncytial virus-infected mice and
987 diminish immunodominance disparities. *J Virol* **83**, 3019-3028, doi:10.1128/JVI.00036-09
988 (2009).
989 48 Hall, A. O. *et al.* The cytokines interleukin 27 and interferon-gamma promote distinct Treg
990 cell populations required to limit infection-induced pathology. *Immunity* **37**, 511-523,
991 doi:10.1016/j.immuni.2012.06.014 (2012).
992 49 Durant, L. R. *et al.* Regulatory T cells prevent Th2 immune responses and pulmonary
993 eosinophilia during respiratory syncytial virus infection in mice. *J Virol* **87**, 10946-10954,
994 doi:10.1128/JVI.01295-13 (2013).
995 50 Schmitz, I. *et al.* IL-21 restricts virus-driven Treg cell expansion in chronic LCMV infection.
996 *PLoS Pathog* **9**, e1003362, doi:10.1371/journal.ppat.1003362 (2013).
997 51 Zhao, J., Zhao, J. & Perlman, S. Virus-specific regulatory T cells ameliorate encephalitis by
998 repressing effector T cell functions from priming to effector stages. *PLoS Pathog* **10**,
999 e1004279, doi:10.1371/journal.ppat.1004279 (2014).
1000 52 Long, S. A. & Buckner, J. H. CD4+FOXP3+ T regulatory cells in human autoimmunity: more
1001 than a numbers game. *J Immunol* **187**, 2061-2066, doi:10.4049/jimmunol.1003224 (2011).
1002 53 Venken, K. *et al.* Natural naive CD4+CD25+CD127low regulatory T cell (Treg) development
1003 and function are disturbed in multiple sclerosis patients: recovery of memory Treg
1004 homeostasis during disease progression. *J Immunol* **180**, 6411-6420,
1005 doi:10.4049/jimmunol.180.9.6411 (2008).
1006 54 Ferraro, A. *et al.* Interindividual variation in human T regulatory cells. *Proc Natl Acad Sci U S*
1007 *A* **111**, E1111-1120, doi:10.1073/pnas.1401343111 (2014).
1008 55 Arvey, A. *et al.* Genetic and epigenetic variation in the lineage specification of regulatory T
1009 cells. *Elife* **4**, e07571, doi:10.7554/eLife.07571 (2015).
1010 56 Nasrallah, R. *et al.* A distal enhancer at risk locus 11q13.5 promotes suppression of colitis by
1011 Treg cells. *Nature* **583**, 447-452, doi:10.1038/s41586-020-2296-7 (2020).
1012 57 Mottet, C., Uhlig, H. H. & Powrie, F. Cutting edge: cure of colitis by CD4+CD25+ regulatory T
1013 cells. *J Immunol* **170**, 3939-3943, doi:10.4049/jimmunol.170.8.3939 (2003).
1014 58 Uhlig, H. H. *et al.* Characterization of Foxp3+CD4+CD25+ and IL-10-secreting CD4+CD25+ T
1015 cells during cure of colitis. *J Immunol* **177**, 5852-5860, doi:10.4049/jimmunol.177.9.5852
1016 (2006).
1017 59 Wan, Y. Y. & Flavell, R. A. Regulatory T-cell functions are subverted and converted owing to
1018 attenuated Foxp3 expression. *Nature* **445**, 766-770, doi:10.1038/nature05479 (2007).
1019 60 Josefowicz, S. Z., Lu, L. F. & Rudensky, A. Y. Regulatory T cells: mechanisms of differentiation
1020 and function. *Annu Rev Immunol* **30**, 531-564,
1021 doi:10.1146/annurev.immunol.25.022106.141623 (2012).

1022 61 Sakaguchi, S. *et al.* Regulatory T Cells and Human Disease. *Annu Rev Immunol* **38**, 541-566,
1023 doi:10.1146/annurev-immunol-042718-041717 (2020).
1024 62 Tahvildari, M. & Dana, R. Low-Dose IL-2 Therapy in Transplantation, Autoimmunity, and
1025 Inflammatory Diseases. *J Immunol* **203**, 2749-2755, doi:10.4049/jimmunol.1900733
1026 (2019).
1027 63 Vogtenhuber, C. *et al.* Constitutively active Stat5b in CD4+ T cells inhibits graft-versus-host
1028 disease lethality associated with increased regulatory T-cell potency and decreased T
1029 effector cell responses. *Blood* **116**, 466-474, doi:10.1182/blood-2009-11-252825 (2010).
1030 64 Sledzinska, A. *et al.* TGF-beta signalling is required for CD4(+) T cell homeostasis but
1031 dispensable for regulatory T cell function. *PLoS Biol* **11**, e1001674,
1032 doi:10.1371/journal.pbio.1001674 (2013).
1033 65 Mombaerts, P. *et al.* Mutations in T-cell antigen receptor genes alpha and beta block
1034 thymocyte development at different stages. *Nature* **360**, 225-231, doi:10.1038/360225a0
1035 (1992).
1036 66 Madisen, L. *et al.* A robust and high-throughput Cre reporting and characterization system
1037 for the whole mouse brain. *Nat Neurosci* **13**, 133-140, doi:10.1038/nn.2467 (2010).
1038 67 Feng, Y. *et al.* A mechanism for expansion of regulatory T-cell repertoire and its role in self-
1039 tolerance. *Nature* **528**, 132-136, doi:10.1038/nature16141 (2015).
1040 68 Campbell, C. *et al.* Extrathymically Generated Regulatory T Cells Establish a Niche for
1041 Intestinal Border-Dwelling Bacteria and Affect Physiologic Metabolite Balance. *Immunity*
1042 **48**, 1245-1257 e1249, doi:10.1016/j.immuni.2018.04.013 (2018).
1043 69 Dobin, A. *et al.* STAR: ultrafast universal RNA-seq aligner. *Bioinformatics* **29**, 15-21,
1044 doi:10.1093/bioinformatics/bts635 (2013).
1045 70 McKenna, A. *et al.* The Genome Analysis Toolkit: a MapReduce framework for analyzing
1046 next-generation DNA sequencing data. *Genome Res* **20**, 1297-1303,
1047 doi:10.1101/gr.107524.110 (2010).
1048 71 Love, M. I., Huber, W. & Anders, S. Moderated estimation of fold change and dispersion for
1049 RNA-seq data with DESeq2. *Genome Biol* **15**, 550, doi:10.1186/s13059-014-0550-8 (2014).
1050 72 van Dijk, D. *et al.* Recovering Gene Interactions from Single-Cell Data Using Data Diffusion.
1051 *Cell* **174**, 716-729 e727, doi:10.1016/j.cell.2018.05.061 (2018).
1052 73 Levine, J. H. *et al.* Data-Driven Phenotypic Dissection of AML Reveals Progenitor-like Cells
1053 that Correlate with Prognosis. *Cell* **162**, 184-197, doi:10.1016/j.cell.2015.05.047 (2015).
1054 74 Wolf, F. A., Angerer, P. & Theis, F. J. SCANPY: large-scale single-cell gene expression data
1055 analysis. *Genome Biol* **19**, 15, doi:10.1186/s13059-017-1382-0 (2018).
1056 75 Stuart, T. *et al.* Comprehensive Integration of Single-Cell Data. *Cell* **177**, 1888-1902 e1821,
1057 doi:10.1016/j.cell.2019.05.031 (2019).
1058

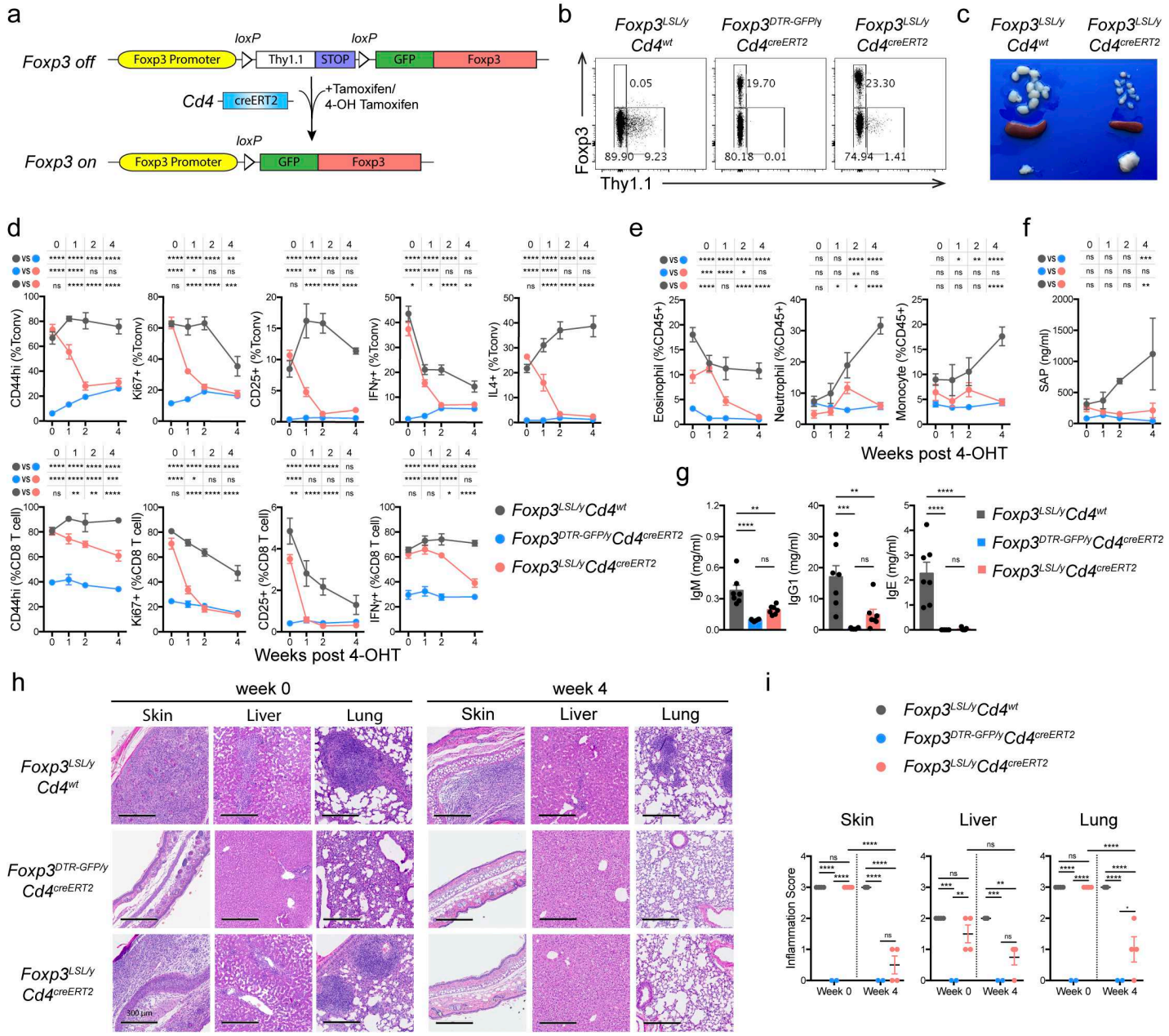

Figure 1 | Restoration of *Foxp3* expression in Treg "wannabes" cures fulminant autoimmunity in male *Foxp3*^{LSL} mice. Mice were treated with 4-hydroxytamoxifen (4-OHT) on postnatal day 14. **a**, Schematic of the *Foxp3*^{LSL} allele. **b**, Flow cytometric analysis of splenic CD4 T cells 1 wk post 4-OHT treatment. **c**, Lymph nodes (top), spleens (middle), and thymi (bottom) of mice of indicated genotypes 4 wks after 4-OHT treatment. **d-f**, Percentages of activated, proliferating, and cytokine-producing splenic T cells (**d**), frequencies of splenic myeloid cell populations (**e**), and serum amyloid P (SAP) levels (**f**) at indicated time points after 4-OHT treatment. **g**, Levels of antibodies in the serum 4 wks post-4-OHT treatment. **h,** Haematoxylin and eosin staining of indicated tissues before and 4 wks after 4-OHT treatment. **i**, Histology scores of indicated tissues before and 4 wks after 4-OHT treatment. For **d-g**, data are combined from three independent experiments with 3 to 12 mice per group per time point. Data are

1070 shown as mean ± s.e.m., two-way (**d-f, i**) or one-way (**g**) ANOVA with Tukey's multiple comparisons test.

1071 ns, non-significant; *, $p < 0.05$; **, $p < 0.01$; ***, $p<0.001$; ****, $p<0.0001$.

1072

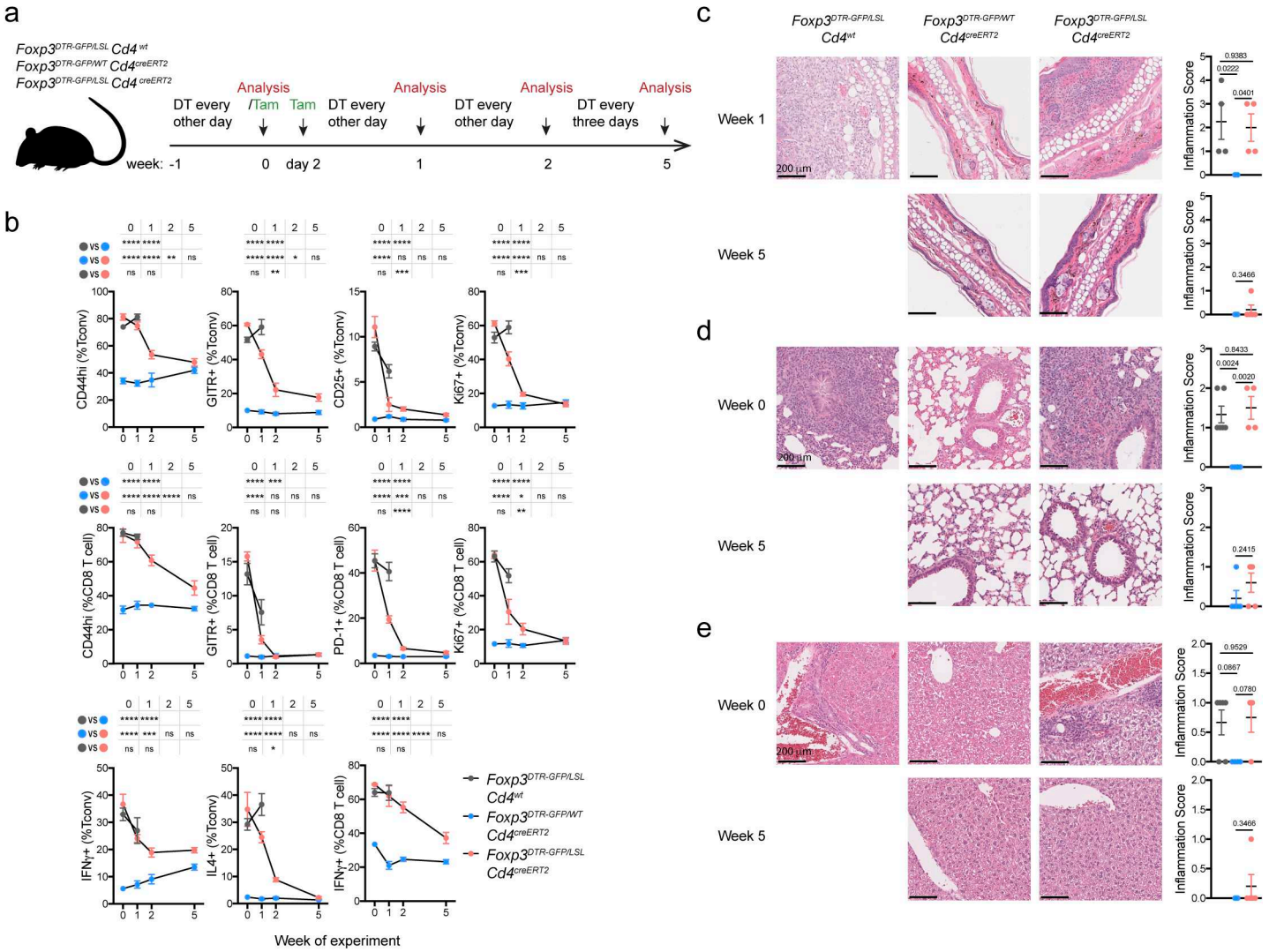

Figure 2 | Restoration of *Foxp3* expression in Treg "wannabe" cells in mosaic adult female *Foxp3*$^{LSL/DTR\text{-}GFP}$ mice suppresses immune activation caused by diphtheria toxin-mediated Treg cell ablation. a, Experimental scheme. 8-10-wk-old female mice were injected with diphtheria toxin (DT) intraperitoneally and given oral gavage of tamoxifen (Tam) on designated days. **b,** Frequencies of activated, proliferating, and cytokine producing splenic conventional CD4 and CD8 T cells at the indicated time points. Data are pooled from two independent experiments with 3 to 5 mice per group per time point. Line graphs show mean percentages ± s.e.m., two-way ANOVA with Tukey's multiple comparison test. ns, non-significant; *, $p < 0.05$; **, $p < 0.01$; ***, $p<0.001$; ****, $p<0.0001$. **c-e,** Haematoxylin and eosin staining of sections of skin (**c**), lung (**d**), and liver (**e**) from mice of indicated genotypes at denoted time points post tamoxifen treatment (left), and their respective inflammation scores (right). Scatter plots show mean score ± s.e.m., one-way ANOVA with Tukey's multiple comparison test.

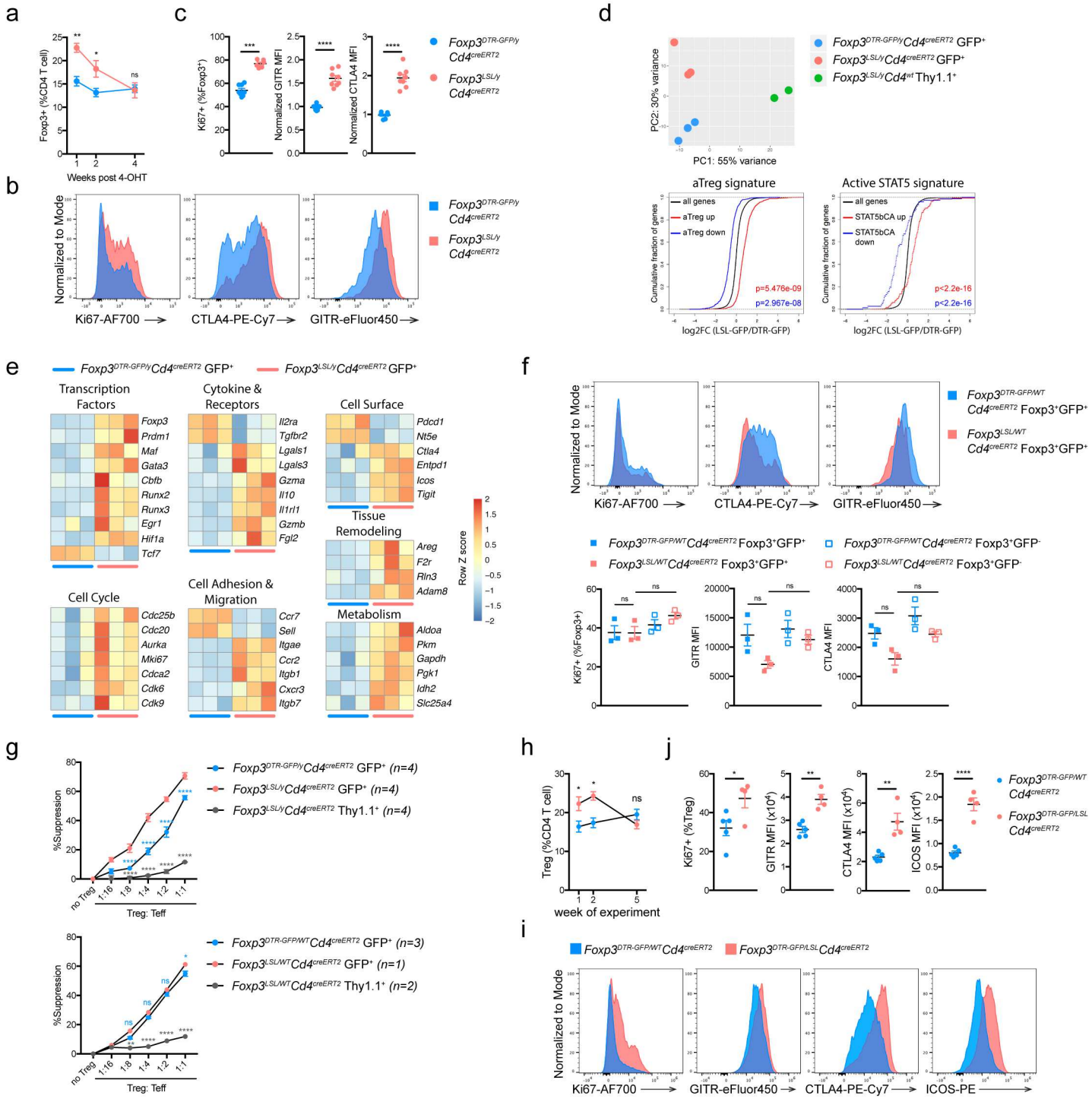

Figure 3 | Rescued Treg cells in inflamed mice are activated and potently suppressive in inflammatory settings. a-c, Male *Foxp3*$^{DTR\text{-}GFP}$*Cd4*^{creERT2} and *Foxp3*^{LSL}*Cd4*^{creERT2} mice were treated with 4-OHT on postnatal day 14. Data are pooled from three independent experiments. **a**, Percentages of splenic Treg cells at indicated time points following 4-OHT treatment. Line graph shows mean ± s.e.m. Multiple *t*-tests with Holm-Sidak multiple comparison. **b, c**, representative histograms (**b**) and combined data (**c**) showing expression of Ki67, CTLA4 and GITR by rescued and control Treg cells on day 7 post 4-OHT treatment from the spleen analyzed by flow cytometry. Scatter plots show mean ± s.e.m. Two-tailed

1094 unpaired *t*-tests. **d, e**, RNA-seq analysis of rescued Treg cells, control Treg cells, and Treg "wannabes"
1095 from male mice of indicated genotypes treated with 4-OHT on postnatal day 14 and analyzed 7 days
1096 afterwards. **d**, Principal component analysis of gene expression in the three indicated cell populations
1097 (top), and empirical cumulative distribution function plots showing gene signatures of activated Treg cells
1098 (bottom left) and Treg cells expressing a constitutively active form of STAT5b (bottom right). Two-sided
1099 Kolmogorov-Smirnov test. **e**, Heatmaps showing expression of curated genes in rescued and control Treg
1100 cells from mice of indicated genotypes. **f**, Expression of Ki67, CTLA4 and GITR by indicated Treg cell
1101 subsets from the spleen of mosaic heterozygous *Foxp3*$^{DTR\text{-}GFP/WT}$*Cd4*^{creERT2} and *Foxp3*$^{LSL/WT}$*Cd4*^{creERT2}
1102 female mice treated with 4-OHT on postnatal day 14 and analyzed after 7 days using flow cytometry. Data
1103 are shown as mean ± s.e.m., one-way ANOVA with Tukey's multiple comparison test. **g**, Suppression of *in*
1104 *vitro* proliferation of conventional CD4 T cells induced by α-CD3 antibody and antigen-presenting cells by
1105 control or rescued Treg cells (GFP^{+}), or Treg "wannabes" (Thy1.1^{+}) from indicated strains of mice on day 7
1106 post 4-OHT treatment. Two-way ANOVA with Tukey's multiple comparison test. Data are shown as mean
1107 %suppression ± s.e.m. Frequencies of Treg cells at the indicated time points. Line graph shows mean
1108 percentages ± s.e.m. Two-way ANOVA with Tukey's multiple comparison test. **h-j**, Adult mosaic
1109 heterozygous female *Foxp3*$^{DTR\text{-}GFP/WT}$*Cd4*^{creERT2} and *Foxp3*$^{DTR\text{-}GFP/LSL}$*Cd4*^{creERT2} mice were treated with DT
1110 and 4-OHT as in **Figure 2a**. **h**, Percentages of splenic Treg cells at indicated time points following 4-OHT
1111 treatment. Line graph shows mean ± s.e.m. Multiple *t*-tests with Holm-Sidak multiple comparison. **i, j,**
1112 Representative histograms (**i**) and combined data (**j**) showing expression of indicated markers by Treg
1113 cells at wk 1. Scatter plots show mean percentages or MFI ± s.e.m., two-tailed unpaired *t*-tests. ns, non-
1114 significant; *, $p < 0.05$; **, $p < 0.01$; ***, $p<0.001$; ****, $p<0.0001$.
1115

1116

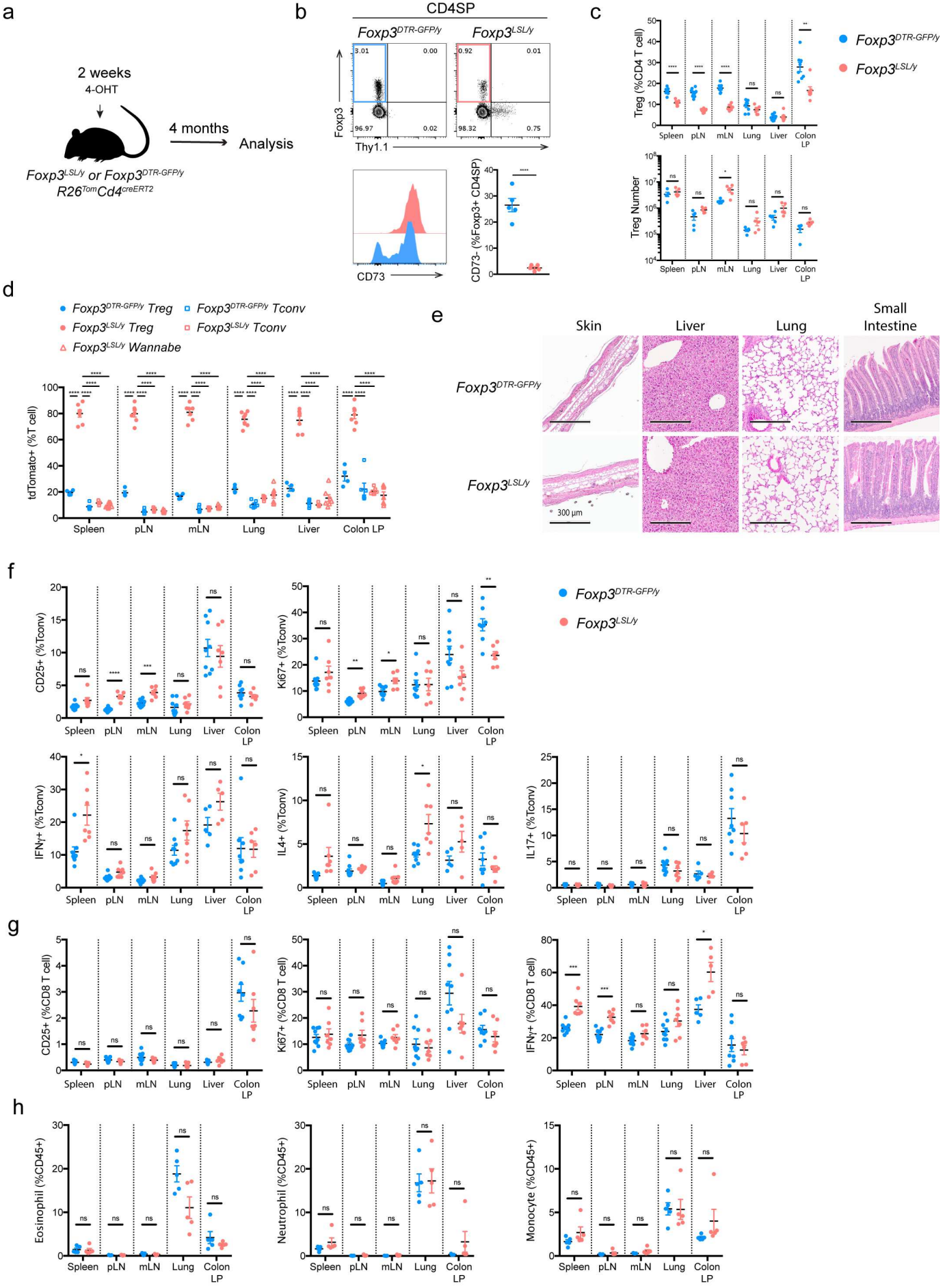
a
2 weeks
4-OHT
4 months
Analysis
Foxp3LSL/y or Foxp3DTR-GFP/y
R26TomCd4creERT2
b
CD4SP
Foxp3DTR-GFP/y
Foxp3LSL/y
Foxp3
Thy1.1
CD73
CD73- (%Foxp3+ CD4SP)
c
Treg (%CD4 T cell)
Treg Number
Spleen
pLN
mLN
Lung
Liver
Colon LP
d
Foxp3DTR-GFP/y Treg
Foxp3LSL/y Treg
Foxp3LSL/y Wannabe
Foxp3DTR-GFP/y Tconv
Foxp3LSL/y Tconv
tdTomato+ (%T cell)
e
Skin
Liver
Lung
Small Intestine
300 µm
f
CD25+ (%Tconv)
Ki67+ (%Tconv)
IFNγ+ (%Tconv)
IL4+ (%Tconv)
IL17+ (%Tconv)
g
CD25+ (%CD8 T cell)
Ki67+ (%CD8 T cell)
IFNγ+ (%CD8 T cell)
h
Eosinophil (%CD45+)
Neutrophil (%CD45+)
Monocyte (%CD45+)

1117 **Figure 4 | Rescued Treg cells in male *Foxp3*^{LSL} mice provide long-term protection from**
1118 **autoimmune inflammatory disease. a,** Experimental design. Mice were treated with a single dose of 4-
1119 OHT at 2 wks of age and analyzed 4 months later. **b,** Flow cytometric analysis of CD73 expression in
1120 Foxp3^{+} CD4 single-positive thymocytes as a discriminating marker of recirculating vs. recently generated
1121 thymic Treg cells. Two-tailed unpaired *t*-test. **c,** Flow cytometric analysis of Treg cell percentages (upper
1122 panel) and absolute numbers (lower panel) in tissues of mice of indicated genotypes. Two-tailed multiple *t*-
1123 tests with Holm-Sidak multiple comparison. **d,** Percentages of lineage-traced (tdTomato^{+}) Treg cells, Treg
1124 "wannabes", and conventional CD4 T cells. One-way ANOVA with Dunnett's multiple hypothesis tests. **e,**
1125 Analysis of histopathology in mice of indicated genotypes. Haematoxylin and eosin staining of sections of
1126 the indicated organs. **f-h,** Percentages of activated, proliferating, and cytokine-producing conventional
1127 CD4 T cells (**f**), CD8 T cells (**g**) and myeloid populations (**h**) from indicated organs. Data are pooled from
1128 two independent experiments. Two-tailed unpaired *t*-tests with Holm-Sidak multiple comparison. pLN,
1129 peripheral (brachial, axillary, and inguinal) lymph nodes; mLN, mesenteric lymph nodes; LP, lamina
1130 propria. Scatter plots show mean ± s.e.m. ns, non-significant; *, $p < 0.05$; **, $p < 0.01$; ***, $p<0.001$; ****,
1131 $p<0.0001$.
1132

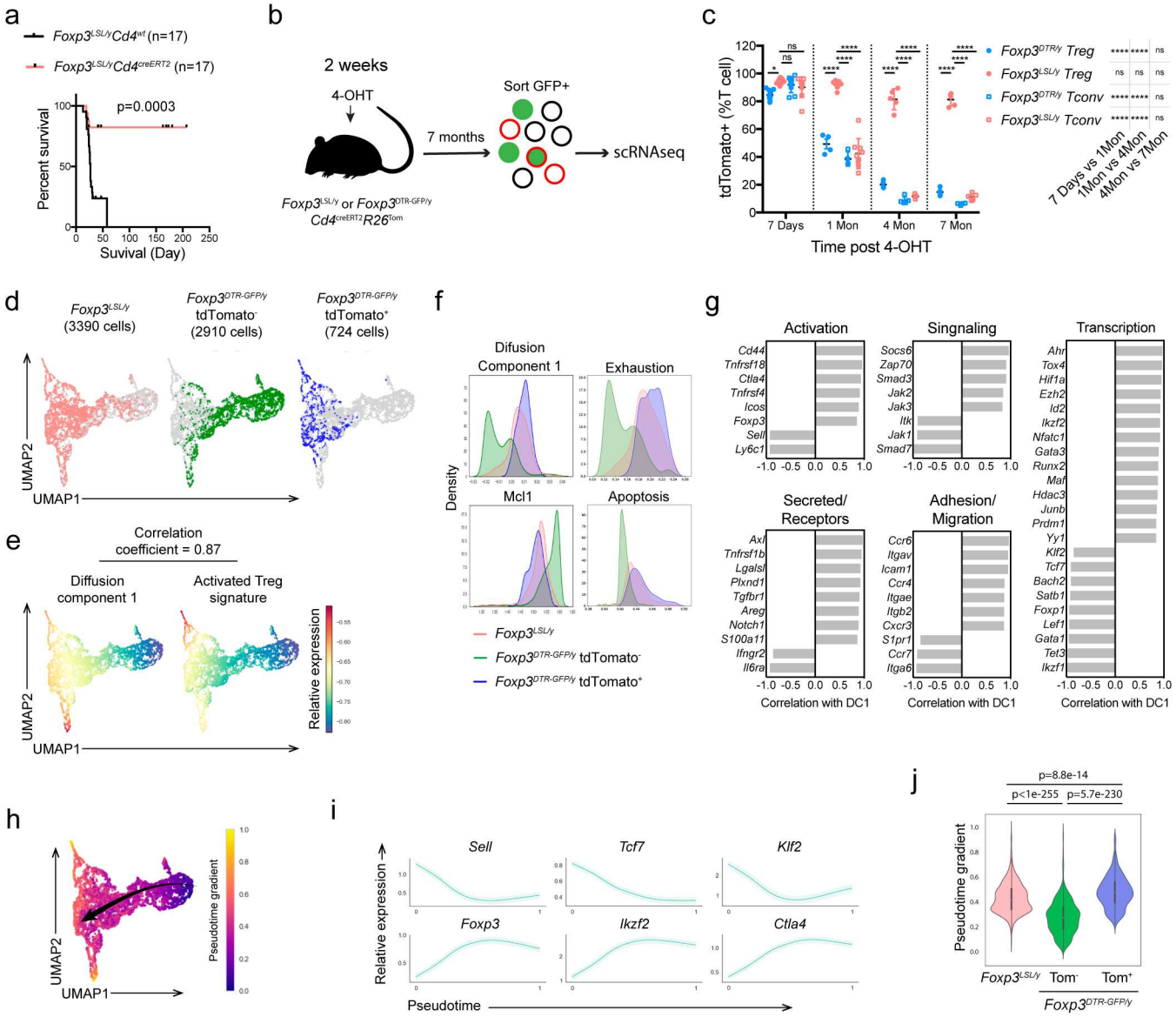

Figure 5 | Single-cell transcriptomic analysis of control and long-lived rescued Treg cells. a, Survival plot of 4-OHT-treated male *Foxp3*^{LSL}*Cd4*^{wt} and *Foxp3*^{LSL}*Cd4*^{creERT2} mice. Mantel-Cox test. **b,** Experimental design. Mice were treated with 4-OHT at 2 wks of age and Foxp3^{+} Treg cells, FACS-purified based on GFP expression, were subjected to scRNA-seq analysis using 10X Genomics platform 7 months later. **c,** Percentages of fate-mapped splenic Treg cells and conventional CD4 T cells in control and rescued mice at indicated time points post 4-OHT treatment. Scatter plot shows mean ± s.e.m. Two-way ANOVA with Tukey's multiple comparisons test. **d,** UMAP visualization of the single-cell transcriptomes of experimental *Foxp3*^{LSL} and control tdTomato^{-} or tdTomato^{+} *Foxp3*$^{DTR\text{-}GFP}$ Treg cells. **e,** UMAP visualization colored by diffusion component 1 (left) and the expression level of activated Treg cell gene signature (right). **f,** Histograms depicting the density of *Foxp3*^{LSL} and tdTomato^{+} or tdTomato^{-} *Foxp3*$^{DTR\text{-}GFP}$ Treg cells along diffusion component 1, *Mcl1* expression, and the average expression levels of indicated gene sets. **g,** Correlation of curated genes with diffusion component 1. **h**, UMAP visualization colored by pseudotime

1146 generated with Palantir. Arrow indicates the direction of differentiation across the map. **i**, Expression of
1147 representative genes along the pseudotime trajectory. **j,** Violin plots showing the medians of pseudotime
1148 values of *Foxp3*^{LSL} and tdTomato^{+} or tdTomato^{-} *Foxp3*$^{DTR\text{-}GFP}$ Treg cells. Thick vertical bars show the
1149 interquartile range.
1150

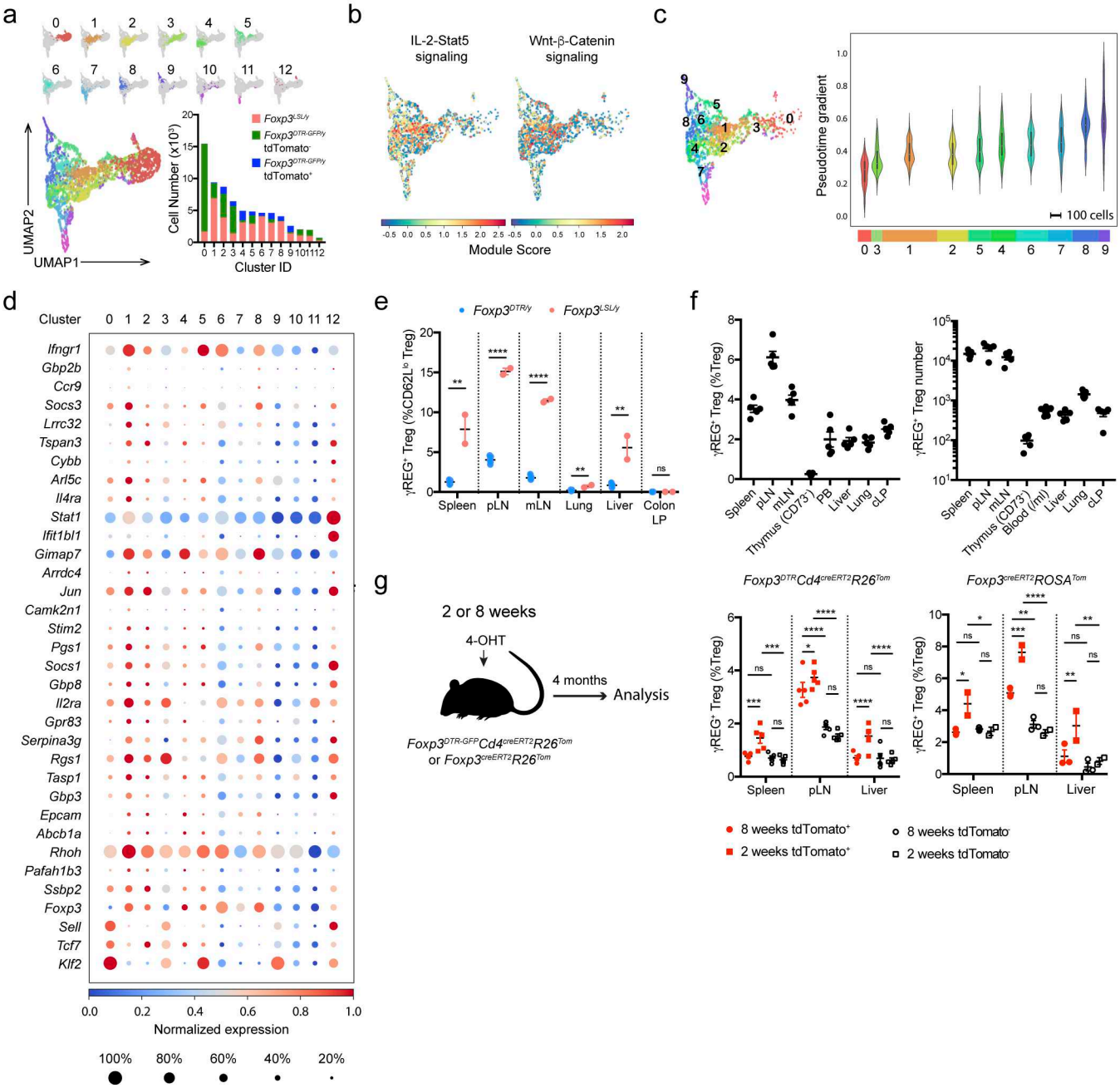

Figure 6 | Identification and analysis of γREG+ Treg cells from the single-cell RNA-seq data. a, UMAP visualization colored by the clusters. Bar graph shows the numbers of cells from each sample that contributed to the individual clusters. **b**, UMAP visualization of *Foxp3*^{LSL} Treg cells colored by the module scores for the indicated gene sets. **c**, Violin plots showing the medians of pseudotime values of *Foxp3*^{LSL} Treg cells from the top 10 clusters. Thick vertical bars show the interquartile range. Horizontal bars show the number of *Foxp3*^{LSL} Treg cells contributing to each cluster. **d**, Dot plot showing the expression of top enriched genes ($p<0.05$) and underrepresented genes from cluster 1 expressed by more than 20% of the cells in at least one cluster. **e**, Frequencies of γREG^{+} Treg cells among CD62L^{lo} Treg cells in rescued and control mice treated with 4-OHT on postnatal day 14 and analyzed 4 months later. Two-tailed unpaired *t*-

1162 tests with Holm-Sidak multiple comparison. **f**, Frequencies (left) and absolute numbers (right) of γREG^{+}
1163 Treg cells in various tissues of unmanipulated 8-wk-old *Foxp3*^{GFP} mice. **g**, Percentages of γREG^{+} Treg
1164 cells among tdTomato^{+} or tdTomato^{-} Treg cells "time-stamped" in adult (8-wk-old) or perinatal (2-wk-old)
1165 mice and analyzed after 4 months. Two-way ANOVA with Tukey's multiple comparison test.
1166

a

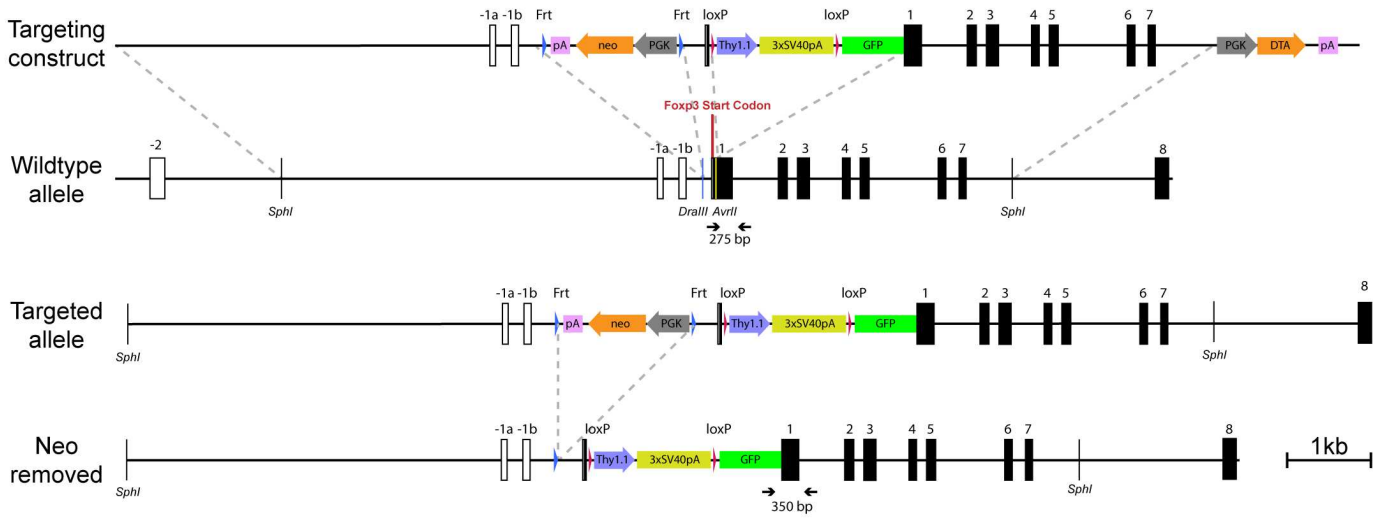
Targeting construct
Wildtype allele
Targeted allele
Neo removed
Foxp3 Start Codon
-1a -1b
Frt
loxP
pA
neo
PGK
Thy1.1
3xSV40pA
GFP
DTA
SphI
DraIII AvrII
275 bp
350 bp
1kb

b

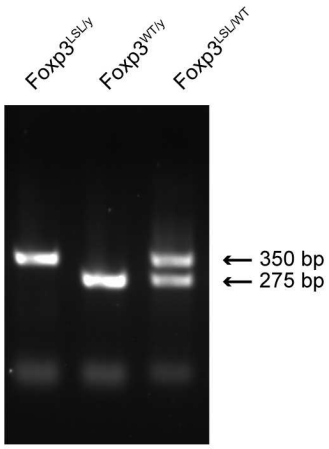
Foxp3LSL/y
Foxp3WT/y
Foxp3LSL/WT
350 bp
275 bp

c

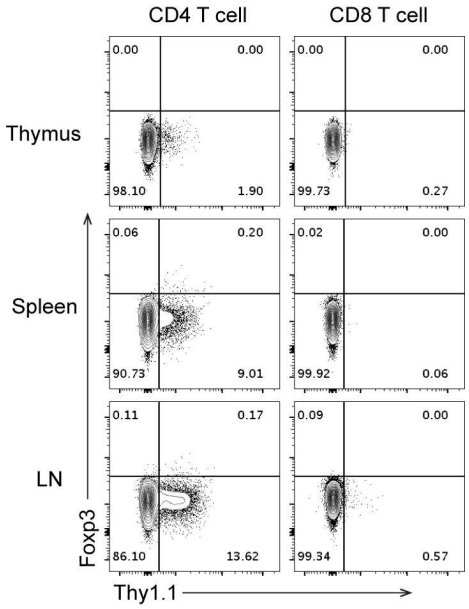
CD4 T cell
CD8 T cell
Thymus
Spleen
LN
Foxp3
Thy1.1
0.00
0.00
0.00
0.00
98.10
1.90
99.73
0.27
0.06
0.20
0.02
0.00
90.73
9.01
99.92
0.06
0.11
0.17
0.09
0.00
86.10
13.62
99.34
0.57

d

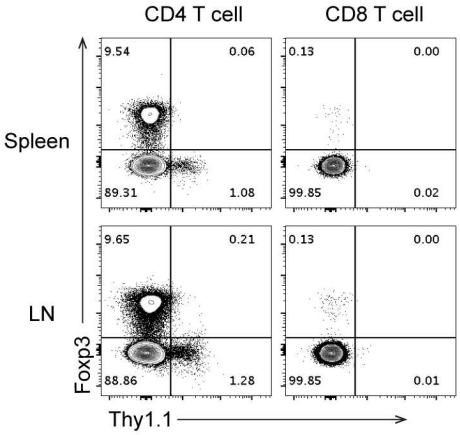
CD4 T cell
CD8 T cell
Spleen
LN
Foxp3
Thy1.1
9.54
0.06
0.13
0.00
89.31
1.08
99.85
0.02
9.65
0.21
0.13
0.00
88.86
1.28
99.85
0.01

e

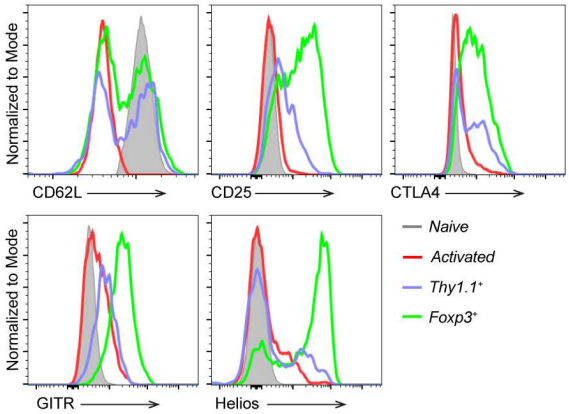
Normalized to Mode
CD62L
CD25
CTLA4
GITR
Helios
Naive
Activated
Thy1.1+
Foxp3+

f

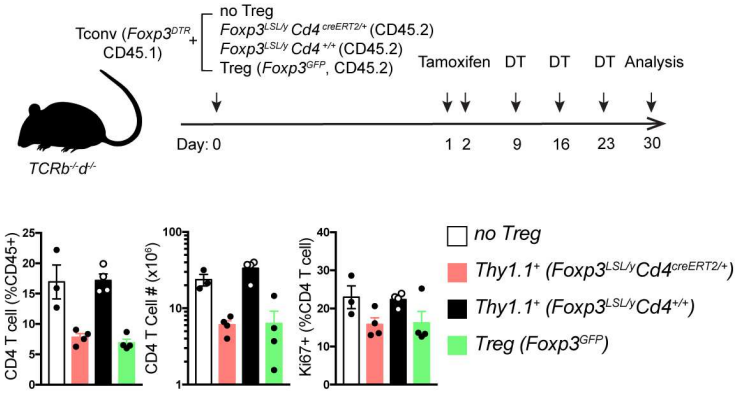
Tconv (Foxp3DTR, CD45.1)
no Treg
Foxp3LSL/y Cd4 creERT2/+ (CD45.2)
Foxp3LSL/y Cd4 +/+ (CD45.2)
Treg (Foxp3GFP, CD45.2)
TCRb-/-d-/-
Tamoxifen
DT
DT
DT
Analysis
Day: 0
1 2
9
16
23
30
CD4 T cell (%CD45+)
CD4 T Cell # (x10^6)
Ki67+ (%CD4 T cell)
no Treg
Thy1.1+ (Foxp3LSL/yCd4creERT2/+)
Thy1.1+ (Foxp3LSL/yCd4+/+)
Treg (Foxp3GFP)

1167

1168 **Extended Data Figure 1 | Generation and characterization of *Foxp3^{LSL}* mice. a**, Schematics of the
1169 targeting construct and the *Foxp3^{LSL}* allele before and after Flp recombinase-mediated removal of the neo
1170 cassette. Homologous regions between the targeting construct and the WT allele are demarcated with
1171 dashed gray lines. Gene map is based on RefSeq record NM_001199347.1. pA, bovine growth hormone
1172 polyadenylation signal; neo, neomycin resistance gene; PGK, mouse phosphoglycerate kinase 1
1173 promoter; 3xSV40pA, triple-tandem SV40 early polyadenylation signals (STOP cassette); DTA, diphtheria
1174 toxin A. **b**, Genotyping PCR showing the WT (275 bp) and knock-in-specific (350 bp) bands using primers
1175 labeled in **a**. **c, d**, Flow cytometric analysis of T cells and TCRβ^{hi} single positive thymocytes from 3-wk-old
1176 male *Foxp3$^{LSL/y}$* (**c**) and 8-10-wk-old female *Foxp3$^{LSL/WT}$* (**d**) mice. LN, lymph nodes. **e**, Expression of
1177 molecules associated with T cell activation in splenic Foxp3^{+} Treg and Thy1.1^{+} Treg "wannabe" cells, and
1178 naïve (CD44^{lo}CD62L^{hi}) and activated (CD44^{hi}CD62L^{lo}) conventional CD4 T cells shown in **d**. **f**, 2x10^{6}
1179 CD45.1^{+}Foxp3^{-} conventional CD4 T cells were co-transferred with 2x10^{5} CD45.2^{+} Treg "wannabes" from
1180 2-3-wk-old *Foxp3$^{LSL/y}$* mice or Treg cells from 6-8-wk-old *Foxp3^{GFP}* mice into *Tcrb$^{-/-}$Tcrd$^{-/-}$* mice. Recipients
1181 were orally gavaged with tamoxifen and injected i.p. with diphtheria toxin (DT) at the indicated time points
1182 (top). DT was administered to deplete the few contaminating DTR-expressing Treg cells in the transferred
1183 FACS-purified conventional T cells or those that were induced to express Foxp3 after transfer. Cellularity
1184 and proliferation of CD45.1^{+} responder cells from lymph nodes were analyzed using flow cytometry
1185 (bottom). Data are representative of two independent experiments. Bar graphs show mean ± s.e.m.
1186

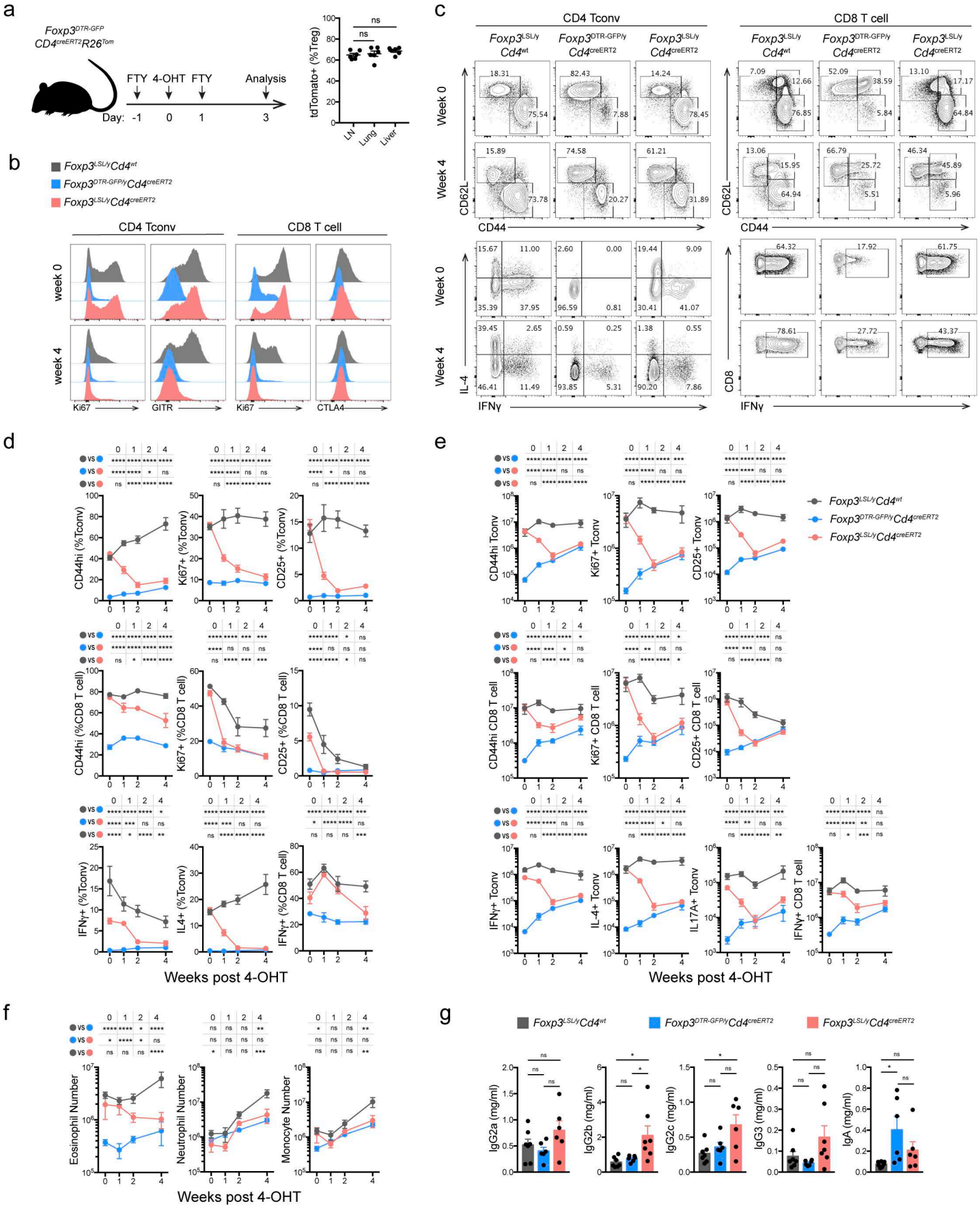
a
Foxp3DTR-GFP CD4creERT2R26Tom
FTY 4-OHT FTY
Analysis
Day: -1 0 1 3
tdTomato+ (%Treg)
ns
LN
Lung
Liver
b
Foxp3LSL/yCd4wt
Foxp3DTR-GFP/yCd4creERT2
Foxp3LSL/yCd4creERT2
CD4 Tconv
CD8 T cell
week 0
week 4
Ki67
GITR
CTLA4
c
CD4 Tconv
CD8 T cell
Week 0
Week 4
CD62L
CD44
IL-4
IFNγ
CD8
d
CD44hi (%Tconv)
Ki67+ (%Tconv)
CD25+ (%Tconv)
CD44hi (%CD8 T cell)
Ki67+ (%CD8 T cell)
CD25+ (%CD8 T cell)
IFNγ+ (%Tconv)
IL4+ (%Tconv)
IFNγ+ (%CD8 T cell)
Weeks post 4-OHT
e
CD44hi Tconv
Ki67+ Tconv
CD25+ Tconv
CD44hi CD8 T cell
Ki67+ CD8 T cell
CD25+ CD8 T cell
IFNγ+ Tconv
IL-4+ Tconv
IL17A+ Tconv
IFNγ+ CD8 T cell
Weeks post 4-OHT
f
Eosinophil Number
Neutrophil Number
Monocyte Number
Weeks post 4-OHT
g
IgG2a (mg/ml)
IgG2b (mg/ml)
IgG2c (mg/ml)
IgG3 (mg/ml)
IgA (mg/ml)

1187

1188 **Extended Data Figure 2 | Restoration of *Foxp3* expression reverses spontaneous lymphocyte**
1189 **expansion, myelo-proliferation, and cytokine production, and normalizes circulatory Ig levels in**
1190 **male *Foxp3*^{LSL} mice. a,** 4-OHT mediated recombination efficiency in lymphoid and non-lymphoid organs.
1191 Experimental scheme (left) and recombination efficiency of *Rosa26*^{Tom} in Treg cells in indicated organs
1192 (right). Scatter plot shows mean ±SEM, One-way ANOVA. **b-g,** Male *Foxp3*^{LSL} mice were treated with 4-
1193 OHT on wk 2 of life and analyzed throughout the following 4 wks. **b,** Representative histograms showing
1194 expression of proliferation and activation markers by splenic conventional CD4 and CD8 T cells at the
1195 indicated time points. **c,** Representative contour plots of flow cytometric analysis of activated and cytokine-
1196 producing splenic conventional CD4 and CD8 T cell populations. **d, e,** frequencies (**d**) and numbers (**e**) of
1197 activated, proliferating and cytokine-producing conventional CD4 and CD8 T cells from lymph nodes of
1198 mice of indicated genotypes at designated time points after 4-OHT treatment. Data shown are mean ±
1199 s.e.m. Two-way ANOVA with Tukey's multiple comparison test. **f,** Numbers of splenic myeloid cell
1200 populations at indicated time points after 4-OHT treatment. Two-way ANOVA with Tukey's multiple
1201 comparison test. **g,** Serum antibody levels as in **Figure 1g.** Data are shown as mean Ig isotype
1202 concentrations ± s.e.m., one-way ANOVA with Tukey's multiple comparison test. ns, non-significant; *, $p < 0.05$; **, $p < 0.01$; ***, $p<0.001$; ****, $p<0.0001$.
1204

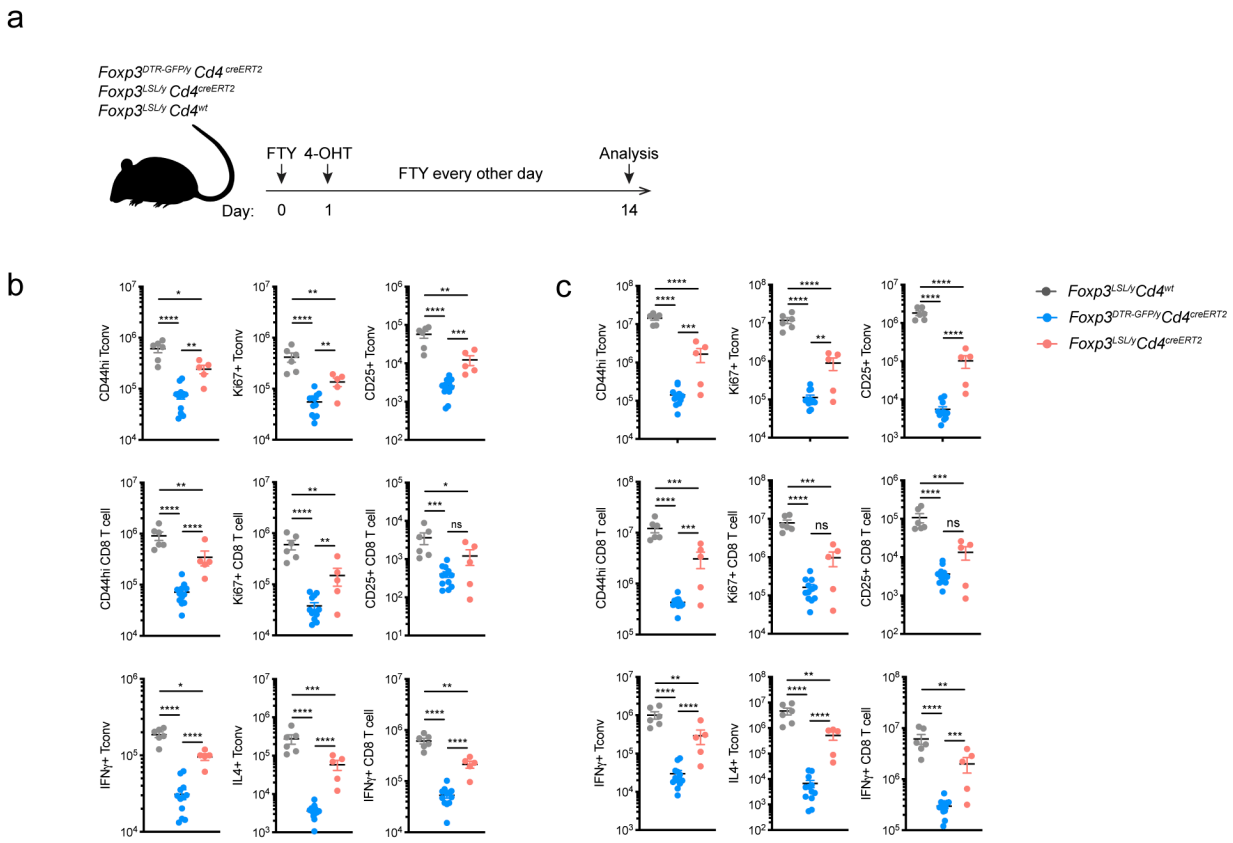

Extended Data Figure 3 | Restoration of *Foxp3* expression in peripheral Treg "wannabes" rescues immune activation in male *Foxp3*^{LSL} mice. a, Experimental Design. Mice were treated with 4-hydroxytamoxifen (4-OHT) at 2 wks of age while being continuously treated with FTY720 to block thymic output. **b, c,** Numbers of activated, proliferating, and cytokine-producing conventional CD4 and CD8 T cells in the spleen (**b**) and lymph nodes (**c**).

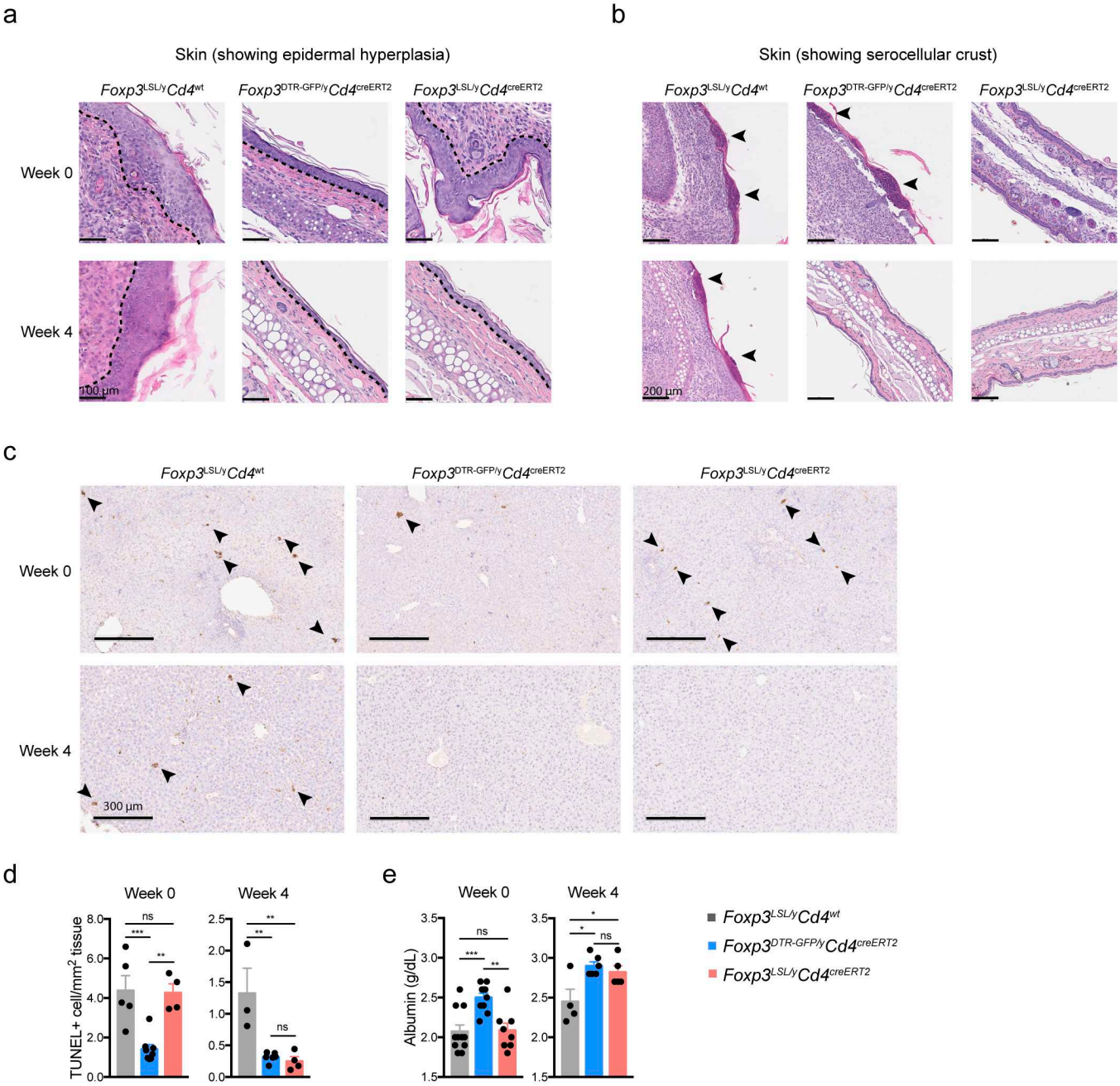

Extended Data Figure 4 | Restoration of *Foxp3* expression in Treg "wannabes" rescues tissue damage in the skin and liver of male *Foxp3*^{LSL} mice. Mice were treated with 4-OHT on postnatal day 14 and examined at the indicated time points post-treatment. **a, b,** H&E staining of skin sections showing epidermal hyperplasia and formation of serocellular crust (arrow heads). Dashed lines demarcate the boundary between epidermis and dermis. **c**, TUNEL (terminal deoxynucleotidyl transferase dUTP nick end labeling) assay followed by immunohistochemistry to visualize apoptotic cells (arrow heads) in H&E counter-stained liver sections from mice of indicated genotypes. **d,** Quantification of TUNEL^{+} cells. **e,** Measurement of serum albumin levels. **d, e,** Data shown are mean ± s.e.m., one-way ANOVA with Tukey's multiple comparison test. ns, non-significant; *, $p < 0.05$; **, $p < 0.01$; ***, $p<0.001$.

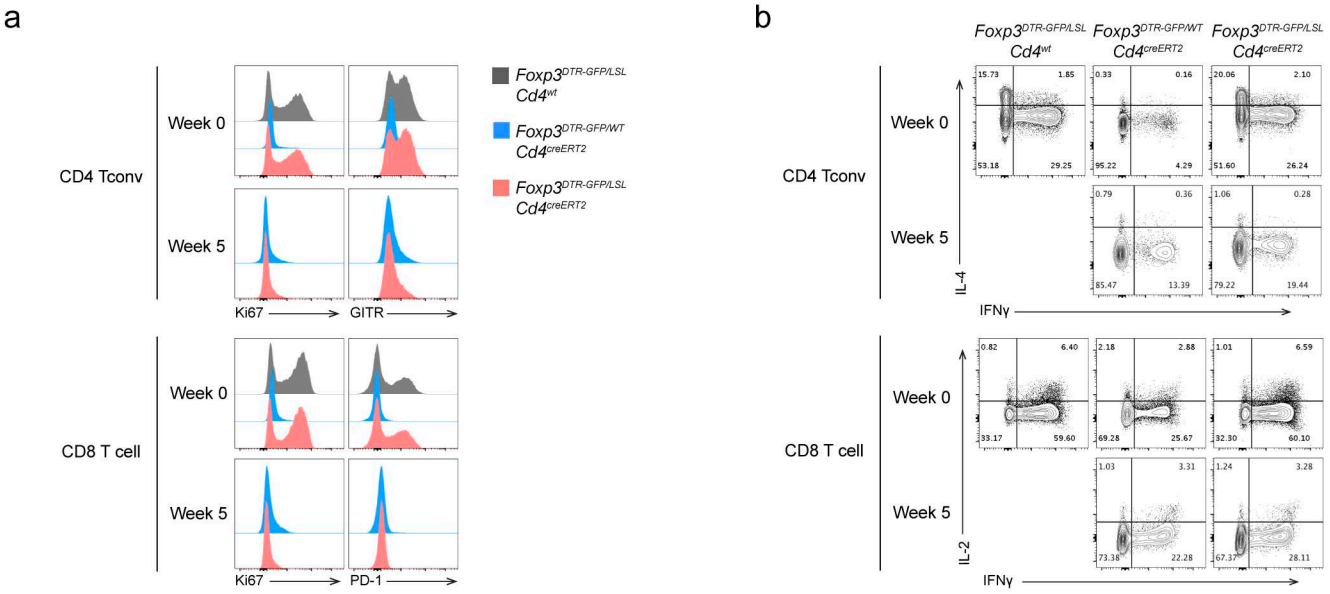

Extended Data Figure 5 | Restoration of *Foxp3* expression in Treg "wannabe" cells in mosaic adult female *Foxp3*$^{LSL/DTR\text{-}GFP}$ mice suppresses immune activation caused by diphtheria toxin-mediated Treg cell ablation. Experimental scheme shown in **Figure 2a**. **a,** Representative histograms showing expression of activation and proliferation markers in splenic conventional T cell populations. **b,** Representative contour plots of splenic conventional CD4 and CD8 T cells showing cytokine production.

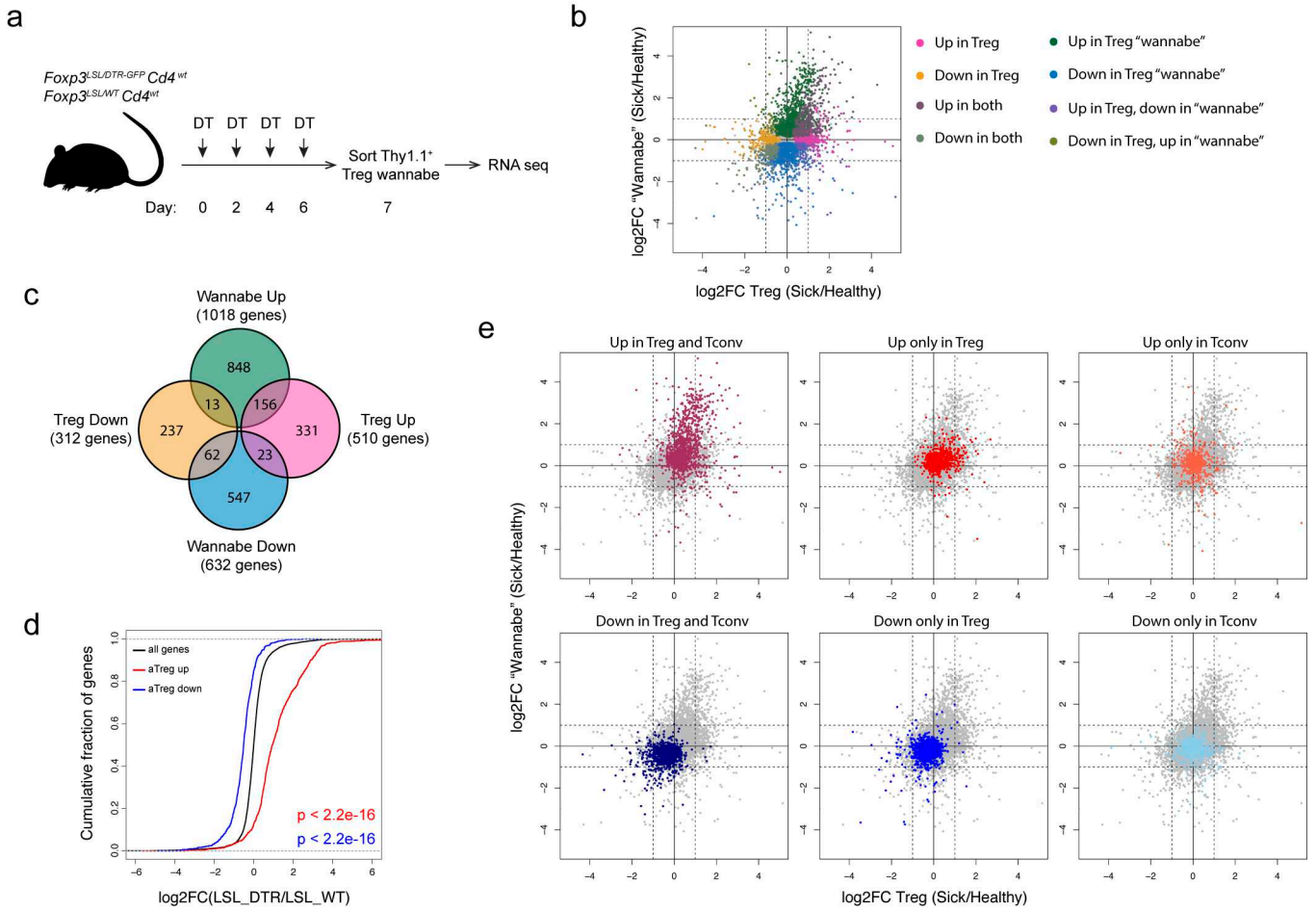

Extended Data Figure 6 | Analysis of gene expression changes in Treg "wannabe" cells induced upon activation. a, Experimental scheme. 8-10-wk-old heterozygous female *Foxp3*$^{LSL/DTR\text{-}GFP}$*Cd4*^{wt} mice were treated with diphtheria toxin (DT) on designated days to deplete *Foxp3*$^{DTR\text{-}GFP}$-expressing Treg cells and induce activation of *Foxp3*^{LSL}-expressing Treg "wannabe" cells which were sorted and analyzed by RNA-seq. **b,** FC-FC plot of activation-induced gene expression changes in Treg cells and "wannabes". Genes with mean normalized counts of >100 are shown. Differentially expressed genes ($p < 0.05$) are colored based on the direction of the change in either or both cell types. **c,** Venn diagram showing the numbers of genes with larger than a 2-fold change in activated Treg and "wannabe" cells. **d,** CDF plots showing expression changes in activated Treg "wannabe" cells for all genes (black) and Treg activation signature genes that are up- (red) or down- (blue) regulated. Two-sided Kolmogorov-Smirnov test. **e,** FC-FC plot showing gene expression changes in Treg vs. "wannabe" cells isolated from sick and healthy mice. Signature genes that are up- or down-regulated in activated Treg and conventional CD4 T cells are highlighted in different colors.

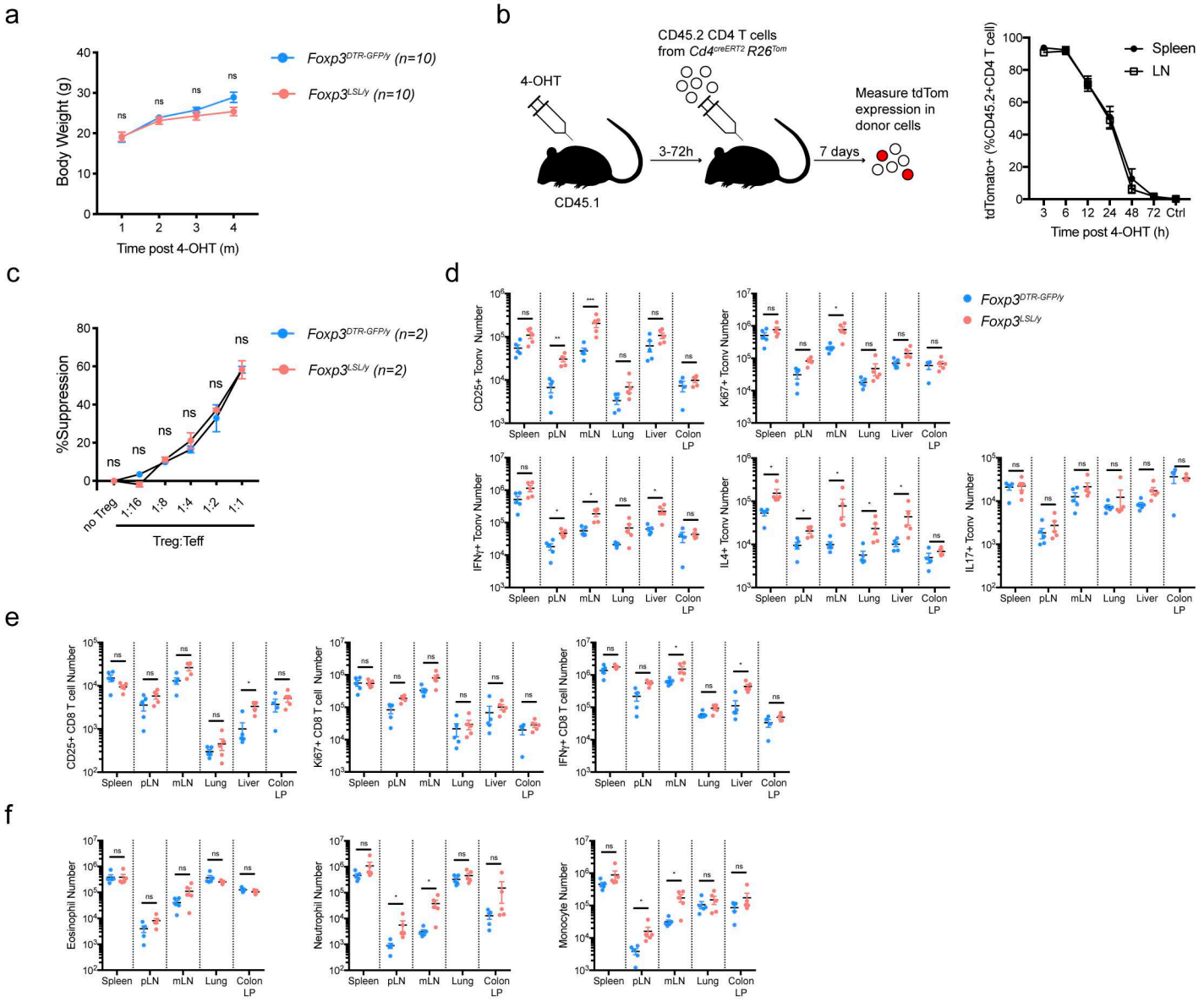

Extended Data Figure 7 | Rescued Treg cells in male *Foxp3^{LSL}* mice exert long-term control of adaptive and innate immune cells. Mice were treated with a single dose of 4-OHT at 2 wks of age and analyzed 4 months later. **a,** Body weight of rescued *Foxp3^{LSL}Cd4^{creERT2}* and control *Foxp3$^{DTR\text{-}GFP}$Cd4^{creERT2}* mice over a 4-month time course. Two-way ANOVA with Sidak's multiple comparison test. **b,** Analysis of 4-OHT "functional" pharmacokinetics in 2-wk-old male mice. Mice were injected with 4-OHT 3-72 hours before transfer of congenically marked recombination-proficient CD4 T cells from *Cd4^{creERT2}R26^{Tom}* mice. 4-OHT-induced recombination was assayed 7 days later by tdTomato expression among donor CD4 T cell as a readout of 4-OHT activity. Data are pooled from two independent experiments with 2 to 4 mice per time point each. Line graph shows mean ± s.e.m. Ctrl, no 4-OHT injection. **c,** Suppression of *in vitro* proliferation of conventional CD4 T cells induced by α-CD3 antibody and antigen-presenting cells by control Treg cells from *Foxp3$^{DTR\text{-}GFP/y}$* or rescued Treg cells from *Foxp3$^{LSL/y}$* mice. Two-way ANOVA with

1257 Tukey's multiple comparison test. Data are shown as mean %suppression ± s.e.m. **d-f,** Numbers of
1258 activated, proliferating, and cytokine-producing conventional CD4 T cells (**d**), CD8 T cells (**e**) and myeloid
1259 populations (**f**) in indicated tissues. pLN, peripheral (brachial, axillary, and inguinal) lymph nodes; mLN,
1260 mesenteric lymph nodes; LP, lamina propria. Data are pooled from two independent experiments. Scatter
1261 plots show mean ± s.e.m. Two-tailed *t*-tests with multiple hypothesis testing correction using the Holm-
1262 Sidak method. ns, non-significant; *, $p < 0.05$; **, $p < 0.01$; ***, $p<0.001$; ****, $p<0.0001$.
1263

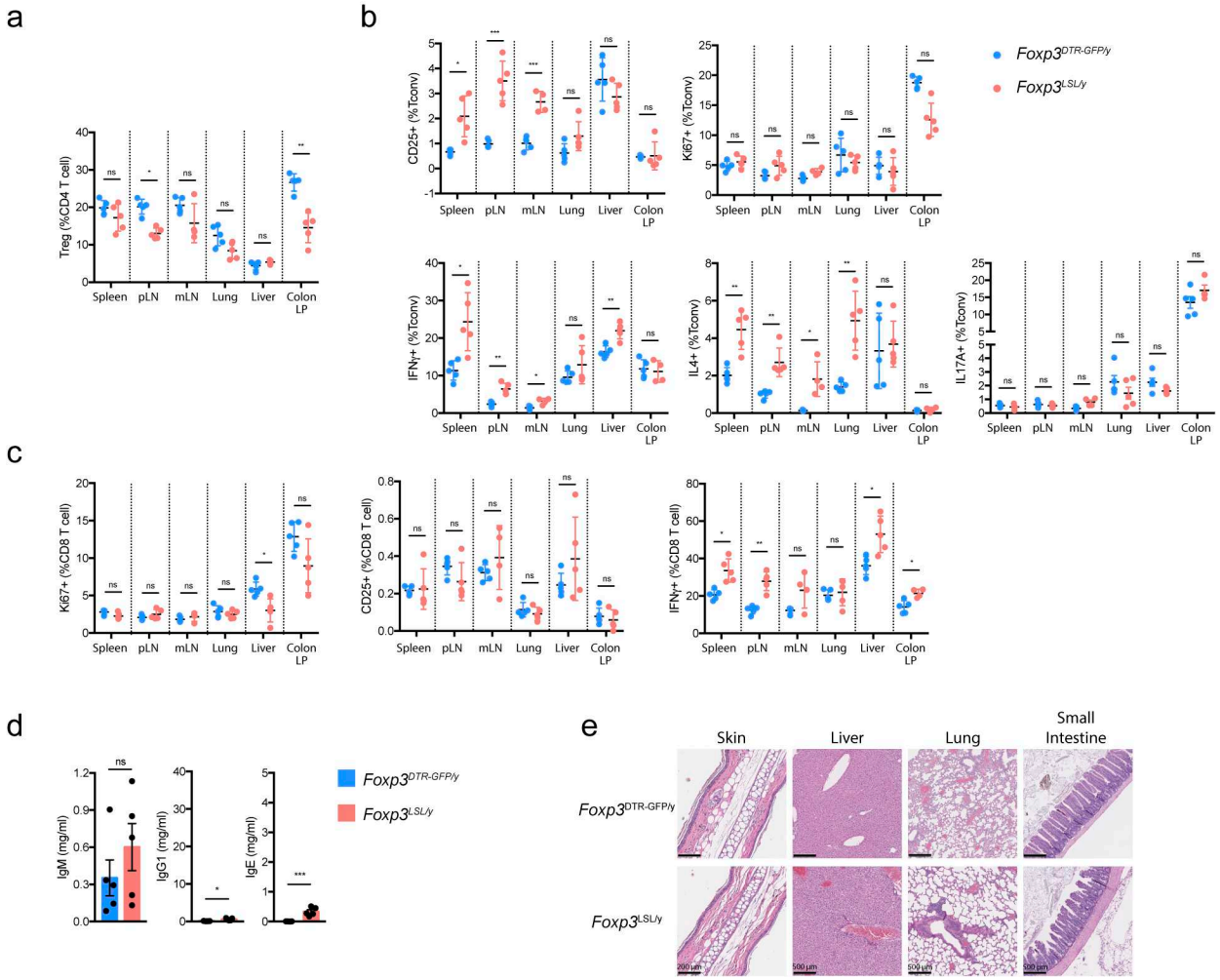

Extended Data Figure 8 | Rescued Treg cell population persisting for 7 months in male *Foxp3^{LSL}* mice prevent relapse of rampant autoimmunity. Mice were treated with 4-OHT on postnatal day 14 and analyzed 7 months later. **a-c,** Frequencies of Treg cells (**a**) and proliferating, activated, and cytokine-producing conventional CD4 (**b**) and CD8 (**c**) T cells. Two-tailed unpaired *t*-tests with multiple hypothesis testing correction using the Holm-Sidak method. **d,** Serum antibody levels. Scales were kept the same as in **Figure 1g**. Two-tailed unpaired *t*-test. **e,** Representative images of haematoxylin and eosin-stained sections of the indicated organs. Scatter plots and bar graphs show mean ± s.e.m. ns, non-significant; *, $p < 0.05$; **, $p < 0.01$; ***, $p<0.001$; ****, $p<0.0001$.

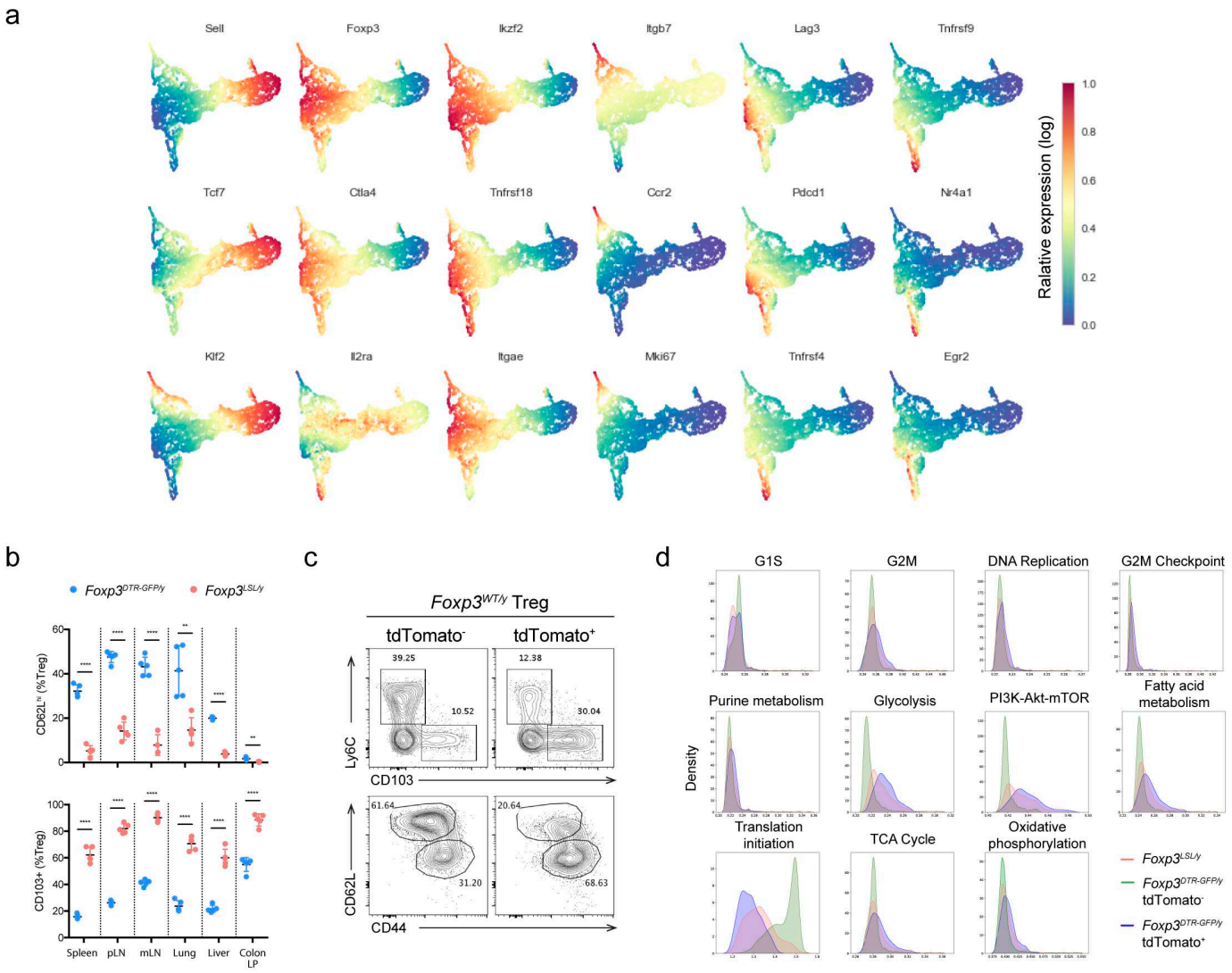

Extended Data Figure 9 | Analysis of long-lived Treg cells in *Foxp3^{LSL}* and control *Foxp3$^{DTR\text{-}GFP}$* mice. Mice were treated with 4-OHT on postnatal day 14 and analyzed 7 months later. **a,** UMAP visualization of the single-cell transcriptomes colored by imputed expression levels of representative genes. **b**, Frequencies of CD62L^{hi} and CD103^{+} cells among Treg cells in rescued *Foxp3^{LSL}Cd4^{creERT2}* and control *Foxp3$^{DTR\text{-}GFP}$Cd4^{creERT2}* mice. Two-tailed multiple *t*-tests. **c,** *Foxp3^{WT}Cd4^{creERT2}R26^{Tom}* mice were treated with 4-OHT on postnatal day 14 and analyzed 4 months later. Representative contour plots show expression of activation markers by tdTomato^{+} and tdTomato^{-} Foxp3^{+} CD4 T cells. **d,** Histogram depicting the density of *Foxp3^{LSL}* and tdTomato^{+} or tdTomato^{-} *Foxp3$^{DTR\text{-}GFP}$* Treg cells along the average expression values for the indicated gene sets. Scatter plots show mean ± s.e.m. ns, non-significant; *, $p < 0.05$; **, $p < 0.01$; ***, $p<0.001$; ****, $p<0.0001$.

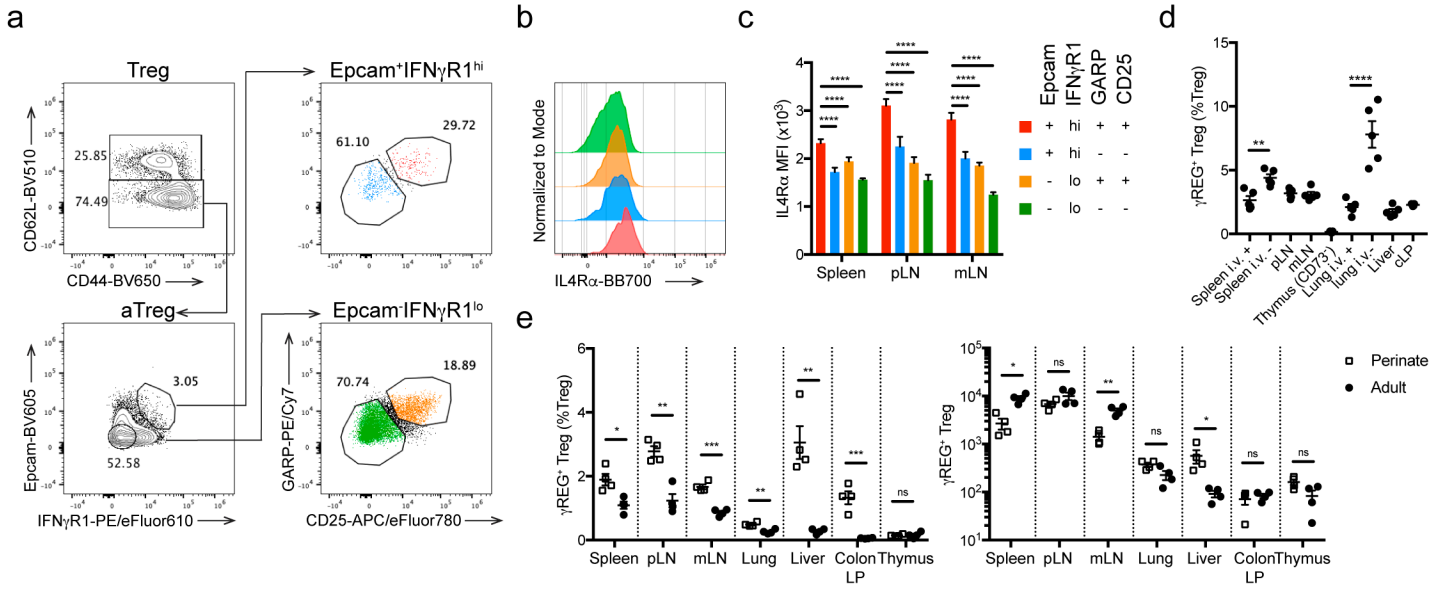

Extended Data Figure 10 | Flow cytometric analysis of γREG⁺ Treg cells. a, Gating strategy for γREG⁺ Treg cells in adult mice. **b, c,** Representative histogram (**b**) and quantification (**c**) of IL4Rα expression in γREG⁺ and other Treg cell populations identified in **a**. Two-way ANOVA with Tukey's multiple comparison test. **d,** Percentages of γREG⁺ Treg cells in lymphoid organs and non-lymphoid tissues of CD45 i.v.-labeled 8-10-wk-old *Foxp3*^{GFP} mice. One-way ANOVA with Sidak's multiple comparison test. **e,** Percentages (left) and numbers (right) of γREG⁺ Treg cells in different organs of 2- or 8-wk-old *Foxp3*$^{GFP\text{-}BirA\text{-}AVI\text{-}TEV}$ mice. Two-sided unpaired *t*-tests with correction for multiple hypothesis testing using the Holm-Sidak method. Bar graph and scatter plots show mean ± s.e.m. ns, non-significant; *, $p < 0.05$; **, $p < 0.01$; ***, $p<0.001$; ****, $p<0.0001$.

Figures

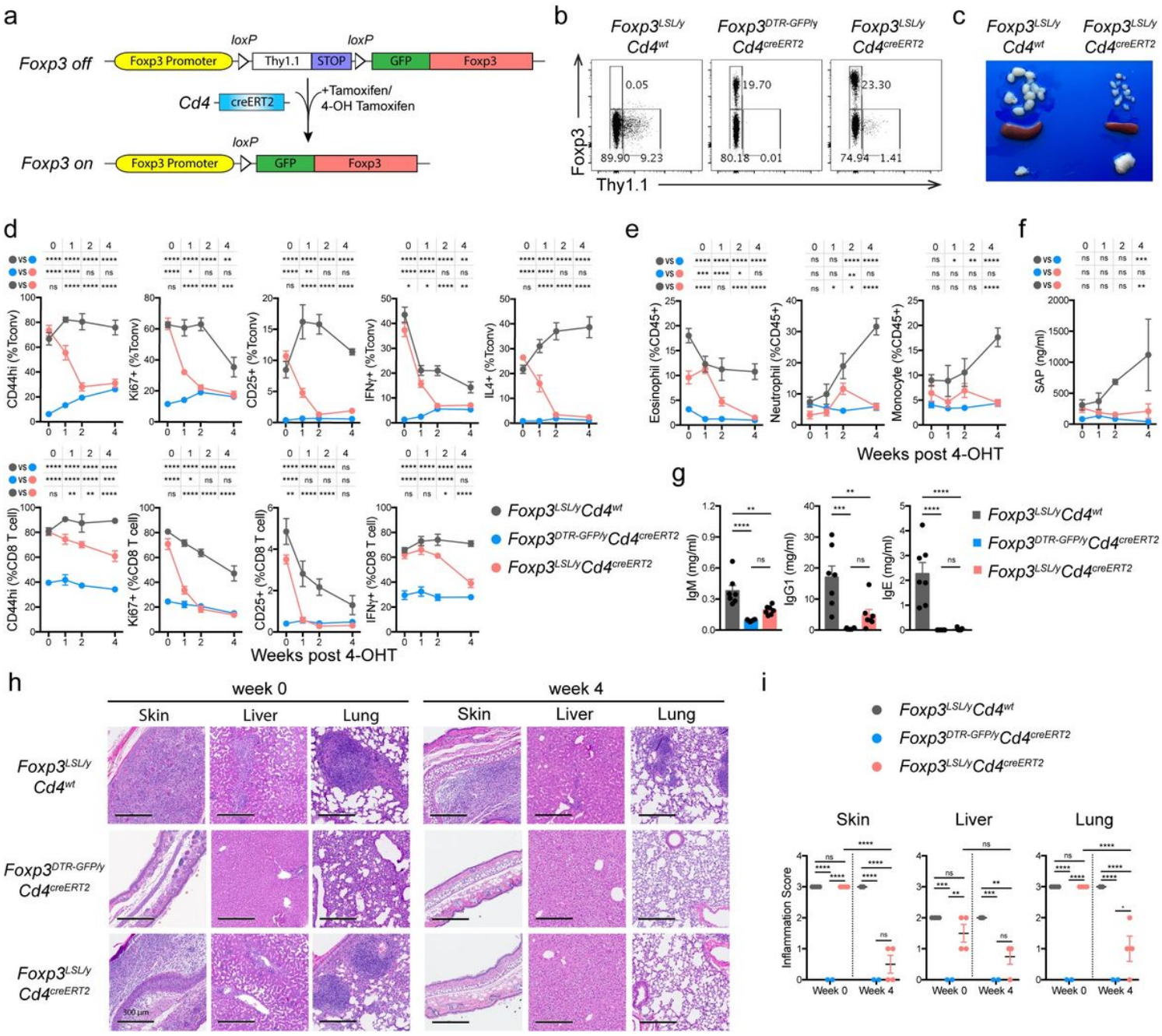

Figure 1

Restoration of Foxp3 expression in Treg “wannabes” cures fulminant autoimmunity in male Foxp3LSL mice. Mice were treated with 4-hydroxytamoxifen (4-OHT) on postnatal day 14. a,Schematic of the Foxp3LSL allele. b, Flow cytometric analysis of splenic CD4 T cells 1 wk post 4-OHT treatment. c, Lymph nodes (top), spleens (middle), and thymi (bottom) of mice of indicated genotypes 4 wks after 4-OHT treatment. d-f, Percentages of activated, proliferating, and cytokine-producing splenic T cells (d), frequencies of splenic myeloid cell populations (e), and serum amyloid P (SAP) levels (f) at indicated time points after 4-OHT treatment. g, Levels of antibodies in the serum 4 wks post-4-OHT treatment. h,

Haematoxylin and eosin staining of indicated tissues before and 4 wks after 4-OHT treatment. i, Histology scores of indicated tissues before and 4 wks after 4-OHT treatment. For d-g, data are combined from three independent experiments with 3 to 12 mice per group per time point. Data are shown as mean ± s.e.m., two-way (d-f, i) or one-way (g) ANOVA with Tukey's multiple 1070 comparisons test. ns, non-significant; *, p < 0.05; **, p < 0.01; ***, p<0.001; ****, p<0.0001.

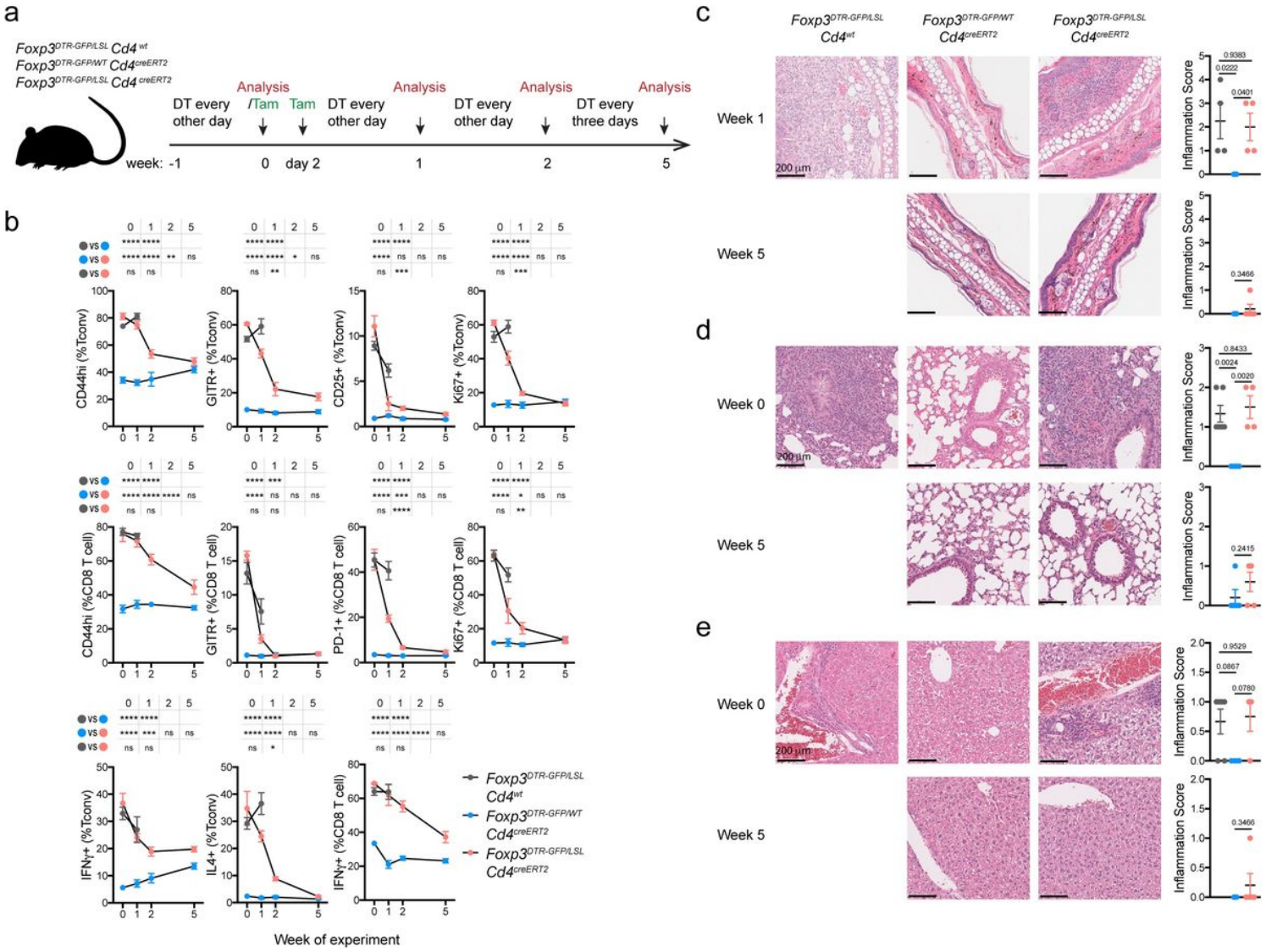

Figure 2

Restoration of Foxp3 expression in Treg "wannabe" cells in mosaic adult female Foxp3LSL/DTR-GFP mice suppresses immune activation caused by diphtheria toxin-mediated Treg cell ablation. a, Experimental scheme. 8-10-wk-old female mice were injected with diphtheria toxin (DT) intraperitoneally and given oral gavage of tamoxifen (Tam) on designated days. b, Frequencies of activated, proliferating, and cytokine producing splenic conventional CD4 and CD8 T cells at the indicated time points. Data are pooled from two independent experiments with 3 to 5 mice per group per time point. Line graphs show mean percentages ± s.e.m., two-way ANOVA with Tukey's multiple comparison test. ns, non-significant; *, p < 0.05; **, p < 0.01; ***, p<0.001; ****, p<0.0001. c-e, Haematoxylin and eosin staining of sections of skin (c), lung (d), and liver (e) from mice of indicated genotypes at denoted time points post tamoxifen

treatment (left), and their respective inflammation scores (right). Scatter plots show mean score ± s.e.m., one-way ANOVA with Tukey's multiple comparison test.

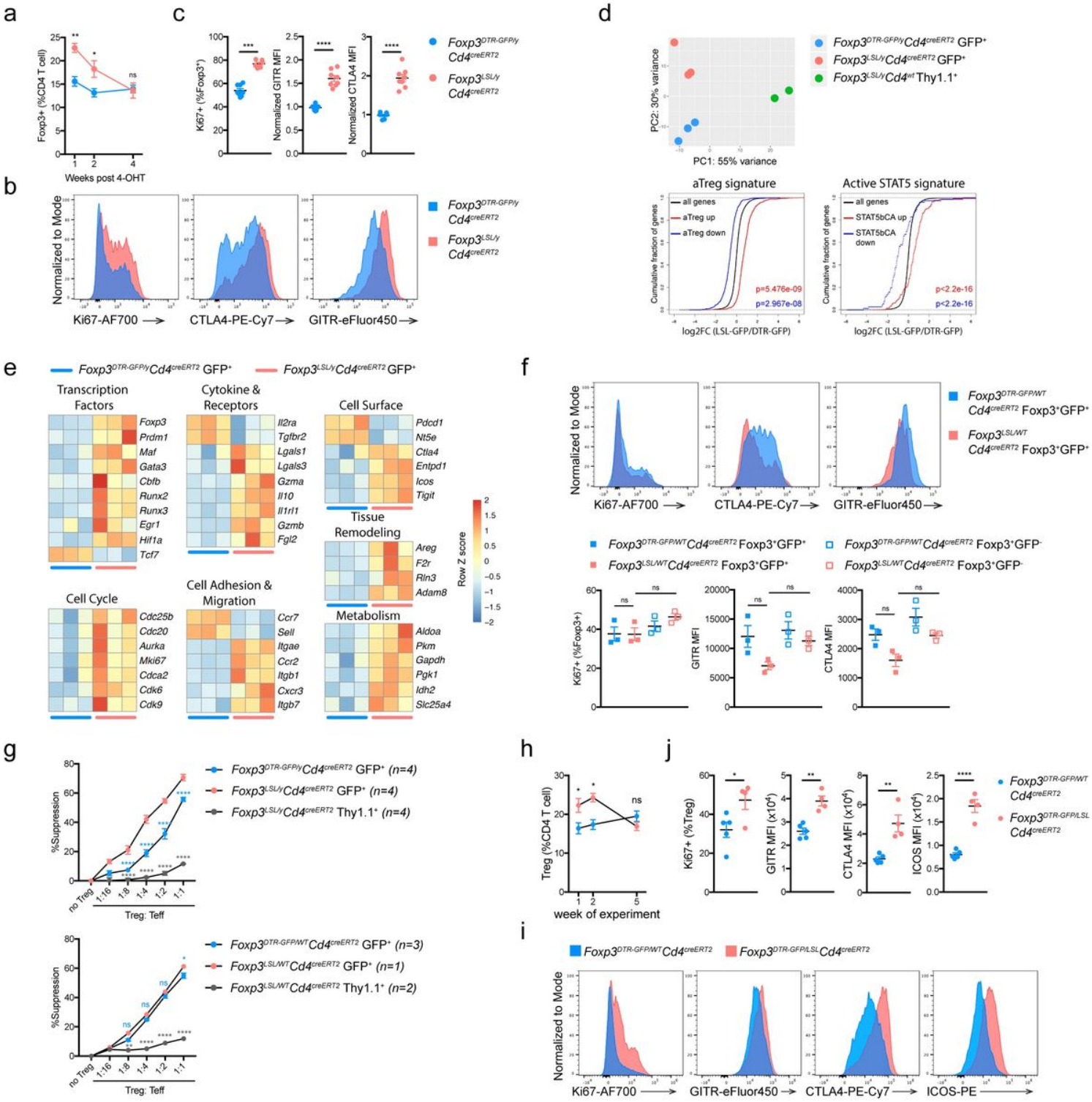

Figure 3

Rescued Treg cells in inflamed mice are activated and potently suppressive in inflammatory settings. a-c, Male Foxp3DTR-GFPCd4creERT2 and Foxp3LSLCd4creERT2 mice were treated with 4-OHT on postnatal day 14. Data are pooled from three independent experiments. a, Percentages of splenic Treg cells at indicated time points following 4-OHT treatment. Line graph shows mean ± s.e.m. Multiple t-tests with

Holm-Sidak multiple comparison. b, c, representative histograms (b) and combined data (c) showing expression of Ki67, CTLA4 and GITR by rescued and control Treg cells on day 7 post 4- OHT treatment from the spleen analyzed by flow cytometry. Scatter plots show mean ± s.e.m. Two-tailed unpaired t-tests. d, e, RNA-seq analysis of rescued Treg cells, control 1094 Treg cells, and Treg “wannabes” from male mice of indicated genotypes treated with 4-OHT on postnatal day 14 and analyzed 7 days afterwards. d, Principal component analysis of gene expression in the three indicated cell populations (top), and empirical cumulative distribution function plots showing gene signatures of activated Treg cells (bottom left) and Treg cells expressing a constitutively active form of STAT5b (bottom right). Two-sided Kolmogorov-Smirnov test. e, Heatmaps showing expression of curated genes in rescued and control Treg cells from mice of indicated genotypes. f, Expression of Ki67, CTLA4 and GITR by indicated Treg cell subsets from the spleen of mosaic heterozygous Foxp3DTR-GFP/WTCd4creERT2 and Foxp3LSL/WTCd4creERT2 female mice treated with 4-OHT on postnatal day 14 and analyzed after 7 days using flow cytometry. Data are shown as mean ± s.e.m., one-way ANOVA with Tukey’s multiple comparison test. g, Suppression of in vitro proliferation of conventional CD4 T cells induced by a-CD3 antibody and antigen-presenting cells by control or rescued Treg cells (GFP+), or Treg “wannabes” (Thy1.1+) from indicated strains of mice on day 7 post 4-OHT treatment. Two-way ANOVA with Tukey’s multiple comparison test. Data are shown as mean %suppression ± s.e.m. Frequencies of Treg cells at the indicated time points. Line graph shows mean percentages ± s.e.m. Two-way ANOVA with Tukey’s multiple comparison test. h-j, Adult mosaic heterozygous female Foxp3DTR-GFP/WTCd4creERT2 and Foxp3DTR-GFP/LSLCd4creERT2 mice were treated with DT and 4-OHT as in Figure 2a. h, Percentages of splenic Treg cells at indicated time points following 4-OHT treatment. Line graph shows mean ± s.e.m. Multiple t-tests with Holm-Sidak multiple comparison. i, j, Representative histograms (i) and combined data (j) showing expression of indicated markers by Treg cells at wk 1. Scatter plots show mean percentages or MFI ± s.e.m., two-tailed unpaired t-tests. ns, nonsignificant; *, $p < 0.05$; **, $p < 0.01$; ***, $p<0.001$; ****, $p<0.0001$.

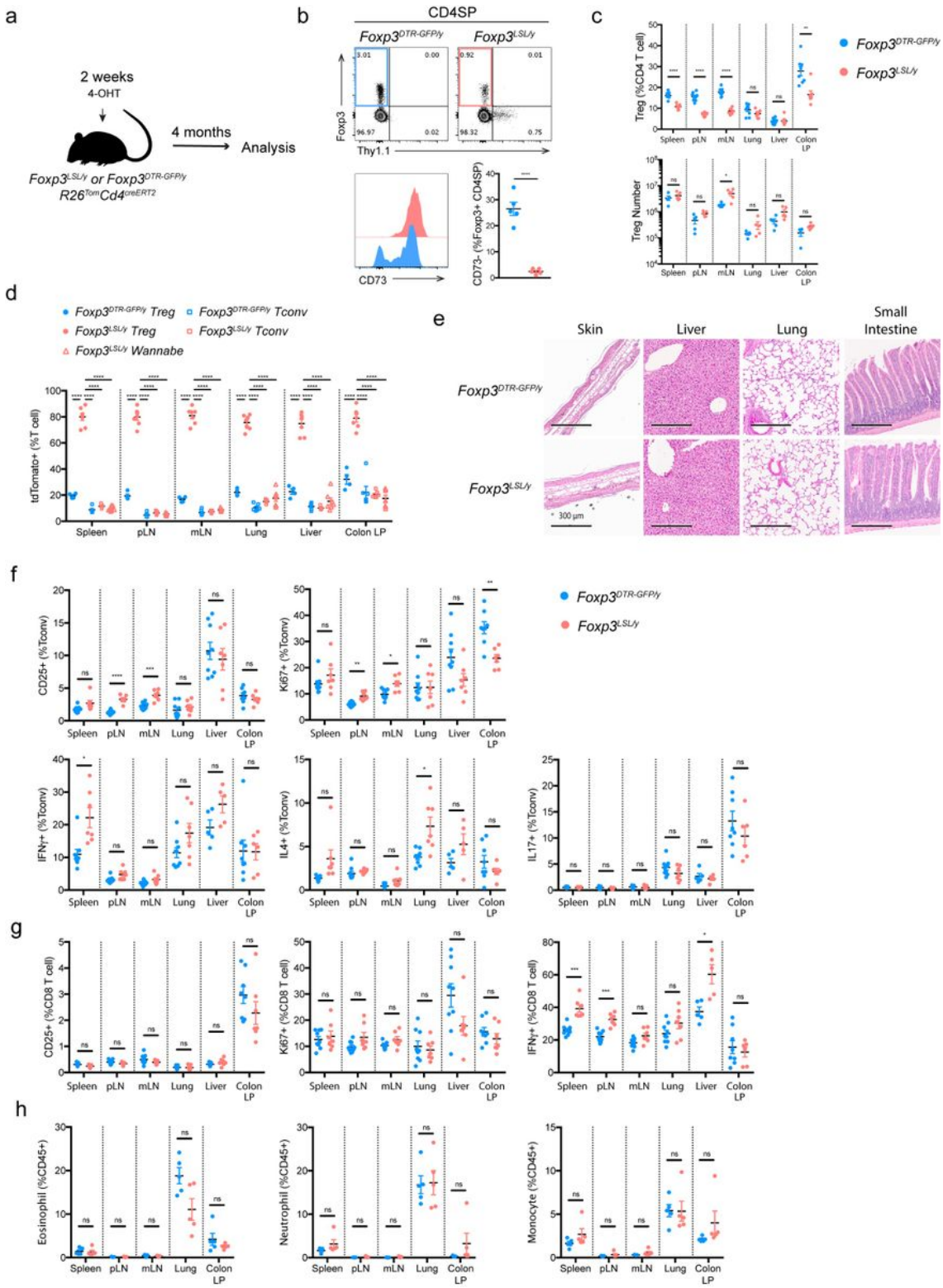

Figure 4

Rescued Treg cells in male Foxp3LSL mice provide long-term protection from autoimmune inflammatory disease. a, Experimental design. Mice were treated with a single dose of 4- OHT at 2 wks of age and analyzed 4 months later. b, Flow cytometric analysis of CD73 expression in Foxp3+ CD4 single-positive thymocytes as a discriminating marker of recirculating vs. recently generated thymic Treg cells. Two-tailed unpaired t-test. c, Flow cytometric analysis of Treg cell percentages (upper panel) and absolute

numbers (lower panel) in tissues of mice of indicated genotypes. Two-tailed multiple t tests with Holm-Sidak multiple comparison. d, Percentages of lineage-traced (tdTomato+) Treg cells, Treg “wannabes”, and conventional CD4 T cells. One-way ANOVA with Dunnett’s multiple hypothesis tests. e, Analysis of histopathology in mice of indicated genotypes. Haematoxylin and eosin staining of sections of the indicated organs. f-h, Percentages of activated, proliferating, and cytokine-producing conventional CD4 T cells (f), CD8 T cells (g) and myeloid populations (h) from indicated organs. Data are pooled from two independent experiments. Two-tailed unpaired t-tests with Holm-Sidak multiple comparison.
pLN, peripheral (brachial, axillary, and inguinal) lymph nodes; mLN, mesenteric lymph nodes; LP, lamina propria. Scatter plots show mean ± s.e.m. ns, non-significant; *, $p < 0.05$; **, $p < 0.01$; ***, $p<0.001$; ****, $p<0.0001$.

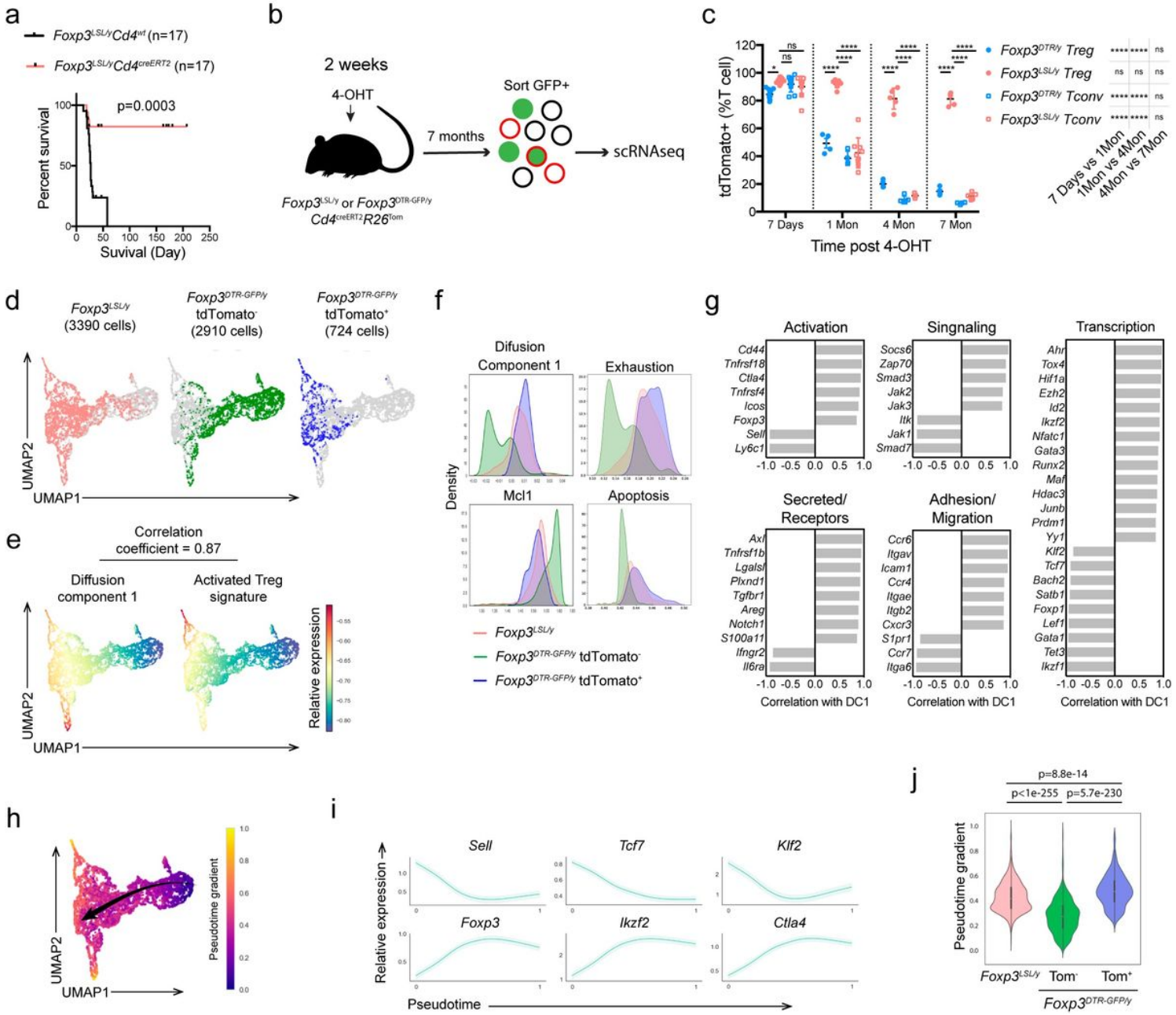

Figure 5

Single-cell transcriptomic analysis of control and long-lived rescued Treg cells. a, Survival plot of 4-OHT-treated male Foxp3LSLCd4wt and Foxp3LSLCd4creERT2 mice. Mantel-Cox test. b, Experimental design. Mice were treated with 4-OHT at 2 wks of age and Foxp3+ Treg cells, FACS-purified based on GFP expression, were subjected to scRNA-seq analysis using 10X Genomics platform 7 months later. c, Percentages of fate-mapped splenic Treg cells and conventional CD4 T cells in control and rescued mice at indicated time points post 4-OHT treatment. Scatter plot shows mean ± s.e.m. Two-way ANOVA with Tukey's multiple comparisons test. d, UMAP visualization of the single-cell transcriptomes of experimental Foxp3LSL and control tdTomato- or tdTomato+ Foxp3DTR-GFP Treg cells. e, UMAP visualization colored by diffusion component 1 (left) and the expression level of activated Treg cell gene signature (right). f, Histograms depicting the density of Foxp3LSL and tdTomato+ or tdTomato- Foxp3DTR-GFP Treg cells along diffusion component 1, Mcl1 expression, and the average expression levels of indicated gene sets. g, Correlation of curated genes with diffusion component 1. h, UMAP visualization colored by pseudotimegenerated with Palantir. Arrow indicates the direction of differentiation across the 1146 map. i, Expression of representative genes along the pseudotime trajectory. j, Violin plots showing the medians of pseudotime values of Foxp3LSL and tdTomato+ or tdTomato- Foxp3DTR-GFP Treg cells. Thick vertical bars show the interquartile range.

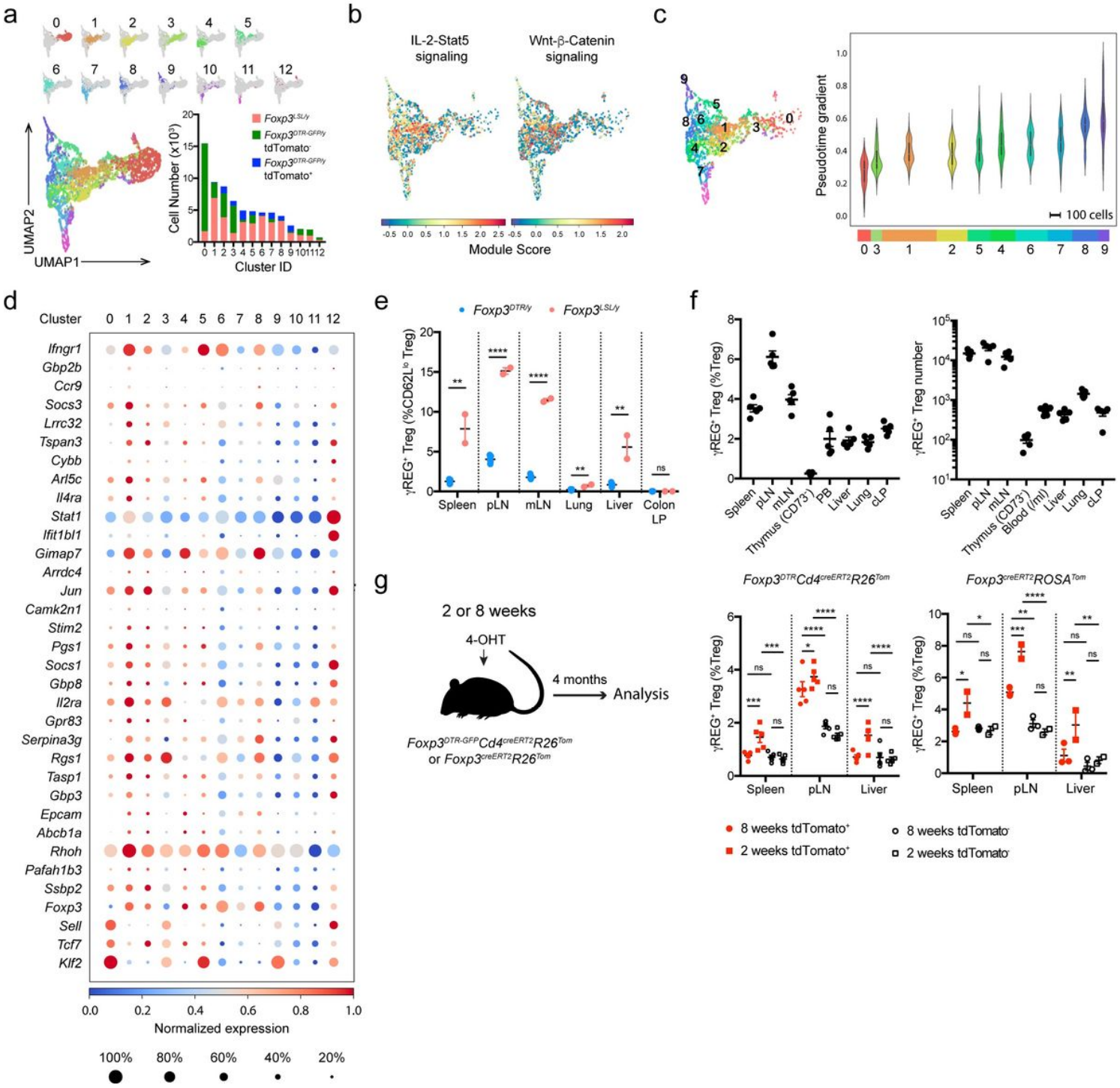

Figure 6

Identification and analysis of gREG+ Treg cells from the single-cell RNA-seq data. a, UMAP visualization colored by the clusters. Bar graph shows the numbers of cells from each sample that contributed to the individual clusters. b, UMAP visualization of Foxp3LSL Treg cells colored by the module scores for the indicated gene sets. c, Violin plots showing the medians of pseudotime values of Foxp3LSL Treg cells from the top 10 clusters. Thick vertical bars show the interquartile range. Horizontal bars show the number of Foxp3LSL Treg cells contributing to each cluster. d, Dot plot showing the expression of top enriched genes ($p<0.05$) and underrepresented genes from cluster 1 expressed by more than 20% of

the cells in at least one cluster. e, Frequencies of gREG+ Treg cells among CD62Llo Treg cells in rescued and control mice treated with 4-OHT on postnatal day 14 and analyzed 4 months later. Two-tailed unpaired t tests with Holm-Sidak multiple comparison. f, Frequencies (left) and absolute 1162 numbers (right) of gREG+ Treg cells in various tissues of unmanipulated 8-wk-old Foxp3GFP mice. g, Percentages of gREG+ Treg cells among tdTomato+ or tdTomato- Treg cells “time-stamped” in adult (8-wk-old) or perinatal (2-wk-old) mice and analyzed after 4 months. Two-way ANOVA with Tukey’s multiple comparison test.

Supplementary Files

This is a list of supplementary files associated with this preprint. Click to download.

- ExtendedDataTable1.xlsx